UNIVERSIDADE FEDERAL DE PERNAMBUCO
CENTRO DE TECNOLOGIA E GEOCIÊNCIAS
DEPARTAMENTO DE ELETRÔNICA E SISTEMAS
PROGRAMA DE PÓS-GRADUAÇÃO EM ENGENHARIA ELÉTRICA

EULOGIO GUTIERREZ HUAMPO

CHIRP-BASED DECOMPOSITIONS FOR COMPUTING FRACTIONAL FOURIER TRANSFORMS

Recife

2025

EULOGIO GUTIERREZ HUAMPO

CHIRP-BASED DECOMPOSITIONS FOR COMPUTING FRACTIONAL FOURIER TRANSFORMS

Thesis submitted to the Graduate Program in Electrical Engineering at the Federal University of Pernambuco, as a partial requirement for obtaining the title of Doctor in Electrical Engineering.

Concentration Area: Communications.

Supervisor: Prof. Dr. Juliano Bandeira Lima.

Co-supervisor: Prof. Dr. José Rodrigues de Oliveira Neto.

Recife

2025

.Catalogação de Publicação na Fonte. UFPE - Biblioteca Central

Gutierrez-Huampo, Eulogio.
Chirp-Based decompositions for computing fractional fourier transforms / Eulogio Gutierrez Huampo. - Recife, 2025.
103f.: il.

Tese (Doutorado)- Universidade Federal de Pernambuco, Centro de Tecnologia e Geociências, Programa de Pós-Graduação em Engenharia Elétrica, 2025.
Orientação: Juliano Bandeira Lima.
Coorientação: José Rodrigues de Oliveira Neto.

1. Transformada fracionária de Fourier; 2. Transformada numérica de Fermat; 3. Estimativa da direção de chegada; 4. Ajuste de múltiplas retas; 5. Chirp linear de banda larga. I. Lima, Juliano Bandeira. II. Oliveira Neto, José Rodrigues de. III. Título.

UFPE-Biblioteca Central

EULOGIO GUTIERREZ HUAMPO

"CHIRP-BASED DECOMPOSITIONS FOR COMPUTING FRACTIONAL FOURIER TRANSFORMS"

Tese apresentada ao Programa de Pós-Graduação em Engenharia Elétrica da Universidade Federal de Pernambuco, como requisito parcial para a obtenção do título de Doutor em Engenharia Elétrica, na área de concentração em Comunicações.

Aprovada em: 03/09/2025

BANCA EXAMINADORA

_____

Prof. Dr. Juliano Bandeira Lima
(Orientador e Examinador Interno)
Universidade Federal de Pernambuco

_____

Prof. Dr. Daniel Pedro Bezerra Chaves
(Examinador Interno)
Universidade Federal de Pernambuco

_____

Prof. Dr. Francisco Madeiro Bernardino Júnior
(Examinador Externo)
Universidade de Pernambuco

_____

Prof. Dr. Vitor de Andrade Coutrinho
(Examinador Externo)
Universidade Federal Rural de Pernambuco

_____

Prof. Dr. Felipe Alberto Barbosa Simão Ferreir
(Examinador Externo)
Universidade Federal Rural de Pernambuco

I would like to dedicate this work to all my family, a special feeling of gratitude to them, and friends with whom I lived in these spaces over the years.

ACKNOWLEDGEMENTS

First of all, I give thanks to God the Creator, a present help in times of distress. Afterward, I would like to express my sincere gratitude to my supervisors, Prof. Juliano B. Lima and Prof. José R. de Oliveira Neto, for their invaluable guidance, support, and encouragement throughout this work. I also wish to thank my professors, colleagues, and members of the Digital Signal Processing Research Group for their insightful discussions and collaborative spirit.

I am deeply grateful to the Federal University of Pernambuco (UFPE) for providing the institutional support and academic environment necessary for the successful completion of my doctoral studies in Electrical Engineering.

Finally, I acknowledge the Coordination for the Improvement of Higher Education Personnel (CAPES) for the financial support that made this research possible.

ABSTRACT

The fractional Fourier transform (FrFT) is a tool for analyzing non-stationary signals, associated with rotations of signal representations through energy distributions in the time-frequency plane. The main numerical algorithm for computing the FrFT is derived from its integral definition and, through sampling, produces a form of discrete FrFT (DFrFT). This thesis focuses on the study of this type of DFrFT and chirp signals, both of which are relevant in various modern systems. There are two chirp-based decompositions for computing the DFrFT: (i) one using chirp convolution and (ii) another relying solely on a discrete Fourier transform (DFT); both are typically implemented via fast Fourier transform (FFT) algorithms. The first contribution of this thesis is the implementation of a simplified FrFT(SmFrFT), with variable frequency scaling, in normalized domains. It is demonstrated that SmFrFT, being a particular case of canonical linear transforms, exhibits distinct properties compared to conventional FrFT and offers advantages in chirp signal processing; the reduction in the number of complex multiplications is approximately 77%. The second contribution of this thesis consists of the reformulation of the previously mentioned chirp convolution as a circular convolution, represented over the ring of integers modulo $2^b + 1$. In this context, an algorithm for computing partial points of an N-point DFrFT based on a 2D convolution scheme is introduced; in this case, it is possible to reduce computational complexity by at least $4N$ multiplications by employing local circular convolution instead of its global version. This approach includes the use of the Fermat Number Transform (FNT), for which local input and output optimizations are proposed to avoid operations involving zero values and to compute only the points of interest. Numerical simulations, including applications in radar echo modeling, are presented to validate the effectiveness of the proposed algorithm. As a final contribution, the SmFrFT is applied to direction-of-arrival (DoA) estimation of wideband chirp signals in scenarios involving one or multiple targets using a uniform linear array. The multi-target case is reformulated as a multi-line fitting problem. In this context, two innovative approaches are considered: piecewise slope fitting and line detection in the Hough space. Numerical simulations demonstrate that both methods achieve low computational complexity. However, for high-precision scenarios, the ESPRIT algorithm with spatial smoothing, incorporating the discrete SmFrFT, is recommended, where a novel preprocessing step—a peak-alignment procedure in the fractional Fourier domain—is introduced.

Keywords: Fractional Fourier transform. Fermat number transform. Direction-of-arrival estimation. Multi-line fitting. Wideband linear chirp.

RESUMO

A transformada fracionária de Fourier (FrFT, do inglês *fractional Fourier transform*) é uma ferramenta para análise de sinais não estacionários, associada a rotações da representação de sinais por meio de distribuições de energia no plano tempo-frequência. O principal algoritmo numérico para cálculo da FrFT parte da definição integral dessa transformada e, empregando amostragem, produz uma espécie de FrFT discreta (DFrFT). Esta tese é centrada no estudo deste tipo de DFrFT e em sinais chirp, ambos relevantes em diversos sistemas modernos. Existem duas decomposições baseadas em modulações chirp para cálculo da DFrFT: (i) uma utilizando convolução chirp e (ii) outra usando apenas uma transformada discreta de Fourier (DFT, do inglês *discrete Fourier transform*); ambas geralmente implementadas por meio de transformadas rápidas de Fourier (FFT, do inglês *fast Fourier transform*). A primeira contribuição desta tese é a implementação de uma FrFT simplificada (SmFrFT), com escalonamento de frequência variável, em domínios normalizados. Demonstra-se que a SmFrFT, sendo um caso particular das transformações lineares canônicas, exibe propriedades distintas em comparação à FrFT convencional e oferece vantagens no processamento do sinal chirp; com uma redução no número de multiplicações complexas que pode atingir aproximadamente 77%. A segunda contribuição desta tese consiste na reformulação da convolução chirp mencionada anteriormente como uma convolução circular, representada sobre o anel dos inteiros módulo $2^b + 1$. Nesse contexto, é apresentado um algoritmo para calcular pontos parciais de uma DFrFT de N pontos com base em um esquema de convolução 2D; nesse caso, é possível reduzir a complexidade do cálculo em pelo menos $4N$ multiplicações ao utilizar convolução circular local em vez da sua versão global. Essa abordagem inclui o uso a transformada numérica de Fermat (FNT, do inglês *Fermat number transform*), para o qual são propostas otimizações locais de entrada e saída, a fim de evitar operações com valores nulos e calcular apenas os pontos de interesse. Simulações numéricas, incluindo aplicações em modelagem de eco de radar, são apresentadas para verificar a eficácia do algoritmo proposto. Como contribuição final, a SmFrFT é aplicada à estimação da direção de chegada (DoA, do inglês *direction-of-arrival*) de sinais chirp de banda larga em cenários com um ou múltiplos alvos, utilizando um arranjo linear uniforme. O caso com múltiplos alvos é reformulado como um problema de ajuste de múltiplas retas. Nesse contexto, duas abordagens inovadoras são consideradas: ajuste de inclinação por partes e detecção de retas no espaço de Hough. As simulações numéricas demonstram que ambos os métodos apresentam baixa complexidade computacional. No entanto, para cenários de alta precisão, recomenda-se o algoritmo ESPRIT com suavização espacial, que incorpora a SmFrFT discreta, no qual uma nova etapa de pré-processamento—um procedimento de alinhamento de picos no domínio da transformada de Fourier fracionária—é proposta.

Palavras-chaves: Transformada fracionária de Fourier. Transformada numérica de Fermat. Estimativa da direção de chegada. Ajuste de múltiplas retas. Chirp linear de banda larga.

LIST OF FIGURES

LIST OF TABLES

LIST OF ABBREVIATIONS AND ACRONYMS

2D	Two-Dimensional.
AWGN	Additive White Gaussian Noise.
CDFrFT	Centered Discrete Fractional Fourier Transform.
CLSM	Constrained Least Squares Method.
CM–CC–CM	Chirp Multiplication – Chirp Convolution – Chirp Multiplication.
CM–FFT–CM	Chirp Multiplication – Fast Fourier Transform – Chirp Multiplication.
CM–LCC–CM	Chirp Multiplication – Local Circular Convolution – Chirp Multiplication.
CSD	Canonical Signed Digit.
DFrFT	Discrete Fractional Fourier Transform.
DFT	Discrete Fourier Transform.
DoA	Direction-of-Arrival.
DSmFrFT	Discrete Simplified Fractional Fourier Transform.
ESPRIT	Estimation of Signal Parameters via Rational Invariance Techniques.
FBSS	Forward-Backward Spatial Smoothing.
FFT	Fast Fourier Transform.
FMCW	Frequency-Modulated Continuous-Wave.
FNT	Fermat Number Transform.
FPGA	Field-Programmable Gate Array.
FrFT	Fractional Fourier Transform.
FT	Fourier Transform.
GSS	Golden-Section Search.
HDFrFT	Hopping Discrete Fractional Fourier Transform.
HT	Hough Transform.
ICS	Inverted Circular Shift.
IEAC	Inverted-End-Around-Carry.
IoUT	Internet of Underwater Things.
IoV	Internet of Vehicles.

LCC	Local Circular Convolution.
LCT	Linear Canonical Transform.
LDFrFT	Local Discrete Fractional Fourier Transform.
LDSmFrFT	Local Discrete Simplified Fractional Fourier Transform.
LFM	Linear Frequency Modulated.
LHS	Latin Hypercube Sampling.
LiDAR	Light Detection and Ranging.
LiFNT	Local-input Fermat Number Transform.
LoIFNT	Local-output Inverse Fermat Number Transform.
LSB	Least Significant Bit.
LSM	Least Squares Method.
MAE	Mean Absolute Error.
MSB	Most Significant Bit.
MUSIC	Multiple Signal Classification.
OaS	Overlap-and-Save.
radar	Radio Detection and Ranging.
RMSE	Root Mean Square Error.
SDFrFT	Sliding Discrete Fractional Fourier Transform.
sonar	Sound Navigation and Ranging.
ULA	Uniform Linear Array.

LIST OF SYMBOLS

$\mathcal{F}^a$	Fractional Fourier transform of a-th order (p. 30).
$\mathcal{F}$	Fourier transform corresponding to FrFT when the order is 1 (p. 30), in its discrete version it is unitary (see Section 3.4.2).
$\mathcal{F}^{-1}$	Inverse Fourier transform corresponding to FrFT when the order is -1 (p. 30), in discrete version it must be unitary (see Section 3.4.2).
α	Angle of rotation of the time–frequency plane, given by $\alpha = a\pi/2$ (see Section 2.2).
A_α	A value that depends on α, but is independent of u and t (p. 30).
$B_{\alpha,u}$	A value that depends on α and u, but is independent of t (see Section 2.2.2).
$\delta(t - t_0)$	The function is an impulse (Dirac delta) centered at $t = t_0$ (see Section 2.2).
$\mathcal{L}^{\mathbf{A}}$	Linear canonical transform, where $\mathbf{A}=(a, b; c, d)$ is a matrix whose entries are real numbers that satisfy $ad - bc = 1$ (see Section 2.3).
$\tau_{m,k}$	Time delay of the signal incident from the k-th source, received by the m-th element relative to the reference element (p. 28).
θ_k	Angle of arrival of the k-th signal of interest (see Figure 29).
m_0	Index corresponding to the reference element in a uniform linear array (see Figure 29).
λ	wavelength calculated by dividing the wave's velocity by its frequency (p. 28).
c	Wave propagation speed (see Section 2.1).
d	Distance between the elements in a uniform linear array (see Section 2.1).
A_k	Constant amplitude of the k-th component of a linear chirp (p. 28).
ϕ_{0k}	Initial phase of the k-th component of a linear chirp (p. 28).
f_{ck}	Center frequency or initial frequency of the k-th component of a linear chirp (p. 28).
μ_k	Chirp rate of the k-th component of a linear chirp (p. 28).

T	Observation time of incident signals (p. 28).
f_c	Center frequency of a single-component LFM signal (see Section 2.1).
μ	Chirp rate of a single-component LFM signal (see Section 2.1).
$\mathbf{x}(t)$	Received signal vector across the uniform linear array (p. 29).
$\mathbf{A}(t)$	Steering matrix whose k-th column is the time-variant steering vector corresponding to direction of arrival θ_k (p. 29).
$\mathbf{s}(t)$	Vector of source signals (p. 29).
$\mathbf{n}(t)$	Additive noise vector (p. 29).
$\mathbb{C}^{M\times K}$	The space of complex-valued matrices of dimension $M \times K$ (p. 29).
r_θ	Index shift of a peak in the fractional Fourier domain when the signal is a delayed chirp, it depends on the direction of arrival, θ (p. 37).
$\mathcal{F}'^a$	Sampling-type DFrFT with axis scaling, constrained by $\Delta_u\Delta_t = \frac{1}{N}\sin\left(a\frac{\pi}{2}\right)$, where Δ_u and Δ_t are the sampling periods along the u- and t-axes (p. 39).
f_s	Sampling frequency, expressed in hertz (Hz), representing the number of samples acquired per second (p. 35).
$\lvert\cdot\rvert$	Euclidean norm (distance from the origin) of the complex number in the complex plane (p. 32).
$\lfloor\cdot\rfloor$	Floor function of its argument (p. 35).
$\lceil\cdot\rceil$	Ceil function of its argument (p. 74).
$x[r]$	Discrete-time signal (p. 35).
$\{x_n\}_{n=0}^{N-1}$	An N-length sequence that can be periodically extended outward with period N (see Section 3.2).
$\mathbf{F}$	The DFT matrix having $\frac{1}{\sqrt{N}}\omega_N^{kn}$, for $n, k = 0, 1, .., N-1$, as the entry in its k-th row and n-th column (p. 42).
$\circledast$	Circular convolution (p. 36).
$*$	Linear convolution (p. 103).
$\mathbb{Z}_{2^b+1}$	The ring of integers modulo $2^b + 1$ (p. 47).
$\mathrm{GF}(p)$	A Galois field, which is a finite field that contains exactly p elements, where p is a prime number (p. 47).

$\langle\cdot\rangle_p$	Modulus operation, which returns the remainder after dividing an integer number by p (p. 47).
$\equiv$	Modular congruence relation, written as $a \equiv b \pmod{p}$, which means a and b leave the same remainder when divided by p (see Section 4.1).
$\oplus$	Bitwise XOR operator (see Section 4.2.1).
$x \ll n$	A left bitwise shift of x by n positions (see Section 4.2.1).
$\mathbf{\Omega}$	A twiddle-factor matrix in the Cooley–Tukey algorithm (see Section 4.1.1).
k_u	The slope of the fitting curve given by $q_m = q_0 + k_u\,(m - m_0)$ (p. 66).
$(\cdot)^{\mathsf{T}}$	The transpose of a matrix or vector that flips it over its main diagonal, converting rows into columns and columns into rows (see Section 6.1.2).
$\mathbf{J}_p^{\mathrm{f}}$	A selection matrix that extracts the p-th forward subarray (see Section 70).
$\mathbf{J}_L$	The exchange L-by-L matrix with ones on its antidiagonal (see Section 70).
$(\cdot)^{\mathsf{H}}$	The Hermitian (conjugate transpose) of a matrix (see Section 70).
$(\cdot)^{\triangle}$	The pseudo-inverse of a matrix (see Section 70).
$(\cdot)^{\dagger}$	Shifting based on the time-shift property to align peaks relative to the peak position of the reference sensor in the fractional Fourier domain, when the DFrFT or DSmFrFT is applied to the received signals in a ULA (see Section 7.3.2.1).
$\mathbf{U}_s$	The signal subspace (see Section 6.2.1.3).
$\mathbf{U}_n$	The signal subspace (see Section 6.2.1.3).
$\mathbf{\Psi}$	The rotational invariance matrix such that $\mathbf{U}_2 = \mathbf{\Psi}\mathbf{U}_1$, where $\mathbf{U}_1$ and $\mathbf{U}_2$ are obtained by removing the last and first rows, respectively, from the signal subspace matrix (p. 70).
(ρ, θ)	A single point in the Hough space; the corresponding line in polar coordinates is given by $x\cos\theta + y\sin\theta = \rho$ (see Section 6.2.2.2).
$\widehat{\theta}$	Estimated direction of arrival corresponding to a single target with true angle of incidence θ (p. 83).

CONTENTS

1 INTRODUCTION

In Engineering, the Fourier transform (FT) constitutes one of the fundamental mathematical tools for signal processing and analysis. Basically, the so-called ordinary FT allows a signal, originally represented as a variation of amplitude over time, to be expressed in terms of its frequency components. However, such a possibility becomes unsuitable for processing non-stationary signals, for which local time-frequency characteristics are essential. To address this limitation, alternative mathematical tools–such as the fractional Fourier transform (FrFT)–have been developed. The FrFT provides a more flexible representation by enabling a continuous transition between the time and frequency domains, making it particularly effective for processing signals whose frequency content evolves over time. In brief, the operator related to a fractional Fourier transform corresponds to a non-integer power of the operator related to the ordinary Fourier transform. To be more specific, in research carried out in the areas of Mathematics and Physics at the beginning of the twentieth century, Wiener (1929) led the Fourier developments to fractional order and Condon (1937) related such a possibility to rotations about a fixed point of the signal representation in the time-frequency plane. After that, FrFT only returned to the scene in the 1980s, when the concept of the fractional-order Fourier transform was formally introduced by Namias (1980). In recent years, it has found applications in optical engineering (HRICHA; YAALOU; BELAFHAL, 2020; DAI et al., 2021), sound classification (ABDUH et al., 2020; TAN et al., 2022), biomedical signal processing (PANAHI; RASHIDI; SHEIKHANI, 2021), image encryption (FARAH et al., 2020; ZHANG et al., 2021), communications (ZHANG et al., 2021; JIA et al., 2022), radar (FANG et al., 2019; PETROV; YAROVOY, 2022), among others (GORBUNOV; DOLOVOVA, 2022; NIEWELT et al., 2023).

In practical scenarios, analytical methods are not used to calculate the FrFT; instead, numerical algorithms are used (SU; TAO; KANG, 2019). A class of algorithms relies on representing the operator as a numerical integration over discrete variables, leading to a sampling-type discrete FrFT (DFrFT). This, in turn, can be decomposed into computational steps involving ordinary discrete FT (DFT) and its standard fast algorithms (FFT, fast Fourier transforms). These algorithms are based on decomposition and decimation (DUHAMEL; VETTERLI, 1990). Although often credited to Cooley and Tukey, the origins of decimation techniques for DFT date back to Carl Friedrich Gauss, who in 1805 devised an efficient method for evaluating trigonometric sums–later recognized as a precursor to modern FFT algorithms (HEIDEMAN; JOHNSON; BURRUS, 1984). The breakthrough occurred in 1965, when Cooley and Tukey formalized such an algorithm (COOLEY; TUKEY, 1965), reducing the computational complexity of the DFT from $\mathcal{O}(N^2)$ to $\mathcal{O}(N \log N)$. It has become considered one of the most important numerical algorithms of our time (STRANG, 1994).

The algorithm most widely used for the aforementioned type of DFrFT is the one proposed in (OZAKTAS et al., 1996); the corresponding quadrature formula is decomposed into

an inner chirp multiplication, a chirp convolution, and an outer chirp multiplication (CM–CC–CM). The algorithmic complexity of this method is $\mathcal{O}(N \log_2 N)$. This form of decomposition plays an important role in the implementation of linear canonical transforms (KOC et al., 2008), simplified fractional transforms (WANG, 2011; TALLA; BATTULA, 2024), generalized convolution theorem (SHI et al., 2014), definition of generalized fractional transforms (WEI; SHEN, 2023; LI et al., 2025), fractional correlation (PETROV; YAROVOY, 2022), and other applications (LUO et al., 2023).

In terms of the exact number of multiplications and additions required to compute the sampling-type DFrFT, a more efficient method involves its decomposition into a chirp multiplication, an ordinary DFT, and another chirp multiplication (PEI; DING, 2000a), with variable frequency scaling (ZAYED, 1996; CARIOLARO et al., 1998) or variable time scaling (MARINHO; BERNARDO, 1998). Since DFT is implemented using a fast algorithm, this type of decomposition is referred to as CM–FFT–CM. In recent years, this approach has been applied to analyze the intrinsic energy distribution of a dynamic time-frequency laser, by decomposing the laser energy with the chirp-frequency waveform as the basic component (LAN et al., 2023b).

An alternative approach is to use simplified forms with the same capabilities as the original FrFT (PEI; DING, 2000b), which emerged and found many applications over the years (ZHANG et al., 2011; ZHANG et al., 2015; ZHAO; LI, 2023). A simplified FrFT is defined as a reformulated version of the conventional FrFT in which the transform kernel is modified to achieve reduced computational complexity while preserving its fundamental time–frequency rotation property. The most relevant simplified FrFT in this context is referred to by the acronym SmFrFT (SANJAY, 2018). It is obtained as a special case of a three-free-parameter linear canonical transform (LCT) and offers two key advantages: the removal of the FrFT outer chirp term and the fact that the sampling parameters do not need to be adjusted in the kernel to become a DFT (PEI; DING, 2002).

Furthermore, computing partial points of a transform refers to evaluating only a subset of its output coefficients. This operation is conceptually equivalent to output pruning, where unnecessary computations in a fast-transform algorithm are omitted to produce only the required outputs with reduced complexity. To be more specific, there are applications that require spectrum analysis over only a subset of the N center frequencies of an N-point DFT. A pioneering solution to this need is the Goertzel algorithm (1958), which provides a recursive and efficient computing method for the selected DFT bins, particularly useful for tone detection (GOERTZEL, 1958). To support real-time and streaming applications, variants such as sliding DFT and hopping DFT were developed, enabling low-overhead spectral tracking over moving windows (JACOBSEN; LYONS, 2003; PARK; KO, 2014). Building on these concepts, real-time applications that require recalculating the DFrFT at each or multiple time steps have led to the development of sliding window algorithms, such as sliding DFrFT (SDFrFT), as well as hopping DFrFT (HDFrFT) (LIU et al., 2021; HUANG; ZHANG; TAO, 2022). Finally, when only partial points of the sampling-

type DFrFT are needed, a local version of this transform has been proposed in (MIAO, 2023). The latter method was applied to the processing of real-world bat echolocation chirp signals.

Other mapping strategies consist of representing the signal in an algebraic structure in changing domains. For example, the Fourier transform can be efficiently computed by converting it into a convolution, while in some cases, using the Fourier transform to perform a convolution is more advantageous(BLAHUT, 2010, p. 91). Discrete-time signals represented as integers can be convolved without round-off errors by using a ring of integers or a finite field (BLAHUT, 2010, p. 311). In this scenario, when the modulus of the arithmetic operations is a Fermat number ($F_t = 2^b + 1$ with $b = 2^t$ for $t = 0, 1, \ldots, 6$), the Fermat number transform (FNT) is obtained by defining it in a manner similar to the DFT, providing a low-complexity solution for circular convolution. To be more precise, for an N-point FNT, selecting the kernel as 2 or $\sqrt{2} = 2^{\frac{b}{4}}(2^{\frac{b}{2}} - 1)$ ensures that N can be a power of two, up to $4b$ (AGARWAL; BURRUS, 1974a). These kernels allow us to use the radix-two algorithm (COOLEY; TUKEY, 1965), and multiplications are converted into combinations of additions and bit-shifting operations (XU; YOU; ZHANG, 2017; SONG et al., 2017; BAOZHOU et al., 2019). In quadratic residue number representations, a complex multiplication can be performed as two multiplications and four additions, instead of the traditional three multiplications and three additions (NUSSBAUMER, 1976; KRISHNAN; JULLIEN; MILLER, 1986; XING et al., 2024); this leads to a reduction of the number of multiplications required for an application.

Finally, considering that a DFT can be expressed as a matrix-vector product, discrete FrFT formulations based on the eigendecomposition of the DFT matrix have been proposed in the literature (PEI; DING, 2000a; CANDAN; KUTAY; OZAKTAS, 2000). Regarding this approach, commonly referred to as the eigendecomposition-based DFrFT, Majorkowska-Mech and Cariow (2017) point out that:

> This type of DFrFT possesses all essential properties which are posed as requirements for DFrFT such as unitarity, additivity, reduction to discrete Fourier transform (when the power is equal to one), and approximation of continuous FrFT (MAJORKOWSKA-MECH; CARIOW, 2017, p. 4119).

On the other hand, the overall time complexity of this method is $\mathcal{O}(N^2)$, which becomes huge for long signals (IRFAN; ZHENG; SHAHZAD, 2013). Various methods have been proposed to reduce this complexity. The low-complexity structures for small-size DFrFT presented in (CARIOW; PAPLIŃSKI; MAJORKOWSKA-MECH, 2019) are not scalable for long signals. To our knowledge, no more efficient method has been reported than the one proposed in (DE OLIVEIRA NETO et al., 2019), which is supported by the hardware architectures presented in (BISPO; NETO; LIMA, 2024). It exploits symmetries and null components present in the eigenvectors of the aforementioned eigendecomposition to reduce the number of additions and multiplications needed to calculate the transform. In any case, this type of method has quadratic arithmetic complexity, and its structure is non-scalable in the sense that it does not make use of the so-called

decimation techniques. Another alternative is the so-called centered DFrFT (CDFrFT), which is based on the Grünbaum eigenvectors of the centered DFT (VARGAS-RUBIO; SANTHANAM, 2005). The CDFrFT offers improved symmetry and superior energy compaction properties, which are particularly advantageous for analyzing chirp signals, making it a well-suited operator for sparse or multi-component chirp estimation (PEACOCK; SANTHANAM, 2011).

Generally speaking, this work explores the aforementioned chirp-based decompositions for computing fractional Fourier transforms. Specifically, we investigate the possibility of incorporating techniques based on tools defined over finite algebraic structures as well as methods for computing partial points of discrete transforms. The development of these algorithms is motivated by applications in radio detection and ranging (radar). Further details on these approaches are presented in the following sections.

1.1 MOTIVATION

In radar signal processing, a linear frequency modulated (LFM) signal, also known as a chirp signal, is a type of signal in which the frequency changes linearly over time; if the signal were audible, it would sound somewhat like the chirp of a bird (KLAUDER et al., 1960; BLOCH, 1973). Chirp signals can arise in moving source problems that involve Doppler effects, particularly when a sinusoidal source undergoes constant acceleration (YETIK; NEHORAI, 2003). An LFM signal is a type of quadratic-phase function signal characterized by constant phase offset, center frequency (or initial frequency), and chirp rate (LIU; XIAO; WANG, 2021; DING; WEI; YU, 2024). A chirp, as a non-stationary signal, offers a low probability of interception and is commonly used in applications such as sound navigation and ranging (sonar) and light detection and ranging (LiDAR) (MAHADI et al., 2021; LIU; XIAO; WANG, 2022). As the line representing the Wigner-Ville distribution of a linear chirp can be established as perpendicular to the frequency variable axis by an FrFT with optimal fractional order a_0, this value depends solely on the chirp rate (AHMAD; LIU; XU, 2010; ALDIMASHKI; SERBES, 2020); such a procedure only requires a one-dimensional search.

Estimating the direction of arrival (DoA) of wideband chirp signals is a well-established research area, particularly effective for chirp-like signals, which is an essential topic in modern radar (ZHANG et al., 2018; KIM et al., 2022), sonar (LEE et al., 2017), and underwater acoustic systems (YIN et al., 2020). Developing DoA estimation algorithms is also a key challenge for mobile agent localization in the Internet of Vehicles (IoV) and Internet of Underwater Things (IoUT) (CUI et al., 2020). In this context, traditional narrowband DoA estimation algorithms, such as subspace decomposition-based methods (SCHMIDT, 1986; ROY; KAILATH, 1989; OTTERSTEN; KAILATH, 1990), are no longer accurate for the referred signals due to their non-stationarity (MULINDE; ATTYGALLE; AZIZ, 2021). As an alternative, mathematical tools such as FrFT have been incorporated into these algorithms to enhance their performance (TAO; ZHOU, 2005; CHONG; XIAOMIN, 2011; YU et al., 2015), providing the benefit that wideband

chirp signals can be processed as narrowband signals in the fractional Fourier domain (ZHONG et al., 2023; ZHAO et al., 2025). The alternative provides better resolution and lower sidelobes compared to FT-based techniques (YIN et al., 2020). Due to these properties, FrFT has been integrated into algorithms related to multiple signal classification (MUSIC) (SCHMIDT, 1986; TAO; ZHOU, 2005) and estimation of signal parameters via rotational invariance techniques (ESPRIT) (ROY; KAILATH, 1989; CHONG; XIAOMIN, 2011). Another approach consists in the slope fitting method in the fractional Fourier domain, offering robust performance with lower computational demands compared to traditional subspace-based techniques (ZHONG et al., 2023). However, this method is limited to single-target scenarios. For multi-target cases (AHMED et al., 2021), FrFT-based ESPRIT, including the principle of spatial smoothing, has been shown to offer an efficient alternative compared to FrFT-based MUSIC for coherent and non-coherent LFM signals (CHONG; XIAOMIN, 2011).

The primary motivation for this work stems from the chirp signals scenario outlined above. However, it is important to note that numerical algorithms involving chirp-based decompositions are not exclusive to the fractional Fourier transform. In fact, the generalization of classical transforms to their fractional-order counterparts has been an active area of research, leading to numerous extensions. Notable examples include the Radon fractional Fourier transform (CHEN et al., 2014), the hyperbolic fractional Fourier transform (MOUSAVI; SHAHZADI, 2015), and more recent developments such as synchrosqueezed fractional variants (SHI et al., 2023). These extensions highlight the growing interest and versatility of fractional domain techniques in time-frequency analysis and signal processing.

1.2 PROBLEM STATEMENT

The problem of digital computation of the FrFT has traditionally been addressed in two main ways. An approach involves evaluating FrFT using numerical methods, which are as accurate as theoretically possible based on time–frequency uncertainty (OKTEM; OZAKTAS, 2009). Another approach defines a DFrFT based on the eigendecomposition of the DFT matrix (CANDAN; KUTAY; OZAKTAS, 2000). This type of DFrFT involves a commuting matrix and is theoretically elegant, unitary, and index additive, but it is computationally intensive. In the context of chirp signal analysis, the former is typically used for peak searching in the fractional Fourier domain (ALDIMASHKI; SERBES, 2020). At the same time, the latter is employed to construct compact fractional domains (SERBES, 2017) to estimate signal parameters, particularly the chirp rate. Although both methods aim to extract similar information, they are based on different principles and may yield results that are not identical. This thesis focuses on the first approach, considering that a FrFT corresponds to a non-integer power of the operator related to the FT. More precisely, the FrFT operator corresponds to the a-th power, $a \in \mathbb{R}$, of the ordinary FT operator, consisting, therefore, of a generalization of the latter (which is obtained if $a = 1$). The parameter a is usually identified as *fractional order*. The choice of this value depends

on the context in which the transform is to be applied (SEJDIĆ; DJUROVIĆ; STANKOVIĆ, 2011; ZHANG et al., 2017; GÓMEZ-ECHAVARRÍA; UGARTE; TOBÓN, 2020). Some specific questions related to this problem can be formulated:

- Is there a way to reduce the arithmetic complexity to levels below what is required in the CM–FFT–CM decomposition?
- Since both the FT and the FrFT can be expressed in terms of the convolution operation, how can one take advantage of the use of fast convolution to compute the FrFT?
- In the process of determining an optimal fractional order, is there any way to reduce the complexity of the method based on finding peaks in the fractional Fourier domain?
- How can simplified FrFT be used to improve subspace-based DoA estimation for wideband chirps, since it has not yet been applied in this context?
- How can the slope-fitting method be performed in the (simplified) fractional Fourier domain and extended for multi-target DoA estimation of wideband linear chirps?

1.3 OBJECTIVES

General Objective:

To propose low-complexity algorithms for computing the fractional Fourier transform by incorporating techniques such as transform decomposition, decimation, subset-based point evaluation, and signal representation over modular algebraic structures, with a focus on the analysis of chirp signals.

Specific Objectives:

In order to achieve the general objective, the specific goals listed in the following items are considered:

1. To systematize the state-of-the-art computing methods for fractional Fourier transforms;
2. To develop a discrete simplified FrFT for chirp signal processing, including its local version;
3. To develop a local circular convolution, over the ring of integers modulo $2^b + 1$, for accelerating the CM–CC–CM decomposition;
4. To verify the effectiveness of simplified FrFT in DoA estimation of wideband linear chirps.

1.4 METHODOLOGY

Essentially, the research strategy adopted is problem-based. That is, both the starting point and the ultimate goal revolve around addressing a specific problem in order to achieve the previously defined objectives. Therefore, to achieve the objectives outlined in Section 1.3, the work plan is structured into the following steps, as summarized below.

- STAGE 1 - *Literature review:* In the initial phase of the project, a comprehensive review of FrFT literature is carried out, including definitions, applications, and discrete implementation methods.
- STAGE 2 - *Theoretical comparison of algorithms:* In this phase of the project, the goal is to identify algorithms with reduced arithmetic complexity for the digital computation of the FrFT.
- STAGE 3 - *Proposing new methods:* In this stage of development, based on state-of-the-art techniques, new computational methods are considered to reduce the arithmetic complexity of FrFT calculations.
- STAGE 4 - *Effectiveness verification:* The execution of this stage leads to determining whether the error generated in the complexity reduction is tolerable; the analysis is carried out involving systems with known performance.
- STAGE 5 - *Risk analysis:* This final stage is the ablation study, that is, possible realistic situations are considered, including some missing or degraded components in the previous stages, for example, spectral analysis of the signals received through noisy channels.

The research stages presented above, depending on the analysis method, can be grouped into two; the analytical method and the numerical method (see Figure 1). In other words, the first two stages involve a literature review and theoretical aspects, while the remaining stages require numerical calculations and computational experiments. Both methods play a role in generating the final report.

In terms of research resources, conceptual maps, diagrams, and comparative tables can be used for the analytical method. In contrast, the numerical method involves signal modeling, algorithm development, simulation, and statistical analysis. Therefore, the means of investigation are as follows:

- Hardware: Desktop Computer.
- Software: Linux Operating System, Jupyter Notebook.
- Programming language: Python.

Figure 1 – Research methods diagram.

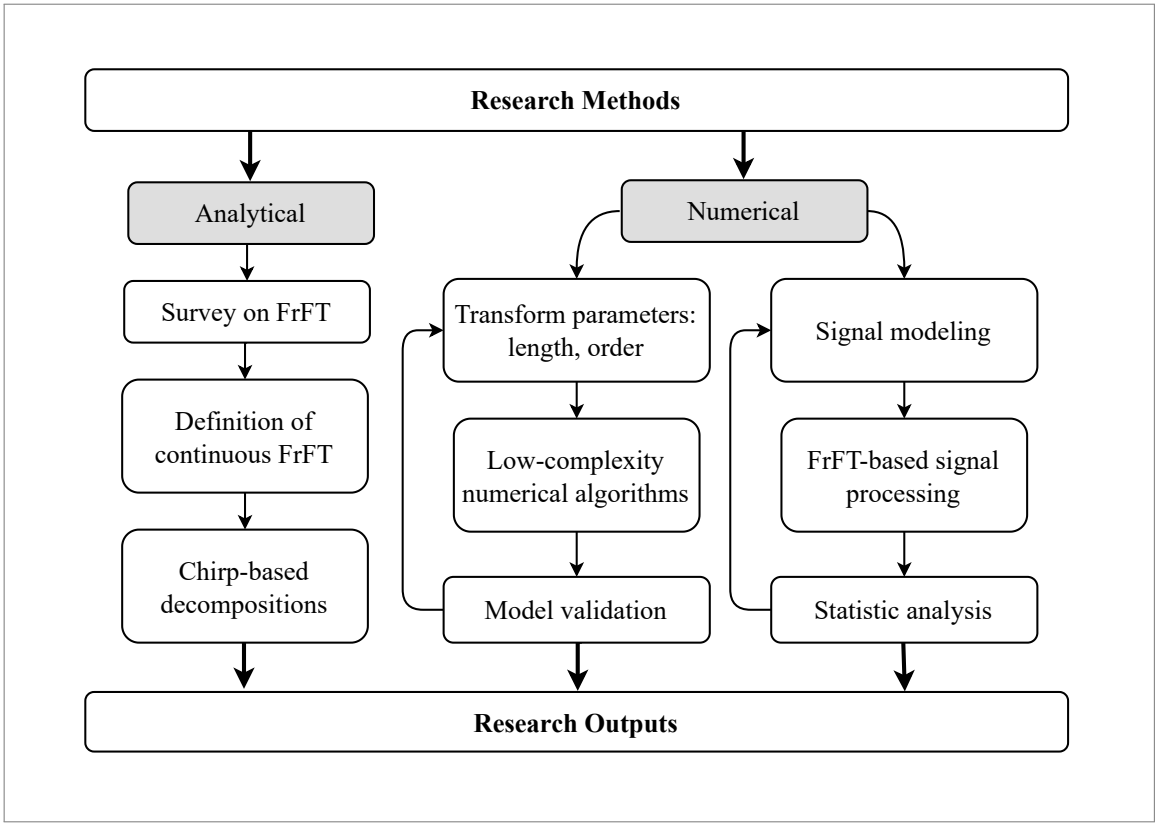

Source: The author (2025).

1.5 CONTRIBUTIONS

In this research, we investigate numerical algorithms based on chirp-based decompositions for the FrFT, exploring two main strategies to reduce algorithmic complexity: (i) the computation of partial transform points and (ii) the incorporation of techniques grounded in finite algebraic structures. For application purposes, we reformulate the multi-target direction-of-arrival (DoA) estimation of wideband linear chirp signals as a multi-line fitting problem in the fractional Fourier domain. In this context, we further propose the use of a frequency-scaled simplified FrFT (SmFrFT) as a replacement for the conventional FrFT within subspace-based techniques. To the best of our knowledge, these approaches have not yet been addressed in the literature. The main contributions of this thesis are summarized as follows:

1. **Frequency-scaled SmFrFT**: We propose that the simplified FrFT with variable frequency scaling be implemented in normalized domains, as this approach is non-trivial due to the operator exhibiting properties that differ from those of the sampling-type DFrFT. For example, to address the issue of high oscillations in the magnitude spectrum of chirp signals, we demonstrate that the cascaded implementation of the corresponding LCT can be decomposed into a circular convolution, which can be efficiently implemented using FFT algorithms.

2. **One-dimensional search**: In preprocessing of chirp signals, we demonstrate that the frequency-scaled SmFrFT, in its discrete form denoted by DSmFrFT, serves as a well-suited operator for estimating the parameters of high-chirp-rate LFM signals. Specifically, selecting the optimal fractional order of DSmFrFT can be achieved through a one-dimensional search for a given center frequency, requiring only the calculation of DSmFrFT at the index corresponding to this frequency. When one or more center frequencies are unknown but lie within a known frequency range, the corresponding peak index interval can be estimated in advance, eliminating the need to compute the full set of DSmFrFT points.

3. **Local DSmFrFT**: We introduce an algorithm for computing partial points of the DSmFrFT, which further reduces the arithmetic complexity without compromising the performance of the DoA estimation. This approach assumes that an N-point DSmFrFT can be decomposed into Q-point DFTs, where N is divisible by Q, resulting in a reduction of N multiplications compared to the similar algorithm proposed in (MIAO, 2023).

4. **Local circular convolution**: Considering that an N-point DFrFT can be decomposed into a two-dimensional (2D) convolution (AGARWAL; BURRUS, 1974b), we introduce a local DFrFT based on local circular convolution; an algorithm to compute L consecutive points of a global circular convolution when N is divisible by L, saving at least $4N$ multiplications. In this context, local adaptations of the FNT are introduced in two forms: a local-input FNT (LiFNT) for calculating the $(2N)$-point FNT of a sequence whose last half consists of null elements; and a local-output inverse FNT (LoIFNT) to obtain the last N points of a $(2N)$-point inverse FNT. These optimizations avoid unnecessary operations.

5. **Improved subspace-based techniques**: We propose the integration of DSmFrFT instead of DFrFT for DoA estimation of chirp signals based on subspace decomposition algorithms, such as MUSIC and ESPRIT with spatial smoothing. In this context, we show that shifting the peak index in the fractional Fourier domain to align with the peak position of the signal received at the reference sensor can improve the precision of subspace-based algorithms.

6. **Multi-line fitting**: As a low-complexity alternative, we propose the use of multi-line fitting for DoA estimation of wideband chirps using a ULA. When the peaks in the fractional Fourier domain can be segmented, piecewise linear regression, the slope-fitting method, can be applied. Otherwise, line detection based on the Hough transform may be employed, which is widely used in image processing (DUDA; HART, 1972).

This work resulted in the preparation of two scientific articles. The first has been published in a peer-reviewed journal, while the second is currently under review:

- E. G. HUAMPO, J. B. LIMA and J. R. d. O. NETO, Direction-of-Arrival Estimation for Wideband Chirps via Multi-Line Fitting in the Fractional Fourier Domain, in **IEEE Access**, vol. 13, pp. 107328-107342, 2025, doi: <https://doi.org/10.1109/ACCESS.2025.3581843>.

- E. G. HUAMPO, J. R. d. O. NETO and J. B. LIMA. Digital Computation of the Fractional Fourier Transform Based on Modulo-$2^b + 1$ Convolutions. Submitted to **Circuits, Systems, and Signal Processing**, 2025. (under review)

These works reflect the main contributions of this thesis, covering the development of efficient algorithms for the sampling-type DFrFT. In the first paper, the effectiveness of the proposed algorithms is demonstrated in both single- and multi-target scenarios, showing a reduction of approximately 77% in the number of arithmetic operations when using the DSmFrFT instead of the conventional DFrFT. The second paper introduces a low-complexity method for computing partial points of the DFrFT by representing chirp convolutions over the ring of integers modulo $2^b + 1$. This method has practical applications in fields such as radar echo modeling. We classify this approach as a local transform version, as it operates from a specified starting point and proceeds over a selected range of output values.

1.6 THESIS OUTLINE

This thesis is structured around the development of numerical algorithms for sampling-type DFrFT based on chirp-based decompositions. Initially, these decompositions are examined in the real field, including a simplified form with axis scaling–a particularly notable variant. The chirp-convolution-based approach is then developed over the ring of integers modulo $2^b + 1$, with emphasis on computing partial transform points. The remainder of this thesis is organized as follows.

- In Chapter 2, preliminaries on FrFT are presented, with a focus on uniform linear arrays and incoming chirp signals. The decomposition of the FrFT in its integral form is given in two ways: one as a convolution operation and the other as a conventional Fourier transform within a variable-frequency scaling scheme. Additionally, we explain how simplified forms of the FrFT can be derived from a linear canonical transform.

- In Chapter 3, the sampling-type DFrFT and its key properties are presented in the normalized and scaled domains, including its application to discrete-time chirp signal processing. Additionally, the frequency-scaled simplified FrFT–derived as a special case of the linear canonical transform–is introduced in its discrete form within normalized domains. This includes discussions on its time-shift property, convertibility property, and localized version.

- In Chapter 4, the theoretical aspects of FNT, diminished-1 arithmetic, complex multiplication, and circular convolution in the ring of integers modulo $2^b + 1$, where $b = 32$ or 64, are presented. The main focus is on the implementation of a chirp convolution, which leads to the introduction of the CM–CC–CM decomposition in the ring $\mathbb{Z}_{2^b+1}$, including the overlap-and-save method for processing long signals.

- In Chapter 5, the key contributions related to the CM–CC–CM method are presented. In this context, the local one- and two-dimensional FNTs are formally defined, incorporating local input and output adaptations. Subsequently, a computational approach for evaluating partial points of the DFrFT based on local circular convolution is proposed.

- In Chapter 6, the estimation of the DoA for wideband linear chirps is introduced as a multi-line fitting problem in the fractional Fourier domain. The previously proposed slope fitting method for single-target scenarios is extended to the multi-target case using piecewise linear regression and line detection in the Hough space. In both scenarios, subspace-based techniques with spatial smoothing are enhanced through the use of simplified FrFT and peak alignment in the preprocessing step.

- In Chapter 7, the results of the computer experiments are presented. Specifically, error analysis and arithmetic complexity are examined, focusing on chirp-based decompositions for the DFrFT over the real field (in floating-point representation) and over the ring of integers modulo $2^b + 1$ (in diminished-1 representation). The effectiveness of the proposed algorithms is validated through DoA estimation for single- and multi-target scenarios involving wideband linear chirps. The simulations also include stationary and non-stationary moving sources.

- In Chapter 8, the main contributions of this work are briefly revisited and potential directions for future research are outlined.

- In Appendix A, the possibilities of multiplying two complex numbers using only three real-valued multiplications and five real-valued additions are discussed. One of these techniques can be applied to chirp multiplications, which are part of the DFrFT decompositions.

- In Appendix B, it is considered that an N-point DFrFT can be reformulated as the computation of partial output points from an infinite linear convolution; this, in turn, can be performed as a circular convolution using an overlap-and-save procedure. Then it is shown that a total of $6N$ real-valued additions can be saved by avoiding unnecessary operations.

2 PRELIMINARIES

In this chapter, we provide an overview of signal modeling and the definition of the continuous FrFT. In this scope, we include chirp signal processing for a uniform linear array receiver, where the FrFT of a delayed signal is essential. Furthermore, we explain how a simplified version of the FrFT can be derived from the linear canonical transforms.

2.1 SIGNAL MODELING

A uniform linear array (ULA) is a set of antenna elements arranged in a straight line with equal spacing between adjacent elements (TREES, 2002, p. 37). This model is commonly used in array signal processing for direction finding due to its simple geometry, well-established mathematical models, and scalability, as the angular resolution can be easily controlled by adding or removing elements. Taking into account a ULA composed of M sensors receiving signals from K far-field sources, the signal received by the m-th element in ULA is a mixed signal, $x_m(t)$, represented as

$$x_m(t) = \sum_{k=0}^{K-1} s_k\left(t - \tau_{m,k}\right) + n_m(t), \quad m = 0, 1, \ldots, M-1, \tag{2.1}$$

where $n_m(t)$ is the additive white Gaussian noise (AWGN). A typical scenario for DoA estimation considers assumptions such as isotropic and linear transmission medium, far field, and AWGN channel (CHEN; GOKEDA; YU, 2010, p. 32). The time delay of the m-th element relative to the reference element (indexed by m_0) is given by

$$\tau_{m,k} = \frac{1}{c}(m - m_0) d \sin\theta_k, \tag{2.2}$$

where c is the wave propagation speed, $d \leqslant \lambda/2$ is the distance between the elements, λ is the wavelength, θ_k is the angle of arrival of the k-th signal of interest (KIM et al., 2022) (see Figure 2). A center-symmetric ULA is formed when $m_0 = \left\lfloor \frac{M}{2} \right\rfloor$ (where $\lfloor \cdot \rfloor$ denotes the floor function). It is preferred for direction finding due to its improved accuracy and reduced sidelobe effects (TREES, 2002, p. 37). In addressing problems involving wideband chirps (KLAUDER et al., 1960; BLOCH, 1973; YETIK; NEHORAI, 2003), the linear frequency-modulated (LFM) signal, $s_k(t)$, is represented by a quadratic phase function, which is

$$s_k(t) = A_k e^{j\phi_{0k}} e^{j\left(2\pi f_{ck} t + \pi \mu_k t^2\right)}, \quad -T/2 \leq t \leq T/2, \tag{2.3}$$

where A_k, ϕ_{0k}, f_{ck}, and μ_k represent constant amplitude, initial phase, center frequency (or initial frequency), and chirp rate of the k-th source, respectively (ALDIMASHKI; SERBES, 2020; LIU; XIAO; WANG, 2021; DING; WEI; YU, 2024). Usually, the time axis t is confined to the symmetric interval $[-T/2, T/2]$, where T represents the duration of the signal. This form of complex (or analytic) signals is supported by most receivers, which decompose received

Figure 2 – Data model for DoA estimation of a k-th target.

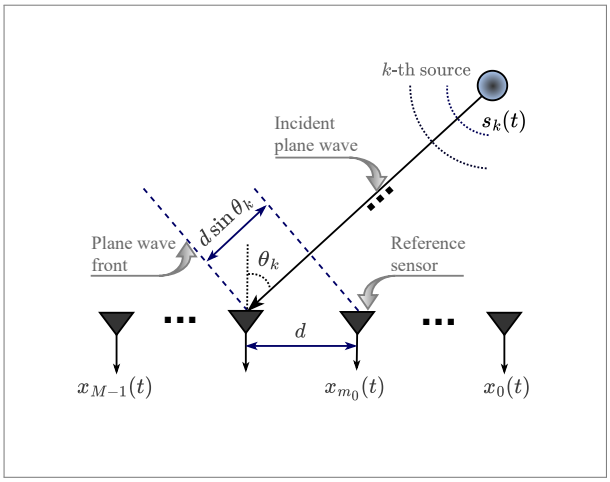

Source: Adapted from Kim et al. (2022).

signals into both in-phase (the real part) and quadrature components (the imaginary part) (CHEN; GOKEDA; YU, 2010, p. 33). The single-component LFM signal is defined as a particular case of $s_k(t)$ when $k = 0$, and is denoted by omitting the subscript, i.e., $s(t)$. The basic form corresponding to the parameter settings $A = 1$ and $\phi_0 = 0$ is used as a reference in subsequent simplified analyses and simulations.

The incident signal, given in (2.1), can be represented by the time-variant steering vector (ZHONG et al., 2023), so that the received signal vector at time t is modeled as

$$\mathbf{x}(t) = \mathbf{A}(t)\,\mathbf{s}(t) + \mathbf{n}(t), \tag{2.4}$$

where:

- $\mathbf{x}(t) \in \mathbb{C}^{M\times 1}$ is the received signal vector across the uniform linear array,
- $\mathbf{A}(t) = [\mathbf{a}(t,\theta_0), \mathbf{a}(t,\theta_1), \ldots, \mathbf{a}(t,\theta_{K-1})] \in \mathbb{C}^{M\times K}$ is the steering matrix, whose k-th column is the time-variant steering vector corresponding to the direction of arrival θ_k,
- $\mathbf{s}(t) = [s_0(t), s_1(t), \ldots, s_{K-1}(t)]^{\mathrm{T}} \in \mathbb{C}^{K\times 1}$ is the vector of source signals,
- $\mathbf{n}(t) \in \mathbb{C}^{M\times 1}$ is the additive noise vector, modeled as spatially white with zero mean.

Each steering vector $\mathbf{a}(t,\theta_k)$ models the relative phase shifts across the sensors due to a plane wave arriving from direction θ_k. For a wideband source, the m-th element of $\mathbf{a}(t,\theta_k)$ is given by

$$a_m(t,\theta_k) = e^{-j2\pi f_k(t)\tau_{m,k}} e^{j\pi\mu_k\tau_{m,k}^2}, \tag{2.5}$$

where $f_k(t) = f_{ck} + \mu_k t$ represents the time-varying frequency.

2.2 FRACTIONAL FOURIER TRANSFORM

The (continuous) fractional Fourier transform, with fractional order $a \in \mathbb{R}$, of a signal $x(t)$ is usually denoted as $X_a(u) = \{\mathcal{F}^a x\}(u)$ and defined as

$$X_a(u) = \int_{-\infty}^{\infty} K_a(u,t)x(t)dt, \tag{2.6}$$

in which $K_a(u,t)$ denotes the FrFT kernel, provided in its general form by

$$K_a(u,t) = \begin{cases} A_\alpha e^{j\pi\left[\left(t^2+u^2\right)\cot\alpha - 2tu\csc\alpha\right]}, & \alpha \neq n\pi, \\ \delta(t-u), & \alpha = 2n\pi, \\ \delta(t+u), & \alpha = (2n+1)\pi, \end{cases} \tag{2.7}$$

where $\alpha = a\pi/2$, $A_\alpha = \sqrt{1 - j\cot\alpha}$, and $j = \sqrt{-1}$. Note that $\alpha = 2n\pi$, with n an integer, reflects the order-4 periodicity of FrFT; increasing a by four yields the same transform, i.e., $\mathcal{F}^a = \mathcal{F}^{a+4}$ for $0 < |a| < 2$. Moreover, calculating the fractional Fourier transform of a signal can be interpreted as a rotation of the same signal in the time-frequency plane, the rotation angle being α. To be more specific, $\alpha = 0$ corresponds to the identity operation, $\alpha = \pi/2$ to obtain FT (ALMEIDA, 1994; OZAKTAS; KUTAY; MENDLOVIC, 1999). In practical scenarios, no analytical methods are used to evaluate this integral; therefore, numerical algorithms are necessary (OZAKTAS et al., 1996). For these numerical methods, this integral can be expressed in two fundamental ways, as outlined below.

1. The decomposition proposed in (OZAKTAS et al., 1996) is also known as the chirp convolution-based method (BULTHEEL; SULBARAN, 2004; IRFAN; ZHENG; SHAHZAD, 2013). The key point in establishing this method is the use of the trigonometric identity

   $$\tan(\alpha/2) = -\cot\alpha + \csc\alpha$$

   to rewrite the FrFT kernel expression for $\alpha \neq n\pi$. This leads to

   $$X_a(u) = A_\alpha e^{-j\pi u^2 \tan\left(\frac{\alpha}{2}\right)} \int_{-\infty}^{\infty} \underbrace{x(t)e^{-j\pi t^2 \tan\left(\frac{\alpha}{2}\right)}}_{g(t)} e^{j\pi(u-t)^2\csc\alpha} dt. \tag{2.8}$$

   In this manner, the isolated integral becomes a convolution operator, $\{g * h\}(u)$, where $h(t) = e^{j\pi t^2 \csc\alpha}$ is a chirp signal with a chirp rate of $\csc\alpha$. Therefore, the FrFT can be decomposed into two chirp multiplications and a chirp convolution. The diagram corresponding to this form of decomposition is shown in Figure 3a. In some applications, the outer chirp term is considered redundant, and it can be removed, giving a simplified FrFT (WANG, 2011; TALLA; BATTULA, 2024).

2. From a different perspective, the FrFT has been shown to be a variation of the standard Fourier transform (ZAYED, 1996; CARIOLARO et al., 1998). This concept can be

illustrated by rewriting the FrFT kernel expression for $\alpha \neq n\pi$, as follows

$$X_a(u) = A_\alpha e^{j\pi u^2 \cot\alpha} \int_{-\infty}^{\infty} \underbrace{x(t) e^{j\pi t^2 \cot\alpha}}_{\tilde{x}(t)} e^{-j2\pi tu \csc\alpha} dt. \tag{2.9}$$

This formulation demonstrates that the FrFT can be decomposed into two chirp multiplications and a single Fourier transform; with scaling of the frequency variable. The corresponding diagram is shown in Figure 3b. The discrete form of this method is presented in (PEI; DING, 2000a), its simplified form in (PEI; DING, 2000b), and its synchrosqueezed transform for time-frequency representation is detailed in (ZHAO; LI, 2023).

Figure 3 – The signal flow graph of the FrFT; diagram corresponding to its decomposition into (a) a chirp convolution, $y(u) = \{g * h\}(u)$, and (b) a Fourier transform with scaling of the frequency variable.

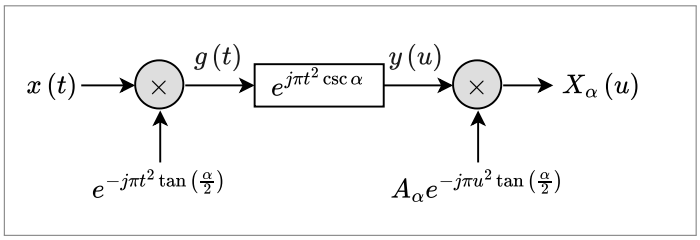

(a)

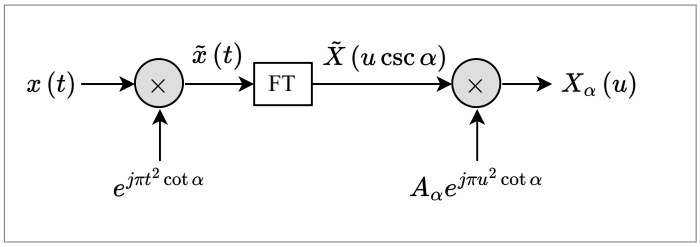

(b)

Source: The author (2025).

2.2.1 FrFT of a Delayed Signal

The FrFT of the received signal at the m-th sensor, delayed by τ_m in the time domain with respect to the reference sensor for an angle of arrival θ, can be expressed according to the operational property of time shifts (OZAKTAS; KUTAY; MENDLOVIC, 1999) as

$$\mathcal{F}^a\{x(t-\tau_m)\} = e^{j\pi\left(\tau_m^2 \sin\alpha\cos\alpha - 2u\tau_m \sin\alpha\right)} X_a(u - \tau_m \cos\alpha), \tag{2.10}$$

where, when τ_m is a small value, as in many practical cases, the delay square τ_m^2 can be neglected. For that reason, the approximated exponential term

$$e^{j\pi\left(\tau_m^2 \sin\alpha\cos\alpha - 2u\tau_m \sin\alpha\right)} \simeq e^{-j2\pi u\tau_m \sin\alpha}$$

can be used to construct the steering vector in the fractional Fourier domain (TAO; ZHOU, 2005; CHONG; XIAOMIN, 2011; YIN et al., 2020); the referred vector can be written as

$$\mathbf{a}_\alpha(u,\theta) = \left[e^{-j2\pi u\tau_0 \sin\alpha} \quad e^{-j2\pi u\tau_1 \sin\alpha} \quad \cdots \quad e^{-j2\pi u\tau_{(M-1)} \sin\alpha}\right]^{\mathsf{T}}.$$

2.2.2 FrFT of an LFM Signal

An LFM signal is a type of signal in which the frequency changes linearly over time, creating as a chirping sound. The FrFT of an LFM signal gradually converges to an impulse in the fractional domain as the fractional order approaches the optimal value (see Figure 4). Estimation

Figure 4 – The FrFT spectrum of an LFM signal.

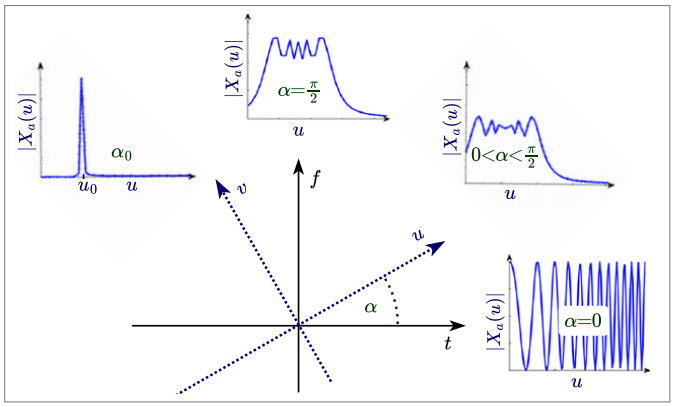

Source: Adapted from Tu et al. (2011).

of the center frequency and frequency modulation rate of chirp signals can be obtained by peak searching in the fractional domain. Substituting (2.3) and (2.7) into (2.6) ($x(t)$ is replaced with $s(t)$), we obtain $\{\mathcal{F}^a s\}(u)$, that is the FrFT of a single-component chirp signal given by

$$\begin{aligned}\{\mathcal{F}^a s\}(u) &= \int_{-T/2}^{T/2} s(t) K_a(t,u)\,dt \\ &= B_{\alpha,u} \int_{-T/2}^{T/2} e^{j\pi\left[2(f_c - u\csc\alpha)t + (\mu+\cot\alpha)t^2\right]}dt,\end{aligned} \tag{2.11}$$

where $B_{\alpha,u} = A_\alpha e^{j\pi u^2 \cot\alpha}$. The optimal order is obtained when the term

$$2\left(f_c - u\csc\alpha\right)t + \left(\mu + \cot\alpha\right)t^2$$

is equal to zero in (2.11). In this way, one obtains the relationships

$$f_c = u_0 \csc\alpha_0, \tag{2.12a}$$

$$\mu = -\cot\alpha_0, \tag{2.12b}$$

where α_0 is the optimal rotation angle and u_0 is the corresponding value in FrFT domain (YIN et al., 2020). At the reference element and considering the noisy channel, the peak searching in the fractional domain can be outlined as

$$\{\widehat{a}_0, \widehat{u}_0\} = \underset{a,u}{\operatorname{argmax}} \left|\{\mathcal{F}^a x_{m_0}\}(u)\right|^2, \tag{2.13}$$

where $\widehat{a}_0$ is the estimated optimum order and $\widehat{u}_0$ is the sampling point corresponding to the maximum peak.

2.3 LINEAR CANONICAL TRANSFORMS

In this section, we explain how (continuous) simplified FrFTs are derived as a special case of the linear canonical transform (LCT) and demonstrate that one of these simplified versions is a well-suited operator for estimating high chirp rates. Therefore, let $X_{\mathbf{A}}(u) = \{\mathcal{L}^{\mathbf{A}}x\}(u)$ denote the LCT of $x(t)$. The corresponding three-free-parameter linear integral transform is defined as in (HEALY et al., 2015, p. 40):

$$X_{\mathbf{A}}(u)=\begin{cases}\sqrt{\frac{1}{jb}}\int_{-\infty}^{\infty}x(t)e^{j\pi\left(\frac{d}{b}u^2-\frac{2}{b}ut+\frac{a}{b}t^2\right)}dt, & b\neq 0,\\ \sqrt{d}e^{j\pi cdu^2}x(du), & b=0,\end{cases} \tag{2.14}$$

where $\mathbf{A}=(a,b;c,d)$ is a matrix whose entries are real numbers that satisfy $ad-bc=1$. The LCT satisfies the cascadability property (HEALY et al., 2015, p. 34), which can be written as

$$\left\{\mathcal{L}^{(a_2,b_2;c_2,d_2)}\left[\mathcal{L}^{(a_1,b_1;c_1,d_1)}x\right]\right\}(u)=\left\{\mathcal{L}^{(a_3,b_3;c_3,d_3)}x\right\}(u),$$

where the matrix $(a_3,b_3;c_3,d_3)$ is determined by the composition of the transformations (PEI; DING, 2002), as

$$\begin{bmatrix}a_3 & b_3\\ c_3 & d_3\end{bmatrix}=\begin{bmatrix}a_2 & b_2\\ c_2 & d_2\end{bmatrix}\begin{bmatrix}a_1 & b_1\\ c_1 & d_1\end{bmatrix}. \tag{2.15}$$

When the matrix $\mathbf{A}$ is specified as $(\cos\alpha,\sin\alpha;-\sin\alpha,\cos\alpha)$, the LCT becomes FrFT (HEALY et al., 2015, p. 42). The FrFT operator can be expressed as $\{\mathcal{F}^a x\}(u)=e^{j\frac{\alpha}{2}}\{\mathcal{L}^{\mathbf{A}}x\}(u)$ and has the additive property as it satisfies (2.15).

The LCT of a single-component LFM signal can be expressed as

$$\{\mathcal{L}^{\mathbf{A}}s\}(u)=\frac{A}{\sqrt{jb}}e^{j\phi_0}e^{j\pi\frac{d}{b}u^2}\int_{t_1}^{t_2}e^{j2\pi\left[\left(f_c-\frac{u}{b}\right)t+\left(\mu+\frac{a}{b}\right)\frac{t^2}{2}\right]}dt.$$

If we assume that the amplitude of $\{\mathcal{L}^{\mathbf{A}}s\}(u)$ reaches its maximum peak for a matrix $\mathbf{A}_0$, given as $(a_0,b_0;c_0,d_0)$, at a sampling point u_0, then the parameters of an LFM signal can be determined using numerical algorithms, as described in (SU; TAO; KANG, 2019). This results in

$$\mu=-a_0/b_0,\ f_c=u_0/b_0,\ \text{and}\ \phi_0=\arg\left[\sqrt{jb_0}e^{-j\pi d_0u_0^2/b_0}\{\mathcal{L}^{\mathbf{A_0}}s\}(u_0)\right].$$

In the following items, we analyze the chirp rate for LCT cases in the form of a simplified FrFT:

1. The operator $\mathcal{L}^{(\cot\alpha,1;-1,0)}$ is a frequency-scaled simplified FrFT (ZAYED, 1996); the chirp rate is $\mu=-\cot\alpha_0$, where $\alpha_0\neq n\pi$ represents the optimal rotation angle in the time-frequency plane. This LCT admits high chirp-rate values, $-\infty\leq\mu\leq\infty$, because the cotangent function has domain and range respectively given by $\mathbb{R}-n\pi$ and $(-\infty,\infty)$.

2. The operator $\mathcal{L}^{(\sin\alpha\cos\alpha,1;-1,0)}$ is a simplified FrFT whose discrete version corresponds to the so-called single-FFT method (MARINHO; BERNARDO, 1998); in this case, one has $\mu = -\sin\alpha_0\cos\alpha_0 = -\frac{1}{2}\sin 2\alpha_0$. The possible chirp rates are limited to low values, $-1/2 \leq \mu \leq 1/2$, because the sine function has domain and range respectively given by $\mathbb{R}$ and $[-1, 1]$.

3. The operator $\mathcal{L}^{(\cos\alpha,1;-1,0)}$ corresponds to a simplified FrFT scheme having both frequency and time scaling. The chirp rate formula is $\mu = -\cos\alpha_0$. In this case, the chirp rate range is twice that of the last item, since the cosine function domain and range are respectively given by $\mathbb{R}$ and $[-1, 1]$. Specifically, the range of possible chirp rate values is $-1 \leq \mu \leq 1$.

In conclusion, the simplified FrFT presented in item 1) is a suitable transform for DoA estimation, since an important aspect, in the referred application, is the quadratic phase signal with high chirp-rate values (MULINDE; ATTYGALLE; AZIZ, 2021). Thus, although this type of simplified FrFT has no additive properties, it is convertible (PEI; DING, 2000b). This convertibility arises from the relationship

$$\begin{bmatrix} \cot\beta & 1 \\ -1 & 0 \end{bmatrix} = \begin{bmatrix} 1 & \cot\alpha - \cot\beta \\ 0 & 1 \end{bmatrix} \begin{bmatrix} \cot\alpha & 1 \\ -1 & 0 \end{bmatrix}. \tag{2.16}$$

In other words, using the cascadability property, the operator $\mathcal{L}^{(\cot\alpha,1;-1,0)}$ can be converted into $\mathcal{L}^{(\cot\beta,1;-1,0)}$ as it satisfies (2.16).

3 CHIRP-BASED DECOMPOSITION ALGORITHMS

This chapter describes the differences among the chirp-based decompositions for the sampling-type DFrFT. Based on the choice of time-frequency representation, we explore definitions in scaled domains. The analysis includes arithmetic complexity, the time-shift property, and places particular emphasis on chirp signals; including the estimation of linear chirp parameters. In this context, we focus on the frequency-scaled simplified FrFT and introduce its local discrete version.

3.1 DISCRETE-TIME SIGNAL

First, let $x[r]$ represent the discrete-time signal obtained by sampling the continuous-time signal $x(t)$. In the context of chirp signal processing with fractional Fourier transforms (MIAO, 2023; ZHONG et al., 2023), an N-length sequence $x[r]$ is defined as

$$x\left[r\right] = x\left(\frac{r}{f_s}\right), \quad r = -N_0, -N_0+1, \ldots, -N_0+N-1, \tag{3.1}$$

where f_s is the sampling rate, $N_0 = \left\lfloor \frac{N}{2} \right\rfloor$ specifies the starting index, and $\lfloor\cdot\rfloor$ denotes the floor function of its argument. For the analysis based on DFrFT, interpolation and decimation are applied to a digital signal, which is derived from an analog signal, to make its Wigner distribution more compact (OZAKTAS et al., 1996). However, these operations are omitted throughout this thesis, as our focus is on exploring numerical algorithms for an N-point DFrFT.

3.2 SAMPLING-TYPE DFrFT ON NORMALIZED DOMAINS

The defining integral (2.6), in its discrete form, can be identified as the sampling-type discrete FrFT (DFrFT) (PEI; DING, 2000a). In time-frequency analysis, the dimensional normalization means that the coordinates (t,u) are scaled to (t/s,us), where s is a scaling parameter given by $s = \frac{\sqrt{N}}{f_s}$ (OZAKTAS et al., 1996). Figure 5 illustrates this concept by showing the Wigner–Ville distribution of a linear chirp signal with center frequency f_0 and chirp rate μ (YU et al., 2015; ZHONG et al., 2025). In such scaled domains, when $\alpha \neq n\pi$, the kernel can be discretized as $K_a[q,r] = K_a(q\Delta, r\Delta)$, where $\Delta = \frac{1}{\sqrt{N}}$ is the normalized sampling period. Therefore, the continuous integral transform can be approximated by a quadrature formula as

$$X_a[q] \triangleq \frac{A_\alpha}{\sqrt{N}} e^{j\frac{\pi}{N}q^2\cot\alpha} \sum_{r=-N_0}^{-N_0+N-1} x[r] e^{-j\frac{\pi}{N}\left(2rq\csc\alpha - r^2\cot\alpha\right)}. \tag{3.2}$$

Notice that the variables a and α, as well as the axes u and v, which belong to normalized domains (see Figure 5), are different from those given in the continuous integral. In this way, the sampling points $u_q = q\Delta$, with $-N_0 \leq q < N_0+N$, correspond to the normalized frequency domain variable; in fact, it is more practical to use normalized coordinates (LIU; XIAO; WANG, 2021;

ZHONG et al., 2023), rather than directly deal with the FrFT time-scaling property (OZAKTAS; KUTAY; MENDLOVIC, 1999). The main drawback of the direct form of discretizing the integral definition is its high computational cost, which is $\mathcal{O}(N^2)$.

Figure 5 – Normalized time-frequency plane (t', f') and coordinates (u, v) rotated by an angle α_0, with the u-axis perpendicular to line representing the Wigner-Ville distribution of a linear chirp: (a) $\mu < 0$, and (b) $\mu > 0$.

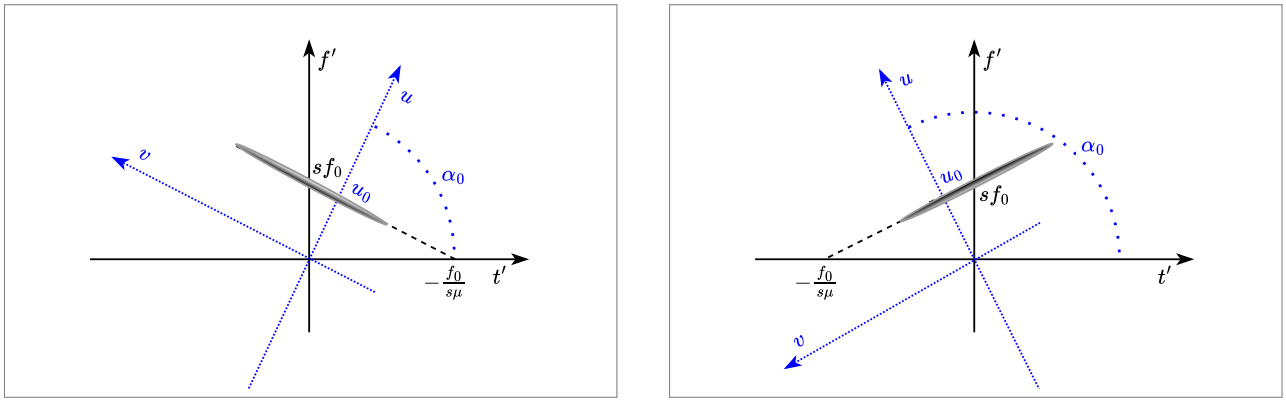

(a) $\mu < 0$ (b) $\mu > 0$

Source: The author (2025).

The most widely used numerical algorithm for DFrFT is a decomposition method proposed in (OZAKTAS et al., 1996), which enables efficient implementation. In such normalized domains, assuming that N is even, the discrete form of the integral definition from (2.8) can be expressed as

$$X_a[q] \triangleq \frac{A_\alpha}{\sqrt{N}} e^{-j\frac{\pi}{N}q^2 \tan\left(\frac{\alpha}{2}\right)} \sum_{r=-N/2}^{N/2-1} \underbrace{x[r] e^{-j\frac{\pi}{N}r^2 \tan\left(\frac{\alpha}{2}\right)}}_{g[r]} e^{j\frac{\pi}{N}(q-r)^2 \csc\alpha}, \tag{3.3}$$

which means the whole algorithm involves one chirp multiplication (inner chirp term), one complex convolution, and one more chirp multiplication (outer chirp term); thus, this method can be identified as CM–CC–CM. The sequence of interest, generated by the summation formula, can be computed as a circular convolution, that is

$$y_n = (g \circledast h)_n = \sum_{i=0}^{N_1-1} g_i h_{(n-i)},\ n = 0, 1, \ldots, N_1 - 1, \tag{3.4}$$

where $N_1 = 2N - 1$. In this operator, $\{g_n\}_{n=0}^{N_1-1}$ and $\{h_n\}_{n=0}^{N_1-1}$ are sequences that can be periodically extended outward with period N_1; their indices are modulo N_1, $n \pmod{N_1}$. Rigorously, the first non-zero N elements of $\{g_n\}$ correspond to the chirp-modulated input signal, and $\{h_n\}$ represents the discrete chirp signal $e^{j\frac{\pi}{N}r^2 \csc\alpha}$, where $-N < r < N$. The first $N-1$ elements of $\{y_n\}$ are rejected; this procedure is well-known in the overlap-and-save method. As stated by the convolution theorem, the cyclic convolution outlined in (3.4) can be implemented through $(2N)$-point FFT algorithms by means of the zero-padding method (AGARWAL; BURRUS,

1974b). In such a way, considering that the DFT of $\{h_n\}$ can be pre-computed, the complexity of an N-point DFrFT consists of $4N$ complex multiplications, one $(2N)$-point FFT and one $(2N)$-point inverse FFT; a complex multiplication can be done as 3 real-valued multiplications and 3 real-valued additions (see Appendix A). The arithmetic complexity of the whole process, in terms of numbers of complex multiplications, $\mathrm{M}_{\mathrm{C}}^{\mathrm{c}}(N)$, and complex additions, $\mathrm{A}_{\mathrm{C}}^{\mathrm{c}}(N)$, is

$$\mathrm{M}_{\mathrm{C}}^{\mathrm{c}}(N) = 4N + 2\mathrm{M}_{\mathrm{C}}(2N), \tag{3.5a}$$

$$\mathrm{A}_{\mathrm{C}}^{\mathrm{c}}(N) = 2\mathrm{A}_{\mathrm{C}}(2N). \tag{3.5b}$$

The terms $\mathrm{M}_{\mathrm{C}}(\cdot)$ and $\mathrm{A}_{\mathrm{C}}(\cdot)$ represent the arithmetic complexity of the DFT/FFT algorithm, where the subscript C refers to the type of operation, in this case, complex. In Appendix B, we detail how $3N$ complex additions can be saved.

3.2.1 DFrFT of a Discrete-Time Delayed Signal

In Section 2.1, we indicated that the signals received by the elements of a ULA have a delay with respect to the reference element. In this scenario, we need to calculate the fractional transform of a discrete-time delayed signal. To be more specific, the goal is to show the relationship that exists between the DFrFT of the received signals. First of all, assuming that the delay τ_m between the m-th element relative to the reference element generates a displacement of r_θ points, that is

$$r_\theta = f_s \tau_m, \tag{3.6}$$

where f_s is the sampling frequency. The DFrFT as a numerical integration of the kernel, does not have scaling on the fractional axis, so that $X_a[q]$, the DFrFT of the discrete-time signal $x[r]$, can be written as

$$X_a[q] = A_{\alpha,q} \sum_{r=-\infty}^{\infty} x[r] e^{-j\frac{\pi}{N}\left(2rq\csc\alpha - r^2\cot\alpha\right)}, \tag{3.7}$$

where $A_{\alpha,q} = \frac{A_\alpha}{\sqrt{N}} e^{j\frac{\pi}{N}q^2\cot\alpha}$. Then, let $\mathcal{F}^a\{x[r-r_\theta]\}$ be the DFrFT of the discrete-time delayed signal $x[r-r_\theta]$, that is

$$\mathcal{F}^a\{x[r-r_\theta]\} = A_{\alpha,q} \sum_{r=-\infty}^{\infty} x[r-r_\theta] e^{-j\frac{\pi}{N}\left(2rq\csc\alpha - r^2\cot\alpha\right)}. \tag{3.8}$$

Performing the substitution $r = n + r_\theta$, (3.8) becomes

$$\mathcal{F}^a\{x[r-r_\theta]\} = A_{\alpha,q} \sum_{n=-\infty}^{\infty} x[n] e^{-j\frac{\pi}{N}\left[2(n+r_\theta)q\csc\alpha - (n+r_\theta)^2\cot\alpha\right]},$$

$$\mathcal{F}^a\{x[r-r_\theta]\} = e^{-j\frac{\pi}{N}\left(2r_\theta q\sin\alpha - r_\theta^2\sin\alpha\cos\alpha\right)} \times A_{\alpha,q-r_\theta\cos\alpha} \sum_{n=-\infty}^{\infty} x[n] e^{-j\frac{\pi}{N}\left[2n(q-r_\theta\cos\alpha)\csc\alpha - n^2\cot\alpha\right]}.$$

Using (3.7), one has

$$\mathcal{F}^a\{x[r-r_\theta]\} = e^{-j\frac{\pi}{N}\left(2r_\theta q\sin\alpha - r_\theta^2\sin\alpha\cos\alpha\right)} X_a[q - r_\theta\cos\alpha].$$

In the context of chirp signal processing in uniform linear arrays, this result indicates that the peak index q_0, corresponding to the DFrFT of the signal received by the reference sensor, is shifted to q_m, as shows in the equation

$$q_m = q_0 + f_s\tau_m\cos\alpha_0, \tag{3.9}$$

where $\alpha_0 = a_0\pi/2$, with a_0 being the optimal order for the DFrFT. Note that q_m represents the index of the peak position in the DFrFT spectrum of the signal received at the m-th sensor.

3.2.2 DFrFT of an LFM Signal

The relationship between the LFM signal parameters and the optimal fractional Fourier order, in discrete form, can be derived straightforwardly by performing energy aggregation analysis, it means identifying peaks in the amplitude spectrum of the DFrFT (ALDIMASHKI; SERBES, 2020). More specifically, let $\{\mathcal{F}^a s\}[q]$ denote the DFrFT of the discrete-time chirp $s[r]$, which represents the discrete form of the signal given in (2.3). It follows that

$$\{\mathcal{F}^a s\}[q] = \frac{A_\alpha}{\sqrt{N}} e^{j\frac{\pi}{N}q^2\cot\alpha} \sum_{r=-N/2}^{N/2-1} e^{j2\pi\left[\left(\frac{f_c}{f_s} - \frac{q\csc\alpha}{N}\right)r + \left(\frac{\mu}{f_s^2} + \frac{\cot\alpha}{N}\right)\frac{r^2}{2}\right]}.$$

The relationship between the chirp signal parameters f_c and μ and the optimal rotation angle α_0 (corresponding to $a_0\pi/2$, where a_0 is the optimal order for the DFrFT) can be determined under the criterion of maximum amplitude by setting the coefficients of the polynomial in r within the exponent to zero. This yields the following formulas:

$$f_c = \tfrac{1}{N} q_0 f_s \csc\alpha_0, \tag{3.10a}$$

$$\mu = -\tfrac{1}{N} f_s^2 \cot\alpha_0. \tag{3.10b}$$

Here, q_0 denotes the peak index.

These expressions enable the estimation of the parameters of a linear chirp signal by searching for peaks in the amplitude spectrum of the DFrFT; representation of the signal received on the reference element. This process can be outlined as

$$\{\widehat{a}_0, \widehat{q}_0\} = \underset{a,q}{\operatorname{argmax}} \left|\{\mathcal{F}^a x_{m_0}\}[q]\right|^2, \tag{3.11}$$

where $\widehat{a}_0$ represents the estimated optimal order of the DFrFT, and $\widehat{q}_0$ denotes the index of the sampling point corresponding to the maximum peak. In (ALDIMASHKI; SERBES, 2020), it was demonstrated that the joint estimation of $\widehat{a}_0$ and $\widehat{q}_0$ in a two-dimensional search space can be achieved by estimating them independently in one-dimensional spaces. The computational cost of the golden-section search (GSS) for a single-component chirp is then $\mathcal{O}(N\log_2^2 N)$, where $\mathcal{O}(N\log_2 N)$ corresponds to the algorithmic cost of a single DFrFT (OZAKTAS et al., 1996).

3.3 SAMPLING-TYPE DFrFT ON SCALED DOMAINS

This section formally presents an alternative to the sampling-type DFrFT. This approach is defined over scaled domains and is affine to a single DFT, incorporating the possibility of scaling the time or frequency axis in the time-frequency representation. We refer to this method as the scaled DFrFT. Given a discrete-time signal as in (3.1), the continuous integral transform of (2.9) can be approximated using a quadrature formula as

$$X_a(u_q) \approx A_\alpha \Delta_t e^{j\pi u_q^2 \cot\alpha} \sum_{r=-N/2}^{N/2-1} \left(x[r] e^{j\pi t_r^2 \cot\alpha} \right) e^{-j2\pi t_r u_q \csc\alpha},$$

where $u_q = q\Delta_u$ and $t_r = r\Delta_t$ represent the discrete domains of the FrFT kernel. The sampling parameter Δ_t is not necessarily equal to $1/f_s$. The points u_q, in general, correspond to the sampling points along the scaled frequency variable axis.

The numerical algorithm for this type of decomposition is based on affine transformations, such as scaling, chirping, and shifting (PEI; DING, 2000a). Let $\{\mathcal{F}'^a x\}[q]$ denote the DFrFT of $x[r]$. Then, this operator can be defined as a one-free-sampling-parameter discrete transform, as

$$\{\mathcal{F}'^a x\}[q] \triangleq A_\alpha \Delta_t e^{j\pi q^2 \Delta_u^2 \cot\alpha} \sum_{r=-N/2}^{N/2-1} \left(x[r] e^{j\pi r^2 \Delta_t^2 \cot\alpha} \right) e^{-j\frac{2\pi}{N} rq}, \tag{3.12}$$

subject to the constraint;

$$\Delta_u \Delta_t = \tfrac{1}{N} \sin\alpha. \tag{3.13}$$

Thus, the entire algorithm consists of an inner chirp multiplication, the ordinary DFT computation of the chirp-modulated signal, and an outer chirp multiplication. This decomposition form (two chirp modulations and one DFT) is referred to as CM–FFT–CM when the DFT is performed using FFT algorithms. Specifically, if we use (3.12), $2N$ complex multiplications and one N-point DFT are required. The arithmetic complexity of (3.12) is given, in terms of numbers of complex multiplications, $\mathrm{M}_\mathrm{C}^{\mathrm{ot}}(N)$, and complex additions, $\mathrm{A}_\mathrm{C}^{\mathrm{ot}}(N)$, by

$$\mathrm{M}_\mathrm{C}^{\mathrm{ot}}(N) = 2N + \mathrm{M}_\mathrm{C}(N), \tag{3.14a}$$

$$\mathrm{A}_\mathrm{C}^{\mathrm{ot}}(N) = \mathrm{A}_\mathrm{C}(N). \tag{3.14b}$$

In practice, N is typically a power of two, allowing the DFT to be computed using a conventional FFT algorithm, such as the Cooley-Tukey algorithm (COOLEY; TUKEY, 1965). In this case, $\mathrm{M}_\mathrm{C}(N)$ and $\mathrm{A}_\mathrm{C}(N)$ are given as $\frac{N}{2}\log_2 N$ and $N\log_2 N$, respectively.

3.3.1 DFrFT of a Discrete-Time Delayed Signal

Similarly to the analysis in Subsection 3.2.1, we present the discrete-time property for the DFrFT. First, (3.12) can be rewritten as

$$\{\mathcal{F}'^a x\}[q] = B_{\alpha,q} \sum_{r=-\infty}^{\infty} x[r] e^{-j\frac{\pi}{N}\left(2rq - r^2\Delta_t^2 N\cot\alpha\right)}, \tag{3.15}$$

where $B_{\alpha,q} = A_\alpha \Delta_t e^{j\pi q^2 \Delta_u^2 \cot\alpha}$. Next, let $\mathcal{F}'^a\{x[r-r_\theta]\}$ denote the DFrFT of the discrete-time delayed signal $x[r-r_\theta]$, given by

$$\mathcal{F}'^a\{x[r-r_\theta]\} = B_{\alpha,q} \sum_{r=-\infty}^{\infty} x_{r-r_\theta} e^{-j\frac{\pi}{N}\left(2rq - r^2\Delta_t^2 N\cot\alpha\right)}. \tag{3.16}$$

As in the previous case, applying the substitution $r = n + r_\theta$, one obtains

$$\begin{aligned}
\mathcal{F}'^a\{x[r-r_\theta]\} &= B_{\alpha,q} \sum_{n=-\infty}^{\infty} x_n e^{-j\frac{\pi}{N}\left[2(n+r_\theta)q - (n+r_\theta)^2\Delta_t^2 N\cot\alpha\right]}, \\
\mathcal{F}'^a\{x[r-r_\theta]\} &= e^{-j\frac{\pi}{N}\left(2r_\theta q\sin^2\alpha - r_\theta^2\Delta_t^2 N\sin\alpha\cos\alpha\right)} \\
&\quad \times B_{\alpha,q-r_\theta\Delta_t^2 N\cot\alpha} \sum_{n=-\infty}^{\infty} x_n e^{-j\frac{\pi}{N}\left[2n(q-r_\theta\Delta_t^2 N\cot\alpha) - n^2\Delta_t^2 N\cot\alpha\right]}.
\end{aligned}$$

Following the notations above, one obtains

$$\mathcal{F}'^a\{x[r-r_\theta]\} = e^{-j\frac{\pi}{N}\left(2r_\theta q\sin^2\alpha - r_\theta^2\Delta_t^2 N\sin\alpha\cos\alpha\right)} \{\mathcal{F}'^a x\}[q - r_\theta\Delta_t^2 N\cot\alpha].$$

From this equation, it can be concluded that the amplitude spectrum of the DFrFT for the signal received at the m-th sensor is a shifted version of the spectrum corresponding to the signal received at the reference sensor. Specifically, the peak index q_0 is shifted to q_m, as indicated in the expression

$$q_m = q_0 + f_s\tau_m\Delta_t^2 N\cot\alpha_0, \tag{3.17}$$

where $\alpha_0 = a_0\pi/2$, with a_0 being the optimal order for DFrFT. Notice that in comparisons between (3.9) and (3.17), the formula for q_m differs in both cases. This is due to the constraint given in (3.13).

3.3.2 DFrFT of an LFM Signal

Analogously to the previous case, the FrFT-based analysis of an LFM signal in discrete form by using DFrFT is as follows. Let $\{\mathcal{F}'^a s\}[q]$ denote the DFrFT of the discrete-time chirp $s[r]$. Considering the expressions that correspond to this method, one obtains

$$\{\mathcal{F}'^a x\}[q] = B_{\alpha,q} \sum_{r=-N/2}^{N/2-1} e^{j2\pi\left[\left(\frac{f_c}{f_s} - \frac{q}{N}\right)r + \left(\frac{\mu}{f_s^2} + \Delta_t^2\cot\alpha\right)\frac{r^2}{2}\right]}.$$

Thus, the parameters f_c and μ are related to the optimal rotation angle α_0 (corresponding to $a_0\pi/2$, where a_0 is the optimal DFrFT order) under the maximum amplitude criterion by setting the polynomial coefficients in r to zero, resulting in the formulas:

$$f_c = \tfrac{1}{N} q_0 f_s, \tag{3.18a}$$

$$\mu = -f_s^2\Delta_t^2\cot\alpha_0. \tag{3.18b}$$

Here, q_0 denotes the peak index. Note that (3.18a) is independent of α. This implies that, given a multi-component LFM signal with f_c in the range between the lower frequency f_1 and the upper frequency f_2, the intervals for the index q_0 can be determined in advance. Specifically, these indices fall within the range $f_1 N/f_s$ to $f_2 N/f_s$. As a result, it is not necessary to compute all the points of the DFrFT. Regarding (3.18b), the following items present some possibilities for the sampling parameter Δ_t:

1. By choosing Δ_t as $1/f_s$, one obtains the formula $\mu = -\cot\alpha_0$.
2. As in normalized domains, Δ_t can be set as $1/\sqrt{N}$. This implies that the magnitude representation corresponds to an amplitude spectrum, with the frequency variable scaled; Δ_u results in $\frac{1}{\sqrt{N}}\sin\alpha$. In addition to that, the formula becomes $\mu = -f_s^2\cot\alpha_0/N$.
3. In a similar way to the previous item, choosing Δ_u as $1/\sqrt{N}$ determines an amplitude spectrum that corresponds to scaling the time variable. In this case, Δ_t is equal to $\frac{1}{\sqrt{N}}\sin\alpha$. Consequently, the formula becomes $\mu = -f_s^2\cos\alpha_0\sin\alpha_0/N$.

In conclusion, the numerical method based on the FrFT–affine Fourier transform differs from the affine chirp convolution, represented respectively by the CM–FFT–CM and CM–CC–CM structures, in terms of the discrete-time shift property, arithmetic complexity, and the representation of chirp signals in the fractional Fourier domain.

3.4 SIMPLIFIED FRACTIONAL FOURIER TRANSFORM

Hereafter, we refer to the LCT with $\mathbf{A} = (\cot\alpha, 1; -1, 0)$ as simplified FrFT (named SmFrFT) (PEI; DING, 2000b), for $\alpha \neq n\pi$, which can be expressed in a linear integral form as

$$\begin{aligned} X_a(u) &\triangleq \{\mathcal{L}^{(\cot\alpha,1;-1,0)}x\}(u) \\ &= \frac{1}{\sqrt{j}}\int_{-\infty}^{\infty} x(t)e^{-j2\pi ut + j\pi t^2\cot\alpha}dt, \end{aligned}$$

where $\alpha = a\pi/2$, with a being the order of SmFrFT. Such a simplified FrFT has remarkable importance due to its greater capability in estimating chirp rate and simpler implementation, since its sampled form becomes a DFT. On normalized domains, the (discrete) simplified FrFT (DSmFrFT) can be given as

$$X_a[q] \triangleq \frac{1}{\sqrt{jN}}\sum_{r=-N/2}^{N/2-1}\left(x[r]e^{j\frac{\pi}{N}r^2\cot\alpha}\right)e^{-j\frac{2\pi}{N}rq}, \tag{3.20}$$

where $\alpha = a\pi/2$, with a being the order of DSmFrFT. Note that the DSmFrFT consists of chirp-modulating the signal and computing a discrete Fourier transform only (there is no outer chirp term nor need for kernel adjustments). Since N is usually a power of two, the N-point DFT can be computed using a conventional FFT algorithm, such as the Cooley-Tukey algorithm (COOLEY;

TUKEY, 1965). Therefore, the arithmetic complexity is given, in terms of the numbers of complex multiplications, $\mathrm{M}_{\mathrm{C}}^{\mathrm{s}}(N)$, and complex additions, $\mathrm{A}_{\mathrm{C}}^{\mathrm{s}}(N)$, by

$$\mathrm{M}_{\mathrm{C}}^{\mathrm{s}}(N) = \tfrac{N}{2}\log_2(N) + N, \tag{3.21a}$$

$$\mathrm{A}_{\mathrm{C}}^{\mathrm{s}}(N) = N\log_2(N). \tag{3.21b}$$

To be more specific, the number of complex arithmetic operations for DFrFT and DSmFrFT is provided in Table 1. In the table, we also include the measures η_{M} and η_{A} for calculating algorithm efficiency, which represent the percentage of multiplications and additions saved, respectively, when using DSmFrFT instead of DFrFT (OZAKTAS et al., 1996). The referred measurements reach $\sim 77\%$ when multiplications and additions are counted.

Table 1 – Arithmetic complexity of DFrFT and DSmFrFT; in terms of the number of complex multiplications and additions.

N	**Multiplications**		η_{M}	**Additions**		η_{A}
	DFrFT	DSmFrFT	(%)	DFrFT	DSmFrFT	(%)
512	12288	2816	77.1	20480	4608	77.5
1024	26624	6144	76.9	45056	10240	77.3

Source: The author (2025).

3.4.1 Cyclic Shift Operator

In this numerical algorithm, we remark that, if we want to compute the DFT of a sequence whose range of index values is as in (3.1), we need to perform a cyclic shift and consider such an adjustment when interpreting the frequency domain. In short, the discrete Fourier transform (DFT) is a linear transformation that converts a discrete-time signal from the time domain to the frequency domain, mapping a sequence of numbers into another sequence representing the signal's frequency components. Specifically, given an input signal vector $\mathbf{v} = \begin{bmatrix} v_0 & v_1 & \cdots & v_{N-1} \end{bmatrix}^{\mathsf{T}}$, the DFT of $\mathbf{v}$ is an output frequency domain vector $\mathbf{V} = \begin{bmatrix} V_0 & V_1 & \cdots & V_{N-1} \end{bmatrix}^{\mathsf{T}}$. The components of $\mathbf{V}$ are given by

$$V_k = \tfrac{1}{\sqrt{N}} \sum_{n=0}^{N-1} e^{-j\frac{2\pi}{N}kn} v_n, \quad k = 0, 1, \ldots, N-1, \tag{3.22}$$

where, $e^{-j\frac{2\pi}{N}}$ is the root of unity and can be denoted as ω_N. The DFT can also be expressed in matrix form as $\mathbf{V} = \mathbf{F} \cdot \mathbf{v}$, where $\mathbf{F}$ is the DFT matrix with entries $F_{k,n} = \frac{1}{\sqrt{N}}\omega_N^{kn}$, for $n, k = 0, 1, \ldots, N-1$, in its k-th row and n-th column. In this form, the DFT is **unitary**, preserving vector inner products and ensuring energy conservation during transformation. In this context, it is important to note that, if we want to compute the DFT of a sequence whose range of index values is as in (3.1), we first need to shift the components with negative indices. A cyclic shift is an operator that shifts the DC component to the center of the spectrum, and an inverse

cyclic shift restores the raw frequency order (VISWANATHAN, 2019). To be more specific, let us represent the chirp-modulated input signal in discrete form as

$$\tilde{x}[r] = x[r]e^{j\frac{\pi}{N}r^2\cot\alpha}, \quad r = -N/2, -N/2+1, \ldots, N/2-1.$$

Then, an inverse cyclic shift is performed before using the DFT, ensuring that the negative-index components are moved to the end. The resulting sequence is expressed in vector form as

$$\mathbf{v} = \begin{bmatrix}\tilde{x}[0] & \tilde{x}[1] & \cdots & \tilde{x}[N/2-1] & \tilde{x}[-N/2] & \tilde{x}[-N/2+1] & \cdots & \tilde{x}[-1]\end{bmatrix}^{\mathsf{T}}.$$

Subsequently, the DSmFrFT of $x[r]$ is the cyclically shifted version of $\frac{1}{\sqrt{j}}\mathbf{F}\cdot\mathbf{v}$.

3.4.2 Convertibility Property

The convertibility property of an LCT enables it to be transformed into another LCT. Specifically, when the order of the DSmFrFT (or DFrFT) approaches the values 0 or ± 2, the transformation may produce high oscillations. In the case of DFrFT, this phenomenon is avoided using the additive property, where the operator $\mathcal{F}^a$ can be expressed as $\mathcal{F}^{a-1}\mathcal{F}$ or $\mathcal{F}^{a+1}\mathcal{F}^{-1}$. By analogy, and as shown in (2.16), the operator $\mathcal{L}^{\mathbf{A}}$, defined by the matrix $(\cot\alpha, 1; -1, 0)$, can be decomposed into two operators, $\mathcal{L}^{\mathbf{A}_2}$ and $\mathcal{L}^{\mathbf{A}_1}$. In this decomposition, the inner operator is determined by the matrix $\mathbf{A}_1 = (0, 1; -1, 0)$, which corresponds to a standard Fourier transform; angle of rotation is $\pi/2$. The outer operator is defined by the matrix $\mathbf{A}_2 = (0, -\cot\alpha; 0, 1)$. In normalized domains, these operators can be expressed in discrete form as

$$\{\mathcal{L}^{\mathbf{A}_1}x\}[q] = \tfrac{1}{\sqrt{jN}}\sum_{r=-N/2}^{N/2-1} x[r]e^{-j\frac{2\pi}{N}rq}, \tag{3.23a}$$

$$\{\mathcal{L}^{\mathbf{A}_2}x\}[q] = \sqrt{\tfrac{j\tan\alpha}{N}}\sum_{r=-N/2}^{N/2-1} x[r]e^{-j\frac{\pi}{N}(q-r)^2\tan\alpha}. \tag{3.23b}$$

Note that the first operator is an N-point DFT multiplied by $\frac{1}{\sqrt{j}}$. The output sequence for the second operator can be calculated as the last N elements of the circular convolution between the input sequence (zero-padded version) and the sequence corresponding to the discrete-time chirp signal $e^{-j\frac{\pi}{N}q^2\tan\alpha}$, where $-N \le q < N$.

To illustrate these properties, we refer to Figs. 6(a–d), which show the FrFT spectra of a single-component chirp ($f_c = 20$, $\mu = 10$, $T = 5$). The index q_0, corresponding to the peak value of the DSmFrFT spectrum, can be easily determined by (3.27a) (i.e., $q_0{=}100$, solid red line in Figure 6c). Figure 6b shows an amplitude spectrum enhanced by the cascability property of DFrFT; as a gets closer to 0 or ± 2, high oscillations appear in the DFrFT spectrum, which can be eliminated by applying the index additivity property, for instance, $\mathcal{F}^a = \mathcal{F}^{a-1}\mathcal{F}$ when $a > 1.5$. In the case of DSmFrFT, in a similar situation, the high oscillations can be eliminated by applying the index convertibility property (see Figure 6d). Specifically, the desired operator $\mathcal{L}^{\mathbf{A}}$,

where $\mathbf{A}$ is the matrix $(\cot\alpha, 1; -1, 0)$, is decomposed as $\mathcal{L}^{\mathbf{A}_2}\mathcal{L}^{\mathbf{A}_1}$ when $a > 1.5$ (or $\alpha > 3\pi/4$). The inner operator corresponds to the matrix $\mathbf{A}_1$, given as $(0, 1; -1, 0)$, which becomes a single DFT. The outer operator is determined by the matrix $\mathbf{A}_2$, given as $(1, -\cot\alpha; 0, 1)$, and can be implemented as a chirp convolution.

Figure 6 – Amplitude spectra, $|X_a[q]|$, corresponding to (a-b) DFrFT and (c-d) DSmFrFT, considering a single-component LFM signal and fractional order range $a \in [1, 1.8]$. The transform length is $N = 1024$.

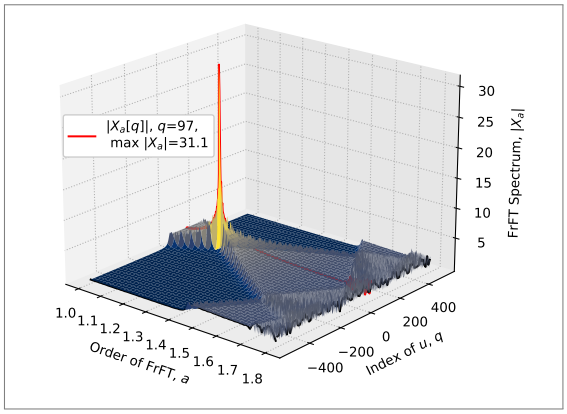

(a) Spectrum of DFrFT, $\mathcal{F}^a$.

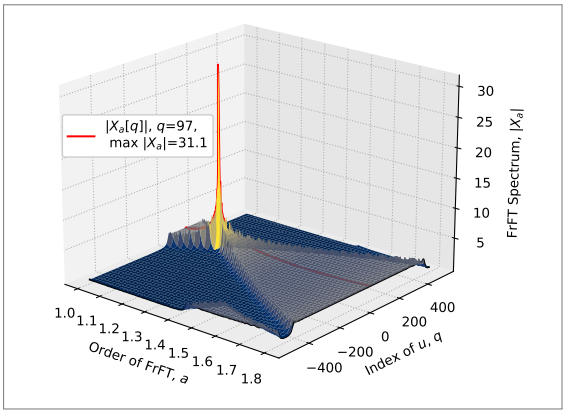

(b) Spectrum of DFrFT, $\mathcal{F}^{a-1}\mathcal{F}$.

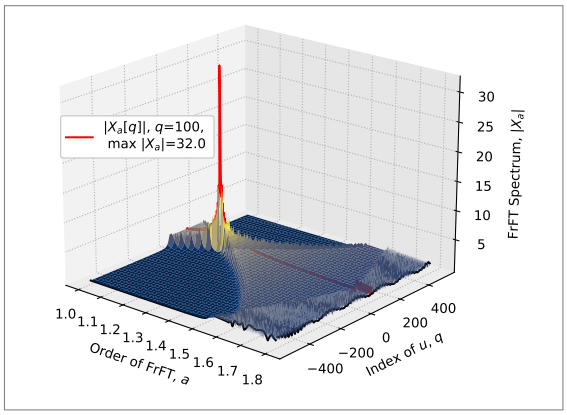

(c) Spectrum of DSmFrFT, $\mathcal{L}^{\mathbf{A}}$.

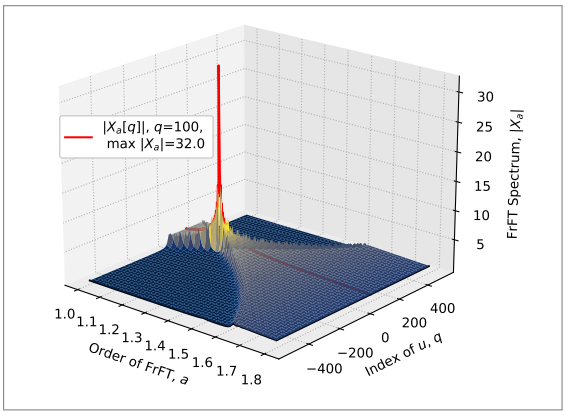

(d) Spectrum of DSmFrFT, $\mathcal{L}^{\mathbf{A}_2}\mathcal{L}^{\mathbf{A}_1}$.

Source: The author (2025).

3.4.3 Local Discrete Simplified FrFT

A local discrete transform is an algorithm for computing partial points of a (global) discrete transform (MIAO, 2023). More specifically, the local discrete SmFrFT (LDSmFrFT) for any Q consecutive points, $q = s, s+1, \ldots, s+Q-1$ and $s \in \{0, 1, \ldots, (P-1)Q\}$, can be defined as

$$X_a[q] = \frac{1}{\sqrt{jN}} \sum_{r=0}^{Q-1} \sum_{p=P_0}^{P_0+P-1} x[p+rP]\mathcal{K}_a[p+rP, q], \tag{3.24}$$

where $N{=}P\,Q$, $P_0{=}{-}N/2$, and $\mathcal{K}_a[n,q] = e^{-j\frac{2\pi}{N}nq + j\frac{\pi}{N}n^2\cot\alpha}$. Then, by substituting $q = s + l$, where $l = 0, 1, \ldots, Q-1$, one obtains

$$X_a[s+l] = \frac{1}{\sqrt{jP}} \sum_{p=P_0}^{P_0+P-1} \underbrace{e^{-j\frac{2\pi}{N}(s+l)p + j\frac{\pi}{N}p^2\cot\alpha}}_{g[p,l]} \times \frac{1}{\sqrt{Q}} \sum_{r=0}^{Q-1} x[p,r] \underbrace{e^{-j\frac{2\pi}{Q}(s-p\cot\alpha)r + j\frac{\pi}{Q}Pr^2\cot\alpha}}_{h[p,r]} e^{-j\frac{2\pi}{Q}lr}.$$

In this way, the LDSmFrFT is different from the general form proposed in (MIAO, 2023); it consists of rearranging the N-length sequence $x[n]$ as a P-by-Q matrix $x[p,r] = x[p + rP]$, element-wise multiplying by the inner chirp matrix $h[p,r]$, performing a Q-point DFT by rows, element-wise multiplying by the outer chirp matrix $g[p,l]$, and summing the elements of each column. Therefore, the arithmetic complexity is given, in terms of numbers of complex multiplications, $\mathrm{M}_{\mathrm{C}}^{\mathrm{o}}(Q)$, and complex additions, $\mathrm{A}_{\mathrm{C}}^{\mathrm{o}}(Q)$, by

$$\mathrm{M}_{\mathrm{C}}^{\mathrm{o}}(Q) = P\tfrac{Q}{2}\log_2(Q) + 2N, \tag{3.25a}$$

$$\mathrm{A}_{\mathrm{C}}^{\mathrm{o}}(Q) = PQ\log_2(Q) + N - Q. \tag{3.25b}$$

Clearly, the reduction in the number of complex multiplications, when LDSmFrFT is used instead of DSmFrFT, is given by $N/2\log_2 P - N$; this means that Q must not be greater than $N/4$ for the algorithm to be efficient. Note that $N\log_2 P - N + Q$ complex additions are also saved.

3.4.4 DSmFrFT of a Discrete-Time Delayed Signal

An important aspect for applications such as DoA estimation concerns the discrete-time-shift property of discrete FrFT. In this context, let $\mathcal{L}^{\mathbf{A}}\{x[r - r_\theta]\}$ be the DSmFrFT of the discrete-time delayed signal $x[r - r_\theta]$. Using (3.20), one has

$$\mathcal{L}^{\mathbf{A}}\{x[r-r_\theta]\} = \frac{1}{\sqrt{jN}} \sum_{r=-\infty}^{\infty} x[r-r_\theta] e^{-j\frac{\pi}{N}\left(2rq - r^2\cot\alpha\right)}.$$

Substituting $r = n + r_\theta$, one obtains

$$\begin{aligned}\mathcal{L}^{\mathbf{A}}\{x[r-r_\theta]\} &= \frac{1}{\sqrt{jN}} \sum_{n=-\infty}^{\infty} x[n] e^{-j\frac{\pi}{N}\left[2(n+r_\theta)q - (n+r_\theta)^2\cot\alpha\right]} \\ &= e^{-j\frac{\pi}{N}\left(2r_\theta q - r_\theta^2\cot\alpha\right)} X_a[q - r_\theta\cot\alpha].\end{aligned}$$

For the estimation of DoA, assume that the delay τ_m between the m-th element relative to the reference element generates a shift of r_θ points, that is, $r_\theta = f_s\tau_m$. Then, the index q_0 corresponding to reference sensor is shifted to

$$q_m = q_0 + f_s\tau_m\cot\alpha_0, \tag{3.26}$$

where q_m is the index of the peak position in the DSmFrFT spectrum of the signal received at the m-th sensor.

3.4.5 DSmFrFT of an LFM Signal

Estimating the parameters of a linear chirp is based on the fact that the FrFT of an LFM signal gradually converges to an impulse in the fractional Fourier domain as the fractional order approaches the optimal value (LIU; XIAO; WANG, 2021). Analogously, the DSmFrFT of a discrete-time chirp signal $s[r]$ can be expressed in its discrete LCT form as

$$\{\mathcal{L}^{\mathbf{A}}s\}[q] = \frac{1}{\sqrt{jN}} \sum_{r=-N/2}^{N/2-1} e^{j2\pi\left[\left(\frac{f_c}{f_s}-\frac{q}{N}\right)r+\left(\frac{\mu}{f_s^2}+\frac{\cot\alpha}{N}\right)\frac{r^2}{2}\right]},$$

when $\mathbf{A} = (\cot\alpha, 1; -1, 0)$. Using an energy aggregation analysis, the peaks can be determined equalling to zero the coefficients of the polynomial in the variable r in the exponent of the last equation. This leads to the following relationships between f_c and the index of peak q_0, as well as μ and the optimal rotation angle α_0:

$$f_c = \tfrac{1}{N} q_0 f_s, \tag{3.27a}$$

$$\mu = -\tfrac{1}{N} f_s^2 \cot\alpha_0. \tag{3.27b}$$

In this case, $\alpha_0 = a_0\pi/2$, with a_0 being the optimal order of DSmFrFT. Table 2 summarizes the formulas for stimating chirp parameters depending on DFrFT and DSmFrFT. It can be observed that DFrFT (CM–FFT–CM) and DSmFrFT result in identical expressions when $\Delta_t = 1/\sqrt{N}$. Consequently, in the subsequent analysis, only the DFrFT (CM–CC–CM) and the DSmFrFT are considered for comparison. Note that, when the center frequency is known, a peak search is required in a 1D space only. In other words, the position of the peak on the fractional axis can be determined directly from the sampling parameters, that is, f_s and N. In this way, we have essentially found two advantages in using DSmFrFT instead of DFrFT: (i) the lower arithmetic complexity, since it requires one DFT only; (ii) for a given f_c, one requires a peak search in 1D space only. Consequently, the overall computational cost of GSS for a single-component chirp is $\mathcal{O}(N\log_2 N)$, since the cost of directly computing the DSmFrFT only at the index q_0 is $\mathcal{O}(N)$. In the case of a multi-component LFM signal with f_c in the range between the lower frequency f_1 and the upper frequency f_2, the intervals for the index q_0 can be determined in advance, when DSmFrFT is used. Specifically, these indices fall into the range f_1N/f_s to f_2N/f_s. As a result, it is not necessary to compute all the points of DSmFrFT.

Table 2 – Formulas for estimating chirp parameters depending on the FrFT Algorithms.

CM–CC–CM	CM–FFT–CM	DSmFrFT
$f_c = \frac{1}{N} q_0 f_s \csc\alpha_0$	$f_c = \frac{1}{N} q_0 f_s$	$f_c = \frac{1}{N} q_0 f_s$
$\mu = -\frac{1}{N} f_s^2 \cot\alpha_0$	$\mu = -f_s^2 \Delta_t^2 \cot\alpha_0$	$\mu = -\frac{1}{N} f_s^2 \cot\alpha_0$
$q_m = q_0 + f_s \tau_m \cos\alpha_0$	$q_m = q_0 + f_s \tau_m \Delta_t^2 N \cot\alpha_0$	$q_m = q_0 + f_s \tau_m \cot\alpha_0$

Source: The author (2025).

4 CM–CC–CM DECOMPOSITION IN $\mathbb{Z}_{2^b+1}$

In this chapter, we first present the preliminaries for performing complex convolution over the ring of integers modulo 2^b+1 (the ring $\mathbb{Z}_{2^b+1}$). In particular, for the fifth- and sixth-order Fermat numbers, the corresponding structures are no longer finite fields but instead form rings of integers. Subsequently, we introduce circular-convolution-based algorithms for the digital computation of the FrFT, showing how these convolutions can be computed efficiently using Fermat number transforms. The adopted strategy evaluates the sampling-type DFrFT based on the CM–CC–CM decomposition in $\mathbb{Z}_{2^b+1}$, where the core stage is a circular convolution. In this context, we also examine the diminished-1 representation, the bounding method used to prevent amplitude aliasing, and the overlap-and-save technique for handling long convolutions.

4.1 FERMAT NUMBER TRANSFORMS

The Fermat number transform (FNT) of the sequence $\{v_i \mid i = 0, 1, \ldots, N-1\}$ over the finite field $\mathrm{GF}(p)$, with $p = 2^b + 1$ a Fermat prime (where $b = 2^t$ for $0 \leq t \leq 4$), is defined as

$$V_k = \sum_{i=0}^{N-1} \omega^{ik} v_i \,(\mathrm{mod}\ p), \quad k = 0, 1, \ldots, N-1, \tag{4.1}$$

where ω is an Nth root of unity over $\mathrm{GF}(p)$, i.e., $\omega^N \equiv 1 \pmod{p}$. It is well known that the element 2 has order $2b$ in $\mathrm{GF}(2^b+1)$, since $2^b + 1 \equiv 0$, $2^b \equiv -1$, and $2^{2b} \equiv 1 \pmod{p}$. This implies that the possible block lengths are given by $N = 2^{t+1}$.

In applications such as digital filtering (DAHER et al., 2021), the algorithm depends on whether the resulting sequence, after applying the FNTs and pointwise multiplication, can be converted back to the original sequence by performing the inverse FNT (IFNT). Specifically, the IFNT of the sequence $\{V_k | k = 0, 1, \ldots, N-1\}$ is defined as

$$v_i = N^{-1} \sum_{k=0}^{N-1} \omega^{-ik} V_k \,(\mathrm{mod}\ p), \quad i = 0, 1, \ldots, N-1, \tag{4.2}$$

where N^{-1} is the inverse of N over $\mathrm{GF}(p)$, $N^{-1}N \equiv 1 \,(\mathrm{mod}\ p)$. Since N is a power of two, its inverse can be obtained as $2^{-n} = -2^{b-n} \,(\mathrm{mod}\ p)$. As a consequence of the element ω being of order N, its inverse can be immediately given as $\omega^{-1} = \omega^{N-1} \,(\mathrm{mod}\ p)$ (AGARWAL; BURRUS, 1974a). One way to use fast FNT algorithms for IFNT is calculating the sequence $v'_i = v_{-i}$, so the final result is obtained by the sequence reversal process, that is, $v_i = v'_{\langle N-i \rangle_N}$.

4.1.1 Radix-2^s Algorithm for FNT

Since the definitions of FNT and DFT are very similar, the Cooley-Tukey algorithm can be used for FNT in an analogous way (COOLEY; TUKEY, 1965). Let us assume that $N = L \cdot M$,

then, the input mapping and the output mapping can be respectively denoted as

$$i = l + mL,\ k = qM + r,\ \begin{cases} l, q = 0, 1, ..., L-1, \\ m, r = 0, 1, ..., M-1. \end{cases} \tag{4.3}$$

After that, two-dimensional (2D) variables can be defined as $v_{l,m} = v_{l+mL}$ and $V_{q,r} = V_{qM+r}$. Substituting i and k in (4.1), considering that ω has order N in $\mathrm{GF}(p)$, that is, $\omega^N{=}1 \pmod p$, the FNT in terms of 2D variables becomes

$$V_{q,r} = \sum_{l=0}^{L-1} \omega^{lqM} \left[\omega^{lr} \sum_{m=0}^{M-1} \omega^{mrL} v_{l,m} \right] \pmod p, \tag{4.4}$$

where ω^{lr} is a twiddle factor in $\mathrm{GF}(p)$. Note that ω^L has order M in $\mathrm{GF}(p)$, $(\omega^L)^M \equiv 1 \pmod p$, which makes the inner sum corresponding to be an M-point FNT. Identically, since ω^M has order L in $\mathrm{GF}(p)$, $(\omega^M)^L \equiv 1 \pmod p$, the outer sum becomes an L-point FNT. The Cooley-Tukey algorithm consists of input mapping, M-point FNTs of the rows (of a matrix), point-wise multiplication with the twiddle-factor matrix $\mathbf{\Omega} = [\omega^{lr}]$, L-point FNTs of the columns and output mapping (DUHAMEL; VETTERLI, 1990). Notice that the twiddle-factor matrix has $L/2 \times M/2$ elements that are odd power of ω.

Figure 7 – Radix-L Cooley-Tukey mapping for an N-point FNT ($L = 2$ and $N = 8$).

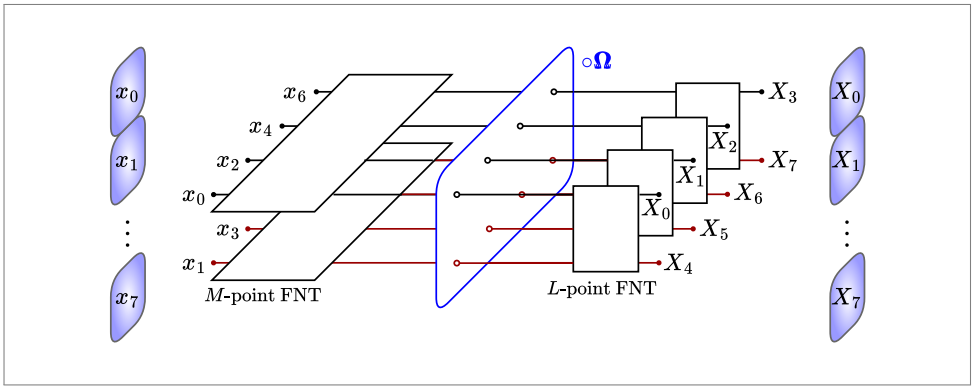

Source: The author (2025).

The 2^n-point FNT, as given in (4.4), where n is a positive integer, with L equal to 2 and M equal to 2^{n-1}, becomes a decimation-in-time radix-two FNT algorithm in $\mathrm{GF}(p)$. This process is illustrated in Figure 7. When $\omega{=}2$, for instance, the 32-point FNT over $\mathrm{GF}(2^{16}+1)$ is given by

$$V_k = \sum_{i=0}^{31} 2^{ik} v_i \pmod p, \quad k = 0, 1, \ldots, 31. \tag{4.5}$$

Thus, an N-point FNT only requires $N \log_2 N$ additions and bit-shifts. As the blocklength $N{=}2b$ can be too short for many applications, one possibility is to use $\sqrt{2}{=}2^{\frac{b}{4}}(2^{\frac{b}{2}} - 1)$ as the kernel of FNT (AGARWAL; BURRUS, 1974a), this element has order $4b$ in $\mathrm{GF}(2^b + 1)$, then the

possible blocklengths are $N = 2^{t+2}$, where $2 \leq t \leq 4$. In a particular way, the 64-point FNT over $\mathrm{GF}(2^{16}+1)$ can be expressed as

$$V_k = \sum_{i=0}^{63} \left(2^{12} - 2^4\right)^{ik} v_i \,(\mathrm{mod}\, p), \quad k = 0, 1, \ldots, 63. \tag{4.6}$$

In this case, as every even power of $\sqrt{2}$ is a power of two, and every odd power of $\sqrt{2}$ is equal to a power of two times $2^{\frac{b}{4}}(2^{\frac{b}{2}} - 1)$ (BLAHUT, 2010, p. 315); given a positive integer d, the $(2d+1)$-th power of $\sqrt{2}$ can be written as $2^{d_1} - 2^{d_2} \,(\mathrm{mod}\, p)$, where $d_1 = d + \frac{3b}{4} \,(\mathrm{mod}\, 2b)$ and $d_2 = d + \frac{b}{4} \,(\mathrm{mod}\, 2b)$ (XING et al., 2024). Therefore, assuming that a subtraction costs the same as an addition, an N-point FNT involves $N/4 + N \log_2 N$ additions and bit-shifts only ($N/4$ is the number of factors in the form $2^{d_1} - 2^{d_2}$).

In general form, considering that the element 2 has order $2b$ in $\mathrm{GF}(2^b+1)$, the kernel ω in terms of the blocklength N can be expressed as $\omega = 2^{\frac{2b}{N}}$, where $N \in \{2, 2^2, \ldots, 2^b\}$. Table 3 provides the possible parameters for the implementation of an N-point FNT. In this context, writing $\omega = \sqrt[m]{2}$, where $m = \frac{N}{2b}$, we can consider that there are m elements whose m-th power equals 2; specifically, $r_i^m \equiv 2 \,(\mathrm{mod}\, p)$ for $1, 2, \ldots, m$. To select the kernel ω, these elements are ordered as $r_1 < r_2 < \ldots < r_m$, and ω is chosen as r_1. When b is 8 or 16, an efficient method for calculating the 2^n-point FNT, where $2^n > 4b$, is the radix-2^s algorithm. This means selecting $L = 2^s$ in (4.4). In such manner, the arithmetic complexity of a 2^n-point FNT over $\mathrm{GF}(2^b+1)$, $s < n \leq b$, in terms of the numbers of multiplications, $\mathrm{M}_b(2^n)$, and additions, $\mathrm{A}_b(2^n)$, in recursive form of radix-2^s algorithm, can be obtained as

$$\mathrm{M}_b(2^n) = 2^s \mathrm{M}_b(2^{n-s}) + 2^{n-s} \mathrm{M}_b(2^s) + \mathrm{M}_b^{\mathbf{\Omega}}(2^n, 2^s);$$
$$\mathrm{A}_b(2^n) = 2^s \mathrm{A}_b(2^{n-s}) + 2^{n-s} \mathrm{A}_b(2^s),$$

where $\mathrm{M}_b^{\mathbf{\Omega}}(2^n, 2^s)$ is the number of non-trivial multiplications needed to compute the element-wise product by the twiddle-factor matrix. Notice that the 2^n-point FNT, where $2 \leq n \leq s$, is a multiplier-less algorithm.

Finally, notice that $\omega^{\frac{m}{2}}$ equals $\sqrt{2}$; however, this value can sometimes correspond to $2^{\frac{b}{4}}(1 - 2^{\frac{b}{2}}) \,(\mathrm{mod}\, p)$ and can serve as the kernel for the $(4b)$-point FNT in the radix-$(4b)$ algorithm, as detailed in Table 4. Taking this into account, the use of $L = 4b$ is more efficient than $2b$ in terms of the number of multiplications, as the smallest possible value of $\mathrm{M}_b^{\mathbf{\Omega}}(2^n, 2^s)$ is obtained as $2^n - 2^s - 2^{n-s}$. This occurs because the first column and the first row of the twiddle-factor matrix contain only ones, and a trivial-factor element $\omega^{lr} = 2^{\frac{b}{2}}$ appears when $l = L/2$ and $r = M/2$. However, since this reduction in multiplications comes at the cost of increasing additions, we consider $L = 2b$ in the subsequent sections.

4.1.2 Two-Dimensional Fermat Number Transform

In convolution implementations, an N_1-length sequence is usually arranged into a $2L \times R$ matrix when $N_1 = L \cdot R$. Therefore, let $[V_{q,r}]$ denote the two-dimensional Fermat number

Table 3 – Possible parameters of the FNT and the root of unity ω for different N.

t	b	F_t	N									
			2	2^2	2^3	2^4	2^5	2^6	2^7	2^8	$\cdots$	2^{16}
0	1	2^1+1	2									
1	2	2^2+1	2^2	2								
2	4	2^4+1	2^4	2^2	2	$\sqrt{2}$						
3	8	2^8+1	2^8	2^4	2^2	2	$\sqrt{2}$	$\sqrt[4]{2}$	$\sqrt[8]{2}$	$\sqrt[16]{2}$		
4	16	2^{16}+1	2^{16}	2^8	2^4	2^2	2	$\sqrt{2}$	$\sqrt[4]{2}$	$\sqrt[8]{2}$	$\cdots$	$\sqrt[2048]{2}$
5	32	2^{32}+1	2^{32}	2^{16}	2^8	2^4	2^2	2	$\sqrt{2}$			
6	64	2^{64}+1	2^{64}	2^{32}	2^{16}	2^8	2^4	2^2	2	$\sqrt{2}$		

Source: Adapted from Xing et al. (2024).

Table 4 – The kernel of 2^n-point FNT over $\mathrm{GF}(2^b + 1)$ is calculated as the m-th root of 2, $\omega = \sqrt[m]{2}$, and its $(m/2)$-th power (modulo $2^b + 1$) is the square root of 2, $\omega^{\frac{m}{2}} = \sqrt{2}$.

n	$b = 8$			$b = 16$		
	m	ω	$\omega^{\frac{m}{2}}$	m	ω	$\omega^{\frac{m}{2}}$
5	2	60	60			
6	4	35	197	2	4080	4080
7	8	42	197	4	4938	4080
8	16	27	197	8	5574	4080
9				16	5589	61457
10				32	5851	61457
11				64	3623	4080
12				128	87	4080
13				256	875	4080
14				512	79	61457
15				1024	367	4080
16				2048	23	4080

Source: The author (2025).

transform (2D-FNT) of $[v_{m,l}]$; this operator is defined as

$$V_{q,r} = \sum_{m=0}^{M-1} \sum_{l=0}^{2L-1} v_{l,m} \omega_{2L}^{lq} \omega_R^{mr} \pmod{p}, \tag{4.7}$$

where $q = 0, 1, \ldots, 2L-1$ and $r = 0, 1, \ldots, R-1$. The elements ω_{2L} and ω_R have order $2L$ and R over $\mathrm{GF}(p)$, respectively. Note that (4.7) can be implemented using one-dimensional butterfly algorithms, i.e., applying (one-dimensional) FNTs to the matrix rows and then to the columns. Therefore, R times $2L$-point FNTs and $2L$ times R-point FNTs are required to compute a 2D-FNT. The back conversion can be performed using the 2D inverse Fermat number transform

(2D-IFNT), which can be written as

$$v_{l,m} = (2N)^{-1} \sum_{r=0}^{R-1} \sum_{q=0}^{2L-1} V_{q,r} \omega_{2L}^{-lq} \omega_{M}^{-mr} \pmod{p}. \tag{4.8}$$

In similar way to the one-dimensional case, the 2D-FNT can be used for computing (4.8) as $v'_{l,m}{=}v_{-l,-m}$, then the sequence reversal is given by $v_{l,m}{=}v'_{\langle 2L-l\rangle_{2L},\langle R-m\rangle_R}$.

In practical scenarios, the Fermat primes $(F_0, F_1, \ldots, F_4)$ may not be large enough for applications involving convolutions. Consequently, it may be necessary to consider F_5 and F_6. However, the corresponding Fermat numbers $2^b + 1$ with $b = 32, 64$ have been proven to be composite, and their prime factors are known to be of the form $k{\cdot}2^{t+2}{+}1$ (AGARWAL; BURRUS, 1974a). As a result, the FNT methods discussed above can still be applied, but the maximum feasible transform length is limited to $N = 2^{t+2}$, where $t = 5, 6$. This upper bound is often too small for many applications, particularly those that require long convolutions. An approach to address this limitation is to map a one-dimensional convolution onto a two-dimensional convolution (AGARWAL; BURRUS, 1974b).

4.2 DIGITAL COMPUTATION OF THE FrFT IN $\mathbb{Z}_{2^b+1}$

In this section, we consider the digital computation of the FrFT through the CM–CC–CM decomposition in the ring $\mathbb{Z}_{2^b+1}$, in which a simple way to implement the chirp convolution stage is to use Fermat number transforms (NUSSBAUMER, 1976). This implies representing the in-phase and quadrature components over the ring of integers modulo Fermat number, $F_t = 2^b + 1$, when $b = 2^t$, $t = 0, 1, \ldots, 6$. Remark that only integers $0, 1, \ldots, 2^b$ are allowed in this modular arithmetic when the elements of the original sequences are given in the range $\left[-2^{b-1}, 2^{b-1}\right]$, negative integers are represented by adding $2^b{+}1$ (AGARWAL; BURRUS, 1974a). In the referred ring of integers, $b + 1$ bits are required to represent all of elements; the additional bit is necessary to represent the value $2^b = -1 \pmod{F_t}$. In binary arithmetic, the diminished-1 representation is a way to avoid additions and multiplications involving the additional bit (LEIBOWITZ, 1976); the integers from 1 to 2^b are represented in binary numbers from 0 to 2^{b-1}.

4.2.1 Diminished-1 Arithmetic

Let x and y be two $(b + 1)$-bit numbers, with $0 \leq x, y \leq 2^b$, and let x_d and y_d represent their diminished-1 forms such that $x_d = \langle x - 1\rangle_{2^b+1}$ and $y_d = \langle y - 1\rangle_{2^b+1}$. Strategically, each arithmetic operation modulo $2^b + 1$ can be expressed as the corresponding diminished-1 operations (LEIBOWITZ, 1976; BAOZHOU et al., 2019), as outlined in the following items:

- *Addition*: The addition of two numbers is determined by their most significant bit (MSB); the operation is inhibited if the MSB of either addend is 1. If this bit of both addend is 0, the operation is performed, then the complement of the carry is added to b least significant

bits (LSBs) of the sum, which can be expressed numerically as

$$f_{\mathrm{A}}(x_d, y_d, b) = \begin{cases} x_d, & y_d = 2^b, \\ y_d, & x_d = 2^b, \\ s - 2^b, & x_d \neq 2^b,\ y_d \neq 2^b,\ s \geq 2^b, \\ s + 1, & x_d \neq 2^b,\ y_d \neq 2^b,\ s < 2^b, \end{cases} \qquad \text{where } s = x_d + y_d.$$

The condition $s \geq 2^b$ is equivalent to detecting a carry–out in the b-bit addition of x_d and y_d, which occurs precisely when the most significant bit of the sum is 1. This operation requires a b-bit inverted-end-around-carry (IEAC) adder for its implementation (XING et al., 2024).

- *Negation*: The negative of a nonzero number is represented by taking the complement of its b LSBs, that is

$$f_{\mathrm{N}}(x_d, b) = \begin{cases} x_d, & x_d = 2^b, \\ x_d \oplus (2^b - 1), & x_d \neq 2^b, \end{cases}$$

where $\oplus$ denotes the bitwise XOR operator; that is to say, a b-bit inversion.

- *Subtraction*: The subtraction of two numbers is achieved by negating the subtrahend and then adding it to the minuend, which can be expressed as follows

$$f_{\mathrm{S}}(x_d, y_d, b) = f_{\mathrm{A}}\left(x_d, f_{\mathrm{N}}(y_d, b), b\right).$$

This operation can be performed using a b-bit inversion followed by a b-bit IEAC adder.

- *Left shift*: Multiplying a number by 2 can be understood as adding the number by itself. This can be expressed as

$$f_{\mathrm{LS}}(x_d, b) = \begin{cases} x_d, & x_d = 2^b, \\ s - 2^b, & x_d \neq 2^b,\ s \geq 2^b, \\ s + 1, & x_d \neq 2^b,\ s < 2^b, \end{cases}$$

where $s = 2x_d$ is a left bit-shift ($s = x_d \ll 1$). Note that multiplying by an n-th power of 2 is the same as applying an inverted circular shift (ICS) $n \pmod{2b}$ times.

- *Multiplication*: One basic method of multiplying two numbers involves converting either the multiplier or the multiplicand to standard binary form (LEIBOWITZ, 1976). Next, residue reduction is done by subtracting the b MSBs of the binary product from its b LSBs using diminished-1 subtraction. In conditional form, it is

$$f_{\mathrm{M}}(x_d, y_d, b) = \begin{cases} f_{\mathrm{N}}(x_d, b), & y_d = 2^b - 1, \\ f_{\mathrm{N}}(y_d, b), & x_d = 2^b - 1, \\ f_{\mathrm{S}}(m_{\mathrm{LSBs}}, m_{\mathrm{MSBs}}, b), & \text{otherwise}, \end{cases}$$

where $m = x \cdot y$ is a binary multiplication. Strategically, one operand can expressed in weighted representation, and the other in diminished-1 representation (VERGOS; DIMITRAKOPOULOS; NIKOLOS, 2005). Let $y = (\beta_b, \beta_{b-1}, \ldots, \beta_0)$ be a binary number; then the weighted multiplication can be represented as

$$f_{\mathrm{W}}(x_d, y, b) = \sum_{i=0}^{b-1} \beta_i \cdot (2^i \cdot x)_d \,(\mathrm{mod}\ 2^b + 1),$$

where $(2^i \cdot x)_d$ denotes the i-th left bit shift, which is part of the diminished-1 operations. In canonical signed digit (CSD) representation, a single constant multiplication is equivalent to $b/3$ additions on average and $b/2$ additions in the worst case (VORONENKO; PÜSCHEL, 2007).

Note that a binary number can be converted to its diminished-1 form by performing a diminished-1 addition between it and the binary value of $2^b - 1$; to be specific, $x_d = f_{\mathrm{A}}\left(x, 2^b - 1, b\right)$. To convert back, complement the MSB of a number in diminished-1 representation and add it to the LSBs.

4.2.2 Complex Multiplication over $\mathbb{Z}_{2^b+1}$

In the commutative ring with unity $\mathbb{Z}_m$, where $m = 2^b + 1$ is a Fermat number, the element 2 is invertible because $\gcd(2, m) = 1$, as m is odd. Similarly, the element $r = 2^{b/2}$ is invertible and satisfies $r^2 \equiv -1 \pmod{m}$. More specifically, the inverses of 2 and r are given by

$$2^{-1} \equiv -2^{b-1}, \qquad r^{-1} \equiv -r \equiv -2^{b/2} \pmod{m}.$$

For any scalars $a, \hat{a}, c, \hat{c} \in \mathbb{Z}_m$, define the Hermitian pairs as

$$u = a + r\hat{a}, \qquad \bar{u} = a - r\hat{a}, \qquad v = c + r\hat{c}, \qquad \bar{v} = c - r\hat{c} \pmod{m}.$$

Let the modular products be $U = uv$ and $\bar{U} = \bar{u}\,\bar{v}$. Then, it follows that

$$U + \bar{U} = 2(ac - \hat{a}\hat{c}), \qquad U - \bar{U} = 2r(a\hat{c} + \hat{a}c) \pmod{m}.$$

Thus, the product $(a + r\hat{a})(c + r\hat{c}) = x + ry$, where

$$x = 2^{-1}(U + \bar{U}), \qquad y = 2^{-1}r^{-1}(U - \bar{U}) \pmod{m},$$

can be computed using only two modular multiplications (to form U and $\bar{U}$), and when $(c \pm r\hat{c})$ can be precomputed, it involves only four modular additions.

4.2.3 Circular Convolution in $\mathbb{Z}_{2^b+1}$

Computing (3.3) in $\mathbb{Z}_{2^b+1}$ requires $4N$ multiplications and $8N$ additions in the chirp multiplication stages, assuming that complex multiplication is performed in quadratic residue number systems (KRISHNAN; JULLIEN; MILLER, 1986), as described above. Furthermore, an efficient way to implement the chirp convolution stage is the method introduced in (NUSSBAUMER, 1976), which, based on the convolution theorem, performs the FNT of the in-phase and quadrature components, followed by pointwise complex multiplication and IFNT of these components. Consequently, an N_1-point complex circular convolution requires two N_1-point FNTs, $2N_1$ multiplications, $4N_1$ additions and two N_1-point IFNTs (XING et al., 2024). Therefore, the arithmetic complexity of an N-point DFrFT can be expressed, in terms of the number of diminished-1 multiplications, $\mathrm{M}_1(\cdot, b)$, and diminished-1 additions, $\mathrm{A}_1(\cdot, b)$, as

$$\mathrm{M}_1\left(N, b\right) = 8N + 4\mathrm{M}_b\left(2N\right); \tag{4.9a}$$

$$\mathrm{A}_1\left(N, b\right) = 16N + 4\mathrm{A}_b\left(2N\right), \tag{4.9b}$$

where $\mathrm{M}_b\left(\cdot\right)$ and $\mathrm{A}_b\left(\cdot\right)$ denotes the arithmetic complexity of the one-dimensional FNT in the diminished-1 representation (modulo $2^b + 1$).

After performing the operations, the final result is obtained by converting back to the interval $\left[-2^{b-1}, 2^{b-1}\right]$. In this context, amplitude overflow (or aliasing) can occur in some scenarios. In the following, we explain how to avoid it. Let $\{g_n\}$ and $\{h_n\}$ be two complex sequences whose elements are given as $a_n + j\hat{a}_n$ and $c_n + j\hat{c}_n$, $n = 0, 1, \ldots, N-1$, respectively. In relation to DFrFT computing via (3.3), the discrete input signal can be represented in polar form as $x_r = |x_r|\, e^{j\phi_r}$, $\phi_r = \arg[x_r]$. Furthermore, each non-zero element of $\{g_n\}$ corresponds to the chirp-modulated input signal, that is

$$g_n = |x_r|\, e^{j\phi_r} e^{-j\frac{\pi}{N} r^2 \tan\left(\frac{\alpha}{2}\right)}, \quad r = n - N/2.$$

Note that the extreme values of g_n are bounded by $|x_r|$. In order to bound the discrete circular convolution $y_n = (g \circledast h)_n$, one assumes that

$$|y_n| \leq \max_r |x_r| \sum_{n=0}^{N-1} \sqrt{c_n^2 + \hat{c}_n^2} \leq F_t/2, \tag{4.10}$$

is satisfied; a generalized form of triangular inequality.

For long signals ($N > 2^b$), the one-dimensional convolution can be remapped into a 2D scheme using the overlap-and-save (OaS) method (AGARWAL; BURRUS, 1974b). Let us assume that the length of the circular convolution given in (3.4) is factored as $N_1 = L \cdot R$, then the 2D mapping is given by

$$n = l + mL,\ i = q + rL,\ \begin{cases} l, q = 0, 1, ..., L-1, \\ m, r = 0, 1, ..., R-1; \end{cases} \tag{4.11}$$

that is, a two-dimensional $L \times R$ array is obtained from the original sequence as $\dot{y}_{(l,m)} = y_{(l+mL)}$; the columns of $[\dot{y}_{l,m}]$ are the blocks of the sequence $\{y_n\}$. Similarly, $\dot{g}_{l,m}$ and $\dot{h}_{l,m}$ are elements of the two-dimensional versions of $\{g_n\}$ and $\{h_n\}$, respectively. After that, let $\ddot{g}$ be the $(2L-1)\times R$ array formed by appending $(L-1)$ rows of zeros to the bottom of $\dot{g}$, and let $\ddot{h}$ be the $(2L-1)\times R$ array formed so that its top columns contain the periodic extension of the original $\dot{h}$ with period N_1. For implementations that use transforms, the arrays are usually extended one additional row to be $2L \times R$ (AGARWAL; BURRUS, 1974b). Therefore, the two-dimensional cyclic convolution of the extend arrays can be denoted as

$$\ddot{y}_{(l,m)} = (\ddot{g} \circledast \ddot{h})_{(l,m)} = \sum_{r=0}^{R-1} \sum_{q=0}^{2L-1} \ddot{g}_{(q,r)} \ddot{h}_{(l-q,m-r)}, \tag{4.12}$$

where the bottom $L \times R$ partition of $\ddot{y}$ is $\dot{y}$, and the columns of $\dot{y}$ are the desired blocks of y in (3.4). In this way, an N_1-length complex circular convolution consumes two 2D-FNTs, two 2D-IFNTs, $4N_1$ multiplications and $8N_1$ additions (XING et al., 2024). If we consider computing an N-point DFrFT, where N is a composite number $N = L \cdot M$, the factor R is $2M$, since N zeros have been appended to the input sequence (see Figure 8). In this case, the arithmetic complexity can be expressed in terms of numbers of diminished-1 multiplications, $\mathrm{M}_2(\cdot, b)$, and diminished-1 additions, $\mathrm{A}_2(\cdot, b)$, as

$$\mathrm{M}_2(N, b) = 12N + 4\mathrm{M}_b(2L, 2M); \tag{4.13a}$$

$$\mathrm{A}_2(N, b) = 24N + 4\mathrm{A}_b(2L, 2M), \tag{4.13b}$$

where $\mathrm{M}_b(\cdot,\cdot)$ and $\mathrm{A}_b(\cdot,\cdot)$ represent the number of multiplications and additions performed when applying two-dimensional FNT (mod $2^b + 1$), respectively.

Figure 8 – Mapping DFrFT as 2D convolution; $[g_{l,m}]$ and $[\ddot{y}_{l,m}]$ are $L \times M$ matrices that respectively represent the input and output of the 2D convolution, $[0]$ represents a null matrix, $[\ddot{h}_{l,m}]$ is a $2L \times 2M$ matrix, and [■] represents a matrix whose elements are ignored when forming the output sequence.

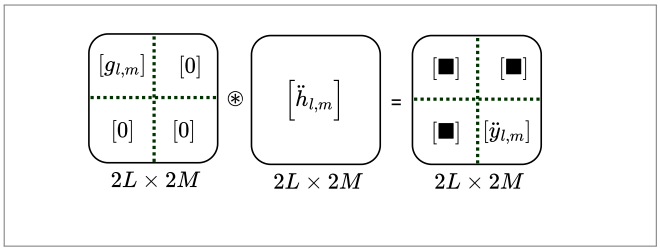

Source: The author (2025).

5 OPTIMIZED CM–CC–CM DECOMPOSITION OVER $\mathbb{Z}_{2^b+1}$

In this chapter, the in-phase and quadrature components of the signals of interest are assumed to be represented in the ring $\mathbb{Z}_{2^b+1}$, with $b = 32$ or 64. The numerical formulation of the fractional Fourier transform is based on a decomposition into circular convolutions – specifically, the CM–CC–CM scheme employed for computing the DFrFT. Within this framework, we introduce the **local Fermat number transforms** and discuss how redundant computations can be eliminated. Moreover, we propose a **local DFrFT**, an algorithm involving two chirp multiplications and a local circular convolution. The latter operation enables the evaluation of partial results of a (global) circular convolution.

5.1 LOCAL FERMAT NUMBER TRANSFORMS

In applications involving circular convolution and its implementation through discrete transforms, one or both input sequences are typically zero-appended. When signals are represented in $\mathbb{Z}_{2^b+1}$, to avoid operations involving null values during computation of the FNT, we propose the use of the local-input Fermat number transform (LiFNT). In this context, computing only a subset of points of the resulting sequence can be an efficient approach; for this purpose, we propose employing the local-output inverse Fermat number transform (LoIFNT).

Theorem 5.1. *Let $\{v_n \mid n = 0, 1, \ldots, N-1\}$ denote a sequence in the ring $\mathbb{Z}_{2^b+1}$. Then its LiFNT, acting as an operator that yields the FNT of a sequence zero-padded in its second half, is the sequence $\{V_k \mid k = 0, 1, \ldots, 2N-1\}$, whose even- and odd-indexed elements are given by*

$$V_{2r} = \sum_{n=0}^{N-1} v_n \omega_N^{nr} \ (\textit{mod}\ 2^b + 1), \tag{5.1a}$$

$$V_{2r+1} = \sum_{n=0}^{N-1} v_n \omega_{2N}^{n} \omega_N^{nr} \ (\textit{mod}\ 2^b + 1), \tag{5.1b}$$

where $r = 0, 1, \ldots, N-1$. Since ω_K, $K = 2N$, is a primitive K-th root of unity in $\mathbb{Z}_{2^b+1}$, it follows that $\omega_N = \omega_K^2$ is an element of order N.

Proof. These two formulas are derived directly from the definition of FNT analogously using the decimation-in-frequency procedure as follows. The K-point FNT over $\mathbb{Z}_{2^b+1}$ is given by

$$V_k = \sum_{n=0}^{K-1} v_n \omega_K^{nk} \ (\text{mod}\ 2^b + 1), \quad k = 0, 1, \ldots, K-1,$$

where ω_K is a K-th root of unity over $\mathbb{Z}_{2^b+1}$. Let v_{q+s}, for $q = 0, 1, \ldots, Q-1$, denote Q consecutive non-zero elements of the input sequence, where s is the starting index. The expression for V_k can be decomposed as

$$V_k = \sum_{n=0}^{s-1} v_n \omega_K^{nk} + \sum_{n=s}^{s+Q-1} v_n \omega_K^{nk} + \sum_{n=s+Q}^{K-1} v_n \omega_K^{nk} \ (\text{mod}\ 2^b + 1). \tag{5.2}$$

Note that the first and third terms are null because $v_n = 0$. By substituting the index $n = q + s$, one obtains

$$V_k = \omega_K^{sk} \sum_{q=0}^{Q-1} v_{q+s} \omega_K^{qk} \pmod{2^b + 1}. \tag{5.3}$$

Furthermore, when $K = P \cdot Q$, the output sequence can be mapped onto a two-dimensional array, $V_{p,r} = V_{p+rP}$, as

$$V_{p+rP} = \omega_K^{s(p+rP)} \sum_{q=0}^{Q-1} v_{s+q} \omega_K^{q(p+rP)} \pmod{2^b + 1}, \tag{5.4}$$

where $p = 0, 1, \ldots, P-1$ and $r = 0, 1, \ldots, Q-1$. Note that $\omega_Q = \omega_K^P$ is an element of order Q. For $K = 2N$, when the last N elements of $\{v_n\}$ are null, the following settings hold: $s = 0$, $P = 2$, and $Q = N$. The expression then becomes

$$V_{2r+p} = \sum_{q=0}^{N-1} v_q \, \omega_K^{qp} \omega_Q^{qr} \pmod{2^b + 1}. \tag{5.5}$$

Equations (5.1a) and (5.1b) are obtained by setting $p = 0$ and $p = 1$ in V_{2r+p}, respectively. □

Theorem 5.2. *Let $\{V_k \mid k = 0, 1, \ldots, 2N-1\}$ denote a sequence in the ring $\mathbb{Z}_{2^b+1}$, which is the FNT of $\{v_n\}$. Then, under the constraint that N is a power of two, the LoIFNT, acting as an operator that yields the last N consecutive elements of $\{v_n\}$, is given by*

$$\begin{aligned} v_{n+N} =& (2N)^{-1} \sum_{r=0}^{N-1} V_{2r} \omega_N^{-rn} \, (\textit{mod}\ 2^b + 1) \\ & - (2N)^{-1} \omega_{2N}^{-n} \sum_{r=0}^{N-1} V_{2r+1} \omega_N^{-rn} \, (\textit{mod}\ 2^b + 1), \end{aligned} \tag{5.6}$$

where $n = 0, 1, \ldots, N-1$. Since ω_K, $K = 2N$, is a primitive K-th root of unity in $\mathbb{Z}_{2^b+1}$, it follows that $\omega_N = \omega_K^2$ is an element of order N.

Proof. The sequence $\{v_n\}$ can be established by definition of the inverse FNT (IFNT) as

$$v_n = K^{-1} \sum_{k=0}^{K-1} V_k \omega_K^{-kn} \pmod{2^b + 1}, \quad n = 0, 1, \ldots, K-1,$$

where ω_K is a K-th root of unity over $\mathbb{Z}_{2^b+1}$. If the transform length is a composite number $K = P \cdot Q$, by mapping the sequence $\{V_k\}$ as a P-by-Q matrix, $V_{p,r} = V_{p+rP}$, one obtains

$$v_n = K^{-1} \sum_{r=0}^{Q-1} \sum_{p=0}^{P-1} V_{p+rP} \omega_K^{-(p+rP)n} \pmod{2^b + 1}.$$

Then, any Q consecutive points of $\{v_n\}$ can be obtained by substituting $n = q + s$, where s is the starting index, that is

$$v_{q+s} = K^{-1} \sum_{p=0}^{P-1} \omega_K^{-ps} \omega_K^{-pq} \sum_{r=0}^{Q-1} V_{p+rP} \omega_K^{-rsP} \omega_K^{-rqP} \pmod{2^b + 1}.$$

where $q = 0, 1, \ldots, Q-1$. Notice that $\omega_Q = \omega_K^P$ is an element of order Q. In a particular way, when $s = N$, $P = 2$, and $Q = N$, the terms ω_K^{-sP} and ω_K^{-s} become trivial factors, as are 1 and $-1 \pmod{2^b + 1}$, respectively. □

Note that a LiFNT (from N to $2N$ points) consumes N multiplications (by the factor ω_{2N}^n) and two N-point FNTs; $2N$ additions are saved by using a LiFNT instead of an FNT. Calculating the last N consecutive points of the $(2N)$-point IFNT, as a LoIFNT (from $2N$ to N points), requires N additions, N multiplications (by the factor ω_{2N}^{-n}), and two N-point IFNTs; N additions are saved by using a LoIFNT instead of an IFNT.

The two-dimensional forms of these transforms are defined as follows. The 2D-LiFNT applies the LiFNT to each row of an $L \times M$ matrix, producing an $L \times 2M$ matrix, and then applies the LiFNT to each column to obtain the final $2L \times 2M$ matrix. In this manner, a total of $6LM$ additions and L instances of $(2M)$-point FNTs are saved when using 2D-LiFNT instead of 2D-FNT. Similarly, the 2D-LoIFNT applies the LoIFNT to each row of a $2L \times 2M$ matrix, producing a $2L \times M$ matrix, and then applies the LoIFNT to each column to obtain the final $L \times M$ matrix. This form saves a total of $3LM$ additions and M instances of $(2L)$-point IFNTs when 2D-LoIFNT is used instead of 2D-IFNT.

5.2 CIRCULAR CONVOLUTION OVER $\mathbb{Z}_{2^b+1}$ FOR DFrFT

In this section, we present how (3.4) can be computed using local Fermat number transforms under two schemes: a one-dimensional scheme and a two-dimensional scheme. These optimized implementations, proposed as the chirp-convolution stage for computing an N-point DFrFT, are shown in Fig. 9.

5.2.1 Proposed 1D Convolution Scheme

The procedure in (3.3) is referred to as the CM–CC–CM (mod 2^b+1) decomposition when implemented over the ring $\mathbb{Z}_{2^b+1}$. This subsection details the realization of its chirp-convolution stage using a one-dimensional circular convolution. The method operates on a chirp-modulated input sequence $\{g_n \mid n = 0, \ldots, N-1\}$ and a chirp sequence $\{h_n \mid n = 0, \ldots, 2N-1\}$. In this context, the last N points of the circular convolution, y_{n+N}, $n = 0, \ldots, N-1$, can be obtained as described in the following steps:

Figure 9 – The signal flow graph of the circular convolution $y_n = (g \circledast h)_n$, with $n = N, N+1, \ldots, 2N-1$, in which the last N elements of the input sequence are null values, that is $g_n = 0$, $N \leq n < 2N$; (a) 1D case and (b) 2D case.

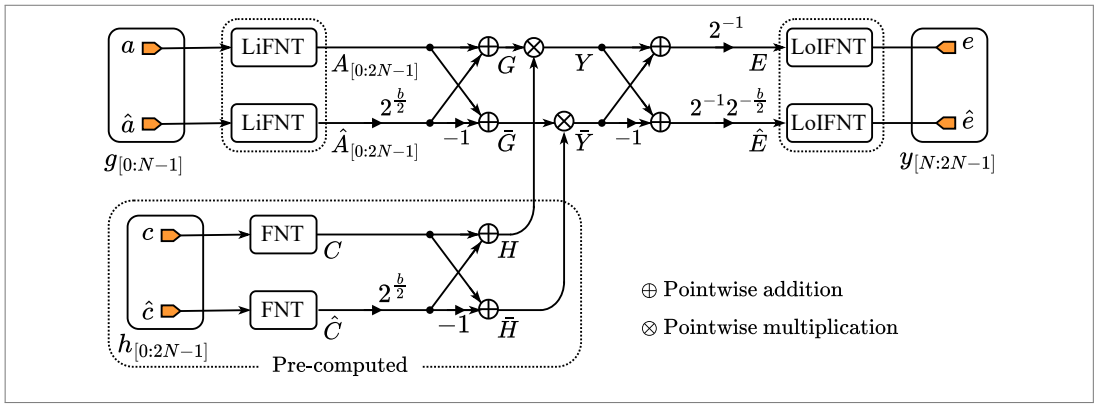

(a) 1D Convolution scheme.

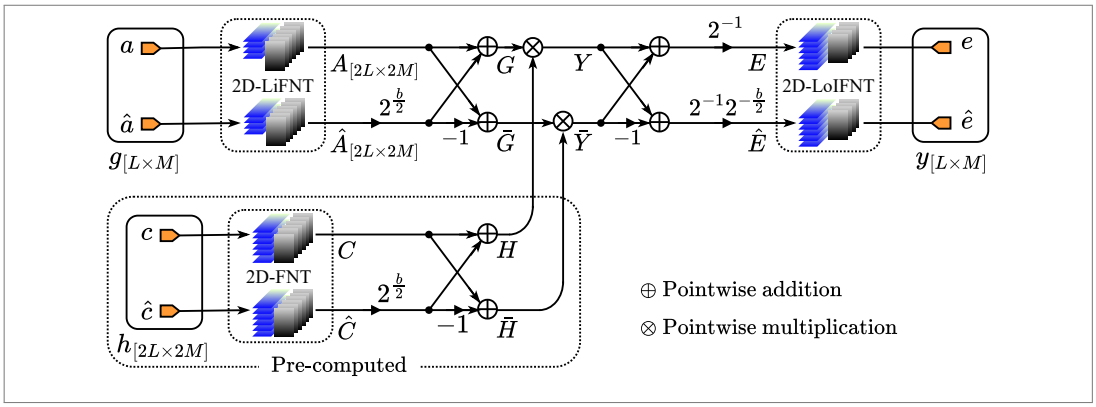

(b) 2D Convolution scheme.

Source: The author (2025).

1. **Computing FNT:** Let C_k and $\hat{C}_k$, $k = 0, 1, \ldots, 2N-1$, be the FNTs of the real and imaginary components of $\{h_n\}$, respectively. Then, their Hermitian pairs are given as

$$H_k = C_k + 2^{\frac{b}{2}} \hat{C}_k \pmod{2^b + 1}, \tag{5.7a}$$

$$\bar{H}_k = C_k - 2^{\frac{b}{2}} \hat{C}_k \pmod{2^b + 1}; \tag{5.7b}$$

2. **Computing LiFNT:** Let A_k and $\hat{A}_k$, $k = 0, 1, \ldots, 2N-1$, be the LiFNTs of the real and imaginary components of $\{g_n\}$, respectively. Then, their Hermitian pairs can be computed as

$$G_k = A_k + 2^{\frac{b}{2}} \hat{A}_k \pmod{2^b + 1}, \tag{5.8a}$$

$$\bar{G}_k = A_k - 2^{\frac{b}{2}} \hat{A}_k \pmod{2^b + 1}; \tag{5.8b}$$

3. **Pointwise product:** $Y_k = G_k H_k$ and $\bar{Y}_k = \bar{H}_k \bar{G}_k \pmod{2^b + 1}$;

4. **Computing LoIFNT:** Let E_k and $\hat{E}_k$, $k = 0, 1, \ldots, 2N-1$, be the FNT of the real and imaginary components of $y_n = (g \circledast h)_n$, which can be calculated as

$$E_k = 2^{-1}\left(Y_k + \bar{Y}_k\right) \pmod{2^b+1}, \tag{5.9a}$$
$$\hat{E}_k = 2^{-1}2^{-\frac{b}{2}}\left(Y_k - \bar{Y}_k\right) \pmod{2^b+1}. \tag{5.9b}$$

   Then, the last N consecutive points of the in-phase and quadrature components of $\{y_n\}$ can be calculated as the LoIFNT of E_k and $\hat{E}_k$, respectively.

Note that item 1) can be precomputed when $\{h_n\}$ is known in advance, which implies a given fractional Fourier order. The scheme corresponding to this algorithm is shown in Figure 9a. In conclusion, as explained in items 2) and 4), a total of $6N$ additions are saved when local FNTs are used to compute (3.3).

5.2.2 Proposed 2D Convolution Scheme

Similarly to the previous subsection, a 2D scheme is proposed in $\mathbb{Z}_{2^b+1}$ to implement (3.4). The method is based on the OaS procedure. The sequences $\{g_n\}$ and $\{h_n\}$ are first mapped to their 2D representations, after which a 2D convolution is performed as detailed in the following steps.

1. **Convolutional-chirp tiling:** Construct the $2L \times 2M$ matrix by vertically stacking two $L \times 2M$ blocks derived from the chirp sequence $\{h_n\}$, as

$$h_{L+l,\,m} = h_{l+mL}, \quad h_{l,\,m} = h_{\langle 2N-L+l+mL\rangle_{(2N)}}, \quad \begin{cases} l = 0, \ldots, L-1, \\ m = 0, \ldots, 2M-1. \end{cases}$$

2. **Computing 2D-FNT:** Let us denote by $[C_{q,r}]$ and $[\hat{C}_{q,r}]$, $q = 0, \ldots, 2L-1$, $r = 0, \ldots, 2M-1$, the 2D-FNT of the real and imaginary components of $[h_{l,m}]$, respectively. Then, the Hermitian pairs of the corresponding 2D-FNTs can be computed as

$$H_{q,r} = C_{q,r} + 2^{\frac{b}{2}}\hat{C}_{q,r} \pmod{2^b+1}, \tag{5.10a}$$
$$\bar{H}_{q,r} = C_{q,r} - 2^{\frac{b}{2}}\hat{C}_{q,r} \pmod{2^b+1}; \tag{5.10b}$$

3. **Input mapping:** Reform the 1D sequence $\{g_n\}$ of length LM into an $L \times M$ matrix, that is $g_{l,m} = g_{l+mL}$, for $l = 0, \ldots, L-1$ and $m = 0, \ldots, M-1$.

4. **Computing 2D-LiFNT:** Let $A_{q,r}$ and $\hat{A}q, r$ denote the elements of the $2L \times 2M$ arrays obtained by applying 2D-LiFNT to the real and imaginary components of $[g_{l,m}]$, respectively. The resulting Hermitian pairs are given by

$$G_{q,r} = A_{q,r} + 2^{\frac{b}{2}}\hat{A}_{q,r} \pmod{2^b+1}, \tag{5.11a}$$
$$\bar{G}_{q,r} = A_{q,r} - 2^{\frac{b}{2}}\hat{A}_{q,r} \pmod{2^b+1}. \tag{5.11b}$$

5. **Pointwise product:** $Y_{q,r}{=}G_{q,r}H_{q,r}$ and $\bar{Y}_{q,r}{=}\bar{H}_{q,r}\bar{G}_{q,r} \pmod{2^b+1}$;

6. **Computing 2D-LoIFNT:** Let $E_{q,r}$ and $\hat{E}_{q,r}$ denote the elements of the 2D-FNT corresponding to the real and imaginary components of the matrix $[y_{l,m}]$, respectively. Then, these elements can be computed as

$$E_{q,r} = 2^{-1}\left(Y_{q,r} + \bar{Y}_{q,r}\right) \pmod{2^b+1}, \tag{5.12a}$$
$$\hat{E}_{q,r} = 2^{-1}2^{-\frac{b}{2}}\left(Y_{q,r} - \bar{Y}_{q,r}\right) \pmod{2^b+1}. \tag{5.12b}$$

   In matrix form, the last N consecutive points of the in-phase and quadrature components of $\{y_n\}$ appear in the bottom right corner of the 2D-IFNT of $E_{q,r}$ and $\hat{E}_{q,r}$, respectively. These matrices of interest can be obtained efficiently using 2D-LoIFNT.

7. **Output mapping:** Flatten the $L \times M$ matrix $[y_{l,m}]$ into a one-dimensional sequence $\{y_n\}$ of length LM (row–column to linear index) using

$$y_{l+mL} = y_{l,m}, \quad l = 0, \ldots, L-1,\ m = 0, \ldots, M-1. \tag{5.13}$$

Notice that items 1) and 2) can be included in the pre-computation step for a given sequence $\{h_n\}$. The 2D scheme is shown in Figure 9b. A total of $18N$ additions are saved by the procedure described in items 4) and 6). Furthermore, $(2M)$-point FNTs across L rows and $(2L)$-point IFNTs across M columns are avoided twice, corresponding to the in-phase and quadrature components, respectively.

5.2.3 Arithmetic Complexity of Optimized Schemes

For comparison purposes, we first consider two alternatives for an N-point DFrFT, where $N = 2^n$, decomposed into two chirp multiplications and one chirp convolution over $\mathrm{GF}(2^{16}+1)$: the first method employs a 1D convolution scheme. In contrast, the second method uses a 2D convolution scheme. For comparison purposes, the arithmetic operations are shown in Figure10, using local FNTs instead of FNTs in both cases. In situations where a second method has a lower number of multiplications (see Figure 10a) but a higher number of additions than the first method (see Figure 10b), the relationship between them can be calculated to ensure that both methods exhibit the same overall complexity, as

$$\rho(N,b) = \frac{\mathrm{A}_2(N,b) - \mathrm{A}_1(N,b)}{\mathrm{M}_1(N,b) - \mathrm{M}_2(N,b)}, \tag{5.14}$$

where $\mathrm{M}_1(\cdot,b)$, $\mathrm{A}_1(\cdot,b)$ and $\mathrm{M}_2(\cdot,b)$, $\mathrm{A}_2(\cdot,b)$ represent the arithmetic complexity of the first and second algorithms, respectively. In CSD representation, for both algorithms to be equivalent on average, this measure must be $b/3$ (VORONENKO; PÜSCHEL, 2007), as the cost of one multiplication is $\rho(N,b)$ times that of one addition. Given that $\rho(N,b) > b/2$, for $n = 7, 8, \ldots, 10$ and $b = 16$, in our assessment of arithmetic operations (see Table 5), we conclude that the DFrFT over $\mathrm{GF}(2^{16}+1)$ is more efficient as a 1D convolution than as a 2D convolution.

Figure 10 – Bar graphs representing the arithmetic complexity of a 2^n-point DFrFT using the CM–CC–CM decomposition over $\mathrm{GF}(2^{16}+1)$; in terms of the number of (a) multiplications, and (b) additions.

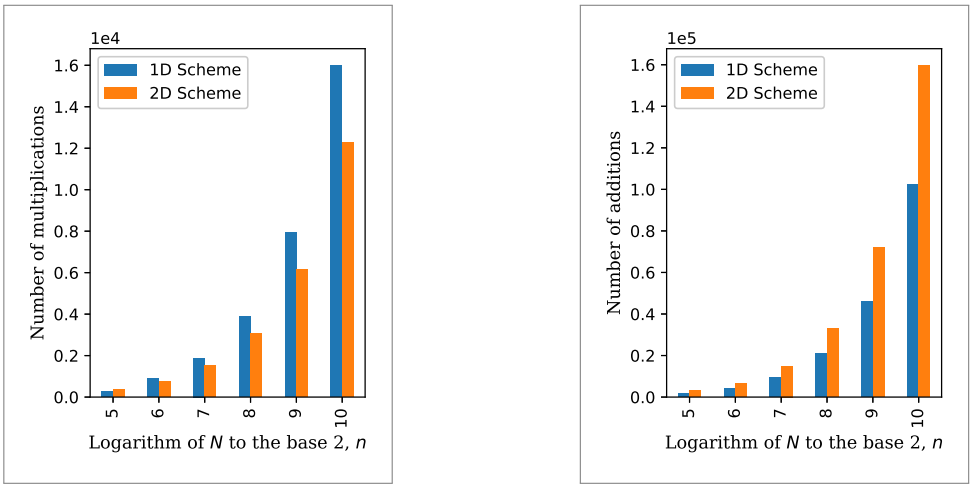

(a) (b)

Source: The author (2025).

Table 5 – Arithmetic complexity of a 2^n-point DFrFT, decomposed as CM–CC–CM modulo 2^b+1 (with $b=16$), in terms of the number of multiplications and additions.

n	**Multiplications**		**Additions**		$\rho(2^n, b)$
	$\mathrm{M}_1(2^n,16)$	$\mathrm{M}_2(2^n,16)$	$\mathrm{A}_1(2^n,16)$	$\mathrm{A}_2(2^n,16)$	
7	1888	1536	9472	14976	15.6
8	3904	3072	20992	33024	14.5
9	7936	6144	46080	72192	14.6
10	16000	12288	102400	159744	15.4

Source: The author (2025).

In summary, the arithmetic complexity of the 1D and 2D structures, in terms of modulo-2^b+1 diminished-1 operations for $b=32$ or 64, is presented in Table 6. Note that the same number of arithmetic operations is obtained for $n=8,9,\ldots,11$, when the length of the matrix columns is arranged as $2L=4b$. The 1D scheme supports transform lengths of up to $2b$, while the 2D scheme extends this limit to $4b^2$. In conclusion, since $b=16$ may be too small for digital representation, only 2D implementations with $b=32$ or 64 are suitable for long-chirp signals, which constitute the focus of the subsequent error analysis.

5.3 LOCAL CIRCULAR CONVOLUTION OVER $\mathbb{Z}_{2^b+1}$ FOR LDFrFT

This section introduces a local DFrFT (LDFrFT) using a 2D convolution approach. We focus on calculating partial points of a circular convolution, which serves as a decomposed module of DFrFT and leads to its local variants. The first L consecutive points of the circular convolution, as given in (3.4), can be obtained through 2D mapping when $m=0$ in (4.11),

Table 6 – Arithmetic complexity of a 2^n-point DFrFT, decomposed as CM–CC–CM modulo $2^b + 1$ (with $b = 32$ or 64), expressed in terms of the number of multiplications and additions.

n	**Multiplications**		**Additions**	
	$\mathrm{M}_1\,(2^n, 32)$	$\mathrm{M}_1\,(2^n, 64)$	$\mathrm{A}_1\,(2^n, 32)$	$\mathrm{A}_1\,(2^n, 64)$
3	64	64	336	336
4	128	128	800	800
5	256	256	1856	1856
6	512	512	4352	4224
7		1024		9728

(a) 1D Convolution scheme

n	**Multiplications**		**Additions**	
	$\mathrm{M}_2\,(2^n, 32)$	$\mathrm{M}_2\,(2^n, 64)$	$\mathrm{A}_2\,(2^n, 32)$	$\mathrm{A}_2\,(2^n, 64)$
7	1536		14976	
8	3072	3072	33024	33024
9	6144	6144	72192	72192
10	12288	12288	156672	156672
11	24576	24576	337920	337920
12	49152	49152	737280	724992
13		98304		1548288
14		196608		3342336

(b) 2D Convolution scheme

Source: The author (2025).

resulting in

$$y_{(l)} = \sum_{r=0}^{2M-1} \sum_{q=0}^{L-1} g_{(q+rL)} h_{(l-q-rL)}, \tag{5.15}$$

where $l{=}0, 1, \ldots, L-1$. Then, any L consecutive points of the sequence resulting in (3.4) can be calculated as

$$y_{(l+s)} = \sum_{r=0}^{2M-1} \sum_{q=0}^{L-1} g_{(q+rL)} h_{(l+s-q-rL)}, \tag{5.16}$$

where s is a starting point $s \in \{0, 1, \ldots, (M-1)L\}$. If we denote $d_{(n)}{=}h_{(n+s)}$ and $z_{(l)}{=}y_{(l+s)}$, then (5.16) can be expressed in matrix form such the elements $y_{(l+s)}$, $l{=}0, 1, \ldots, L-1$, are the bottom elements of a 2D convolution column of the respective extended versions, that is

$$\ddot{z}_{(l)} = \sum_{r=0}^{2M-1} \sum_{q=0}^{2L-1} \ddot{g}_{(q,r)} \ddot{d}_{(l-q,-r)}. \tag{5.17}$$

Note that $\ddot{g}_{(q,r)}{=}0$, when $L{\leq}\, q{<}\, 2L$ or $M{\leq}\, r{<}\, 2M$, in the case of this operation is part of DFrFT. Figure 11 illustrates how (5.17) can be implemented as the sum of the last L elements of the 1D convolutions per column. In this form, the cyclic convolutions originally formulated

Figure 11 – Mapping Local DFrFT; $[g_{q,r}]$ is an input $L \times M$ matrix, $[\ddot{d}_{q,\langle -r \rangle_{2M}}]$ is a $2L \times M$ matrix, $\circledast'$ represents the local FNT-based circular convolution of the columns of the aforementioned matrices, y_{l+s} is the output L-length vector obtained by adding the rows of the matrix $[f_{q,r}]$.

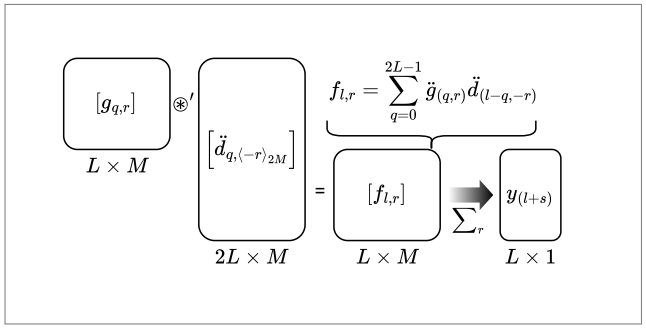

Source: The author (2025).

in one dimension can be recursively extended to two-dimensional structures to support larger transform lengths.

The local DFrFT, which is based on the circular convolution decomposition previously introduced, is hereafter denoted as CM–LCC–CM. This formulation relies on a local circular convolution (LCC), whose implementation consists of the following sequential steps:

1. Cyclic shift of the discrete chirp sequence, that means $d_{(n)} = h_{\langle n+s \rangle_N}$, $n = 0, \ldots, 2N-1$;
2. Mapping the sequence obtained in the previous item as $2L \times M$ matrix (its top columns are periodic extension), whose elements are obtained from the original extended matrix as $\ddot{d}_{q,\langle -r \rangle_{2M}}$, where $q = 0, 1, \ldots, 2L-1$ and $r = 0, 1, \ldots, M-1$;
3. Mapping the input sequence as an unextended $L \times M$ matrix, whose elements are denoted as $g_{q,r}$ and obtained as $g_{(q+rL)}$, $q = 0, 1, \ldots, L-1$ and $r = 0, 1, \ldots, M-1$;
4. Circular convolution of each column of the matrix $[g_{q,r}]$ and a column of $[\ddot{d}_{q,\langle -r \rangle_{2M}}]$. This step involves M instances of $(2L)$-length convolutions (see Figure 8).
5. Summing the elements of each row of the $L \times M$ matrix resulting in the last item gives a sequence of length L that contains the local points of the circular convolution. This step requires $2L(M-1)$ additions.

This algorithm is denoted as CM–LCC–CM (mod $2^b + 1$), where the circular convolution in item 4) can be implemented as a one- or two-dimensional scheme. In the 1D case, note that the $2L$- and $2M$-point FNTs can be implemented as algorithms that do not contain multiplications; a total of $4N$ multiplications are saved when the local circular convolution is used instead of the global 2D circular convolution; in the local case, each convolution consumes $4L$ pointwise multiplications (in total $4LM$), while in the global case, a 2D convolution consumes $8N$ pointwise

multiplications. Furthermore, $N - L$ complex multiplications (corresponding to the outer chirp term) are saved using LDFrFT instead of DFrFT; a complex multiplication can be done as two multiplications and four additions.

Regarding the proposed LDFrFT using the CM–LCC–CM (mod $2^b + 1$) decomposition, Figure 12 illustrates the reduction in the number of multiplications, η_{M}, and additions, η_{A}, when computing only Q consecutive points of an N-point DFrFT, where $N = 2^n$. To be more specific, in Figure 12a and Figure 12c, it can be observed that η_{M} increases as the number of Q points decreases, and for longer transform lengths, η_{M} also reaches higher values. This measure ranges give: from 46% to 50% for $b = 32$ and from 42% to 50% for $b = 64$. Similarly, Figure 12b and Figure 12d illustrates how the measurement η_{A} varies within an expanded percentage range: from 23% to 80% for $b = 32$ and from 13% to 82% for $b = 64$. These results confirm that the proposed LDFrFT provides significantly higher computational efficiency than the conventional DFrFT, especially when processing only a subset of the total transform points. This advantage becomes more pronounced for longer transform lengths, where both the reduced number of arithmetic operations and the modular arithmetic structure lead to lower computational complexity and improved scalability for real-time or resource-constrained implementations.

Figure 12 – Bar graph depicting the percentage reduction in arithmetic operations for an N-point DFrFT ($N = 2^n$) when only Q local points ($Q = 2^q$) are calculated; reductions in the number of (a,c) multiplications, and (b,d) additions.

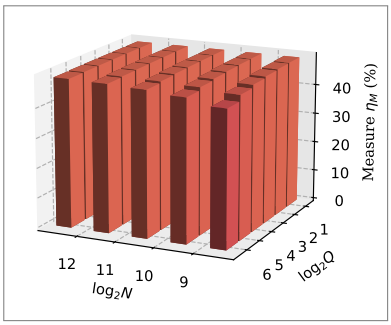

(a) $b = 32$

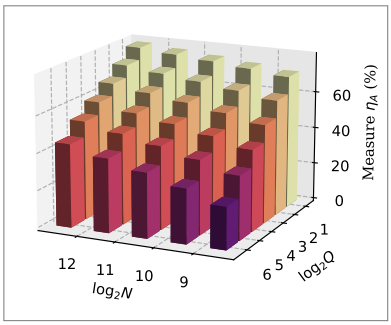

(b) $b = 32$

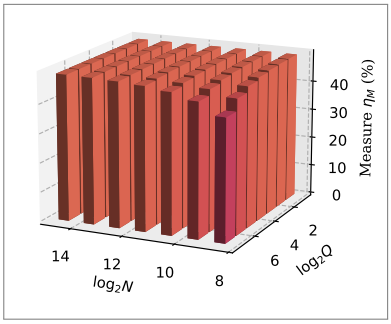

(c) $b = 64$

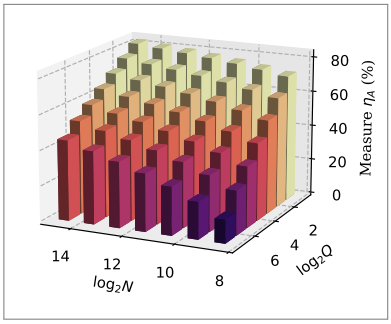

(d) $b = 64$

Source: The author (2025).

6 DIRECTION-OF-ARRIVAL ESTIMATION FOR WIDEBAND CHIRPS

In this chapter, we explore chirp-based decompositions, with the main contribution being the use of DSmFrFT instead of DFrFT, for direction-of-arrival (DoA) estimation of wideband linear chirps, addressing both single- and multi-target scenarios. Considering the direction-of-arrival (DoA) estimation problem using a uniform linear array, the single-target case is formulated as a least-squares problem, in which we explain the use of LDSmFrFT. The multi-target case is reformulated as a multi-line fitting problem in the fractional Fourier domain. Moreover, we consider the use of subspace-based methods with spatial smoothing.

6.1 SINGLE-TARGET DIRECTION FINDING

In this section, as a key contribution, we introduce the estimation of DoA for wide-band linear chirps using slope fitting in the simplified fractional Fourier domain, a process that involves the DSmFrFT. Finally, we provide a brief explanation of the use of partial points of the DSmFrFT for DoA estimation with outlier detection.

6.1.1 Least Square Problem

After determining the optimal rotation angle α_0, at the reference sensor, the peak position q_m at the m-th sensor, as a function of θ, can be obtained by substituting τ_m in (3.26). This provides

$$q_m = q_0 + (m - m_0) \underbrace{f_s d \sin\theta \cot\alpha_0 / c}_{\text{slope}}. \tag{6.1}$$

For $\theta \in [-\pi/2, \pi/2]$, the index q_m can be bounded within the range $[q_0 - \psi, q_0 + \psi]$, where $\psi = f_s \left(m - m_0\right) d \cot\alpha_0 / c$; peaks outside this range are considered outliers. In this context, LDSmFrFT can be used to reduce the complexity of peak searching. To achieve this, we choose Q to be the smallest power of two such that $Q \geq 2\psi$, and $\psi \leq q_0 - s \leq Q - \psi$. From (6.1), denoting the slope as k_u, the angle-of-arrival value is given by

$$\theta = \arcsin\left(\frac{k_u c}{d f_s \cot\alpha_0}\right), \tag{6.2}$$

where k_u, the slope of the fitting curve, can be calculated using the CLSM (ZHONG et al., 2023). For comparison purposes, Table 7 presents the formulas for the DoA estimation of a chirp signal. The equations corresponding to DFrFT were provided in (ZHONG et al., 2023).

6.1.2 Constrained Least Squares Method

In the least squares method (LSM), given a set of points $\{x_i, y_i\}_{i=0}^{N-1}$, the goal is to find a line $y = a_0 + a_1 x$ that best fits the given data points, where a_1 is the slope of the line and a_0 is

Table 7 – Formulas for DoA estimation depending on numerical algorithms for FrFT.

DFrFT	DSmFrFT
$q_m = q_0 + f_s \tau_m \cos \alpha_0$	$q_m = q_0 + f_s \tau_m \cot \alpha_0$
$\theta = \arcsin\left(\frac{k_u c}{df_s \cos \alpha_0}\right)$	$\theta = \arcsin\left(\frac{k_u c}{df_s \cot \alpha_0}\right)$

Source: The author (2025).

the y-intercept. The first-order polynomial associated with this least squares problem has the form

$$\widehat{y}_i = a_0 + a_1 x_i, \quad i = 0, 1, ..., N-1, \tag{6.3}$$

where a_0 and a_1 are the coefficients found by least squares regression. In the case of DoA estimation in the fractional domain, for a ULA with M elements, N is bounded as $1 < N \leq M$, due to the outlier detection method. The first order solution by least squares regression can be represented by matrix operations as follows

$$\underbrace{\begin{bmatrix} q_0 \\ q_1 \\ \vdots \\ q_{N-1} \end{bmatrix}}_{\mathbf{Y}} = \underbrace{\begin{bmatrix} 1 & x_0 \\ 1 & x_1 \\ \vdots & \vdots \\ 1 & x_{N-1} \end{bmatrix}}_{\mathbf{XA}} \begin{bmatrix} a_0 \\ a_1 \end{bmatrix}, \quad \mathbf{Y} = \begin{bmatrix} q_0 & q_1 & \cdots & q_{N-1} \end{bmatrix}^{\mathsf{T}}, \quad \mathbf{A} = \begin{bmatrix} a_0 & a_1 \end{bmatrix}^{\mathsf{T}} \tag{6.4}$$

where $\mathbf{Y}$ is the vector of the peak positions of the received signal, $\mathbf{X}$ is the Vandermonde matrix and $\mathbf{A}$ is the coefficient vector. By the principle of LSM, the solution is given by

$$\mathbf{A} = \left(\mathbf{X}^{\mathsf{T}}\mathbf{X}\right)^{-1} \mathbf{X}^{\mathsf{T}}\mathbf{Y}, \tag{6.5}$$

where $\mathbf{A} = \begin{bmatrix} a_0 & a_1 \end{bmatrix}^{\mathsf{T}}$. Then, the slope k_u of the fitted curve is a_1. Since $\arcsin$ of x is defined as the inverse sine function when $-1 \leq x \leq 1$, when DSmFrFT is employed, the target slope must be constrained as

$$|a_1| - |df_s \cot \alpha_0 / c| \leq 0;$$

it converts the least square problem into a Lagrange duality problem as well as LSM becomes CLSM (ZHONG et al., 2023). Therefore, the obtained solution can be expressed as

$$\mathbf{A} = \left(\mathbf{X}^{\mathsf{T}}\mathbf{X} + \lambda \mathbf{p}^{\mathsf{T}}\mathbf{p}\right)^{-1} \mathbf{X}^{\mathsf{T}}\mathbf{Y}, \tag{6.6}$$

where $\mathbf{A} = \begin{bmatrix} a_0 & a_1 \end{bmatrix}^{\mathsf{T}}$, $\mathbf{p} = \begin{bmatrix} 0 & 1 \end{bmatrix}$ and λ is the Lagrange multiplier, $\lambda \geq 0$. Similarly, the slope k_u is given by the coefficient a_1.

For visual inspection and comparisons, the DFrFT, DSmFrFT, and LDSmFrFT spectra of the noise-free signal at the first eight ULA elements are shown in Figure 13. In which, to

illustrate the use of LDSmFrFT instead of DFrFT, we present the same example and data as in (ZHONG et al., 2023). In such a figure, we observe that the peaks can be determined using LDSmFrFT at optimal fractional order.

Figure 13 – Fractional Fourier–domain spectra of chirp signals received by the first eight ULA elements, computed using DFrFT, DSmFrFT, and LDSmFrFT, with $N = 1024$.

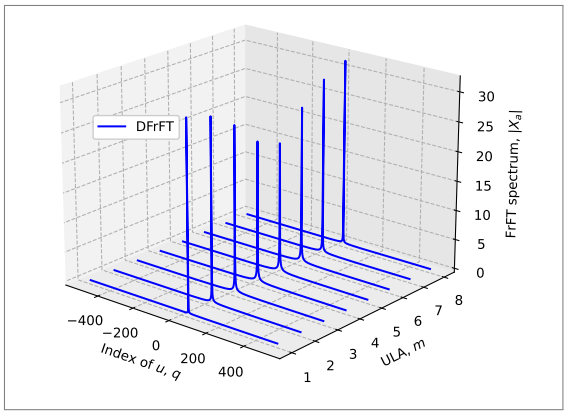

(a) DFrFT

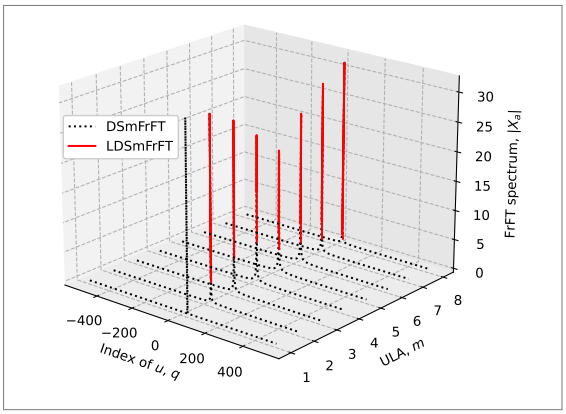

(b) DSmFrFT

Source: The author (2025).

Table 8 details the total number of complex multiplications and additions reduced in estimating the DoA with an ULA of 40 elements, when using LDSmFrFT instead of DSmFrFT, for $N = 1024$. In percentage terms, the aforementioned reductions are 32.1% and 48.7%, respectively.

Table 8 – Reduction in number of complex multiplications and additions when using LDSmFrFT instead of DSmFrFT, $N = 1024$.

m	Q	$N/2 \log_2 P - N$	$N \log_2 P - N + Q$
From 2 to 4	4	3072	7172
From 5 to 10	8	2560	6152
From 11 to 22	16	2048	5136
From 23 to 40	32	1536	4128
Total:		76800	194364

Source: The author (2025).

6.2 MULTI-TARGET DIRECTION FINDING

In this section, we present two approaches for multi-target DoA estimation of wideband chirp signals in the fractional Fourier domain, including the simplified FrFT. First, we introduce peak alignment as a pre-processing step for subspace-based algorithms. Second, we propose a multi-line fitting approach, where the lines can either be non-intersecting or intersecting. The corresponding methods for this approach are piecewise linear regression and Hough transform-based line detection.

6.2.1 Subspace-Based Algorithms

In a manner analogous to the traditional narrowband subspace methods, we first propose the incorporation of peak alignment into the preprocessing stage of subspace-based algorithms for DoA estimation of LFM signals. Subsequently, spatial smoothing and angle-of-arrival calculating are also described.

6.2.1.1 Peak Alignment

For improving DoA estimation of wideband linear chirp signals, it is proposed that the peaks in the fractional Fourier domain should be aligned. Let Δ_q denote the difference between the peak index corresponding to the m-th sensor and that of the reference sensor. Depending on the computational method, Δ_q can be utilized as described in the following items:

1. In the case of DFrFT, considering the time-shift property (see Section 3.2.1), under the constraint $2q \gg f_s \tau_{m,k} \cos\alpha_0$, the steering vector corresponding to the k-th source, $\mathbf{a}[q_{0k}, \alpha_{0k}, \theta_k]$, can be derived in the DFrFT domain. The m-th element of this vector can be expressed as

$$a_m(q_{0k}, \alpha_{0k}, \theta_k) = e^{-j\frac{2\pi}{N} f_s \tau_{m,k} q_{0k} \sin\alpha_{0k}}, \tag{6.7}$$

   where q_{0k} and α_{0k} represent the peak index and the optimal DFrFT order for the k-th target, respectively. This vector is typically used in subspace-based algorithms (QU et al., 2006; CHONG; XIAOMIN, 2011). Then, let $g[r]$ represent the shifted signal $x[r - r_\theta]$. The DFrFT of $g[r]$ is denoted by $G_a[q]$. In this context, aligning the peaks corresponds to applying the following shift:

$$Y_a[q] = G_a[q + \Delta_q] = e^{-j\frac{\pi}{N}\left(2r_\theta q + r_\theta^2 \cos\alpha\right)\sin\alpha} X_a[q].$$

   The value of Δ_q can be estimated by a peak search procedure. The elements of the steering vector in the DFrFT domain remain as given in (6.7), as long as $2q \gg f_s \tau_{m,k} \cos\alpha_0$.

2. In the case of DSmFrFT, note that the FrFT of $x(t)$ can be expressed as

$$\{\mathcal{F}^a x\}(u) = \sqrt{j} A_\alpha e^{j\pi u^2 \cot\alpha} \{\mathcal{L}^{\mathbf{A}} x\}(u \csc\alpha),$$

   where $\mathbf{A} = (\cot\alpha, 1; -1, 0)$. This implies that the peaks obtained using DSmFrFT must be shifted to the position corresponding to the peak index when using DFrFT and multiplied by the term $\sqrt{j} A_\alpha e^{j\frac{\pi}{N} q_0^2 \cot\alpha_0}$, where α_0 is the optimal order of DSmFrFT and q_0 is the peak index given in (3.10a).

In the case of multi-target DoA estimation, peaks can be detected and extracted to form new snapshots in the fractional Fourier domain; that is, nonzero values correspond only to the detected peaks. If two peaks are to be shifted to the same position, the resulting peak can be obtained by summing them. This step requires KM complex multiplications when the DSmFrFT is employed.

6.2.1.2 Spatial Smoothing

Consider a uniform linear array (ULA) with M elements. Let $\mathbf{Y}_a \in \mathbb{C}^{M\times N}$ denote the snapshot matrix obtained after discrete fractional Fourier transform (DFrFT) processing and peak alignment. The array is divided into $P = M - L + 1$ overlapping subarrays, each of length L. The p-th subarray snapshot is then formed as

$$\mathbf{Y}_p^{\mathrm{f}} = \mathbf{J}_p^{\mathrm{f}} \mathbf{Y}_a, \quad p = 1, 2, \ldots, P,$$

where $\mathbf{J}_p^{\mathrm{f}} \in \mathbb{R}^{L\times M}$ is a selection matrix that extracts the p-th forward subarray. The backward snapshots are given as $\mathbf{Y}_p^{\mathrm{b}} = \mathbf{J}_L(\mathbf{Y}_p^{\mathrm{f}})^*$, where $\mathbf{J}_L \in \mathbb{R}^{L\times L}$ is the exchange matrix with the ones on the antidiagonal, used to reverse the sensor order. To enhance the rank and robustness of the covariance estimate, forward–backward (FB) averaging is then applied to each subarray, and the corresponding sample covariance matrix is given by

$$\mathbf{R}_{\mathrm{FB}} = \frac{1}{2P} \sum_{p=1}^{P} \left[\mathbf{Y}_p^{\mathrm{f}} (\mathbf{Y}_p^{\mathrm{f}})^{\mathsf{H}} + \mathbf{Y}_p^{\mathrm{b}} (\mathbf{Y}_p^{\mathrm{b}})^{\mathsf{H}} \right],$$

where $(\cdot)^{\mathsf{H}}$ denotes the Hermitian (conjugate transpose) of a matrix. The procedure described above is referred to as forward-backward spatial smoothing (FBSS). The time complexity of this step is $\mathcal{O}(PL^2N)$.

6.2.1.3 Methods for Estimating the Angle of Arrival

Given the covariance matrix $\mathbf{R}_{\mathrm{FB}}$, the signal and noise subspaces can be obtained by eigendecomposition, resulting in $\mathbf{U}_s \in \mathbb{C}^{L\times K}$ and $\mathbf{U}_n \in \mathbb{C}^{L\times(L-K)}$, respectively. Subsequently, two methods can be employed to estimate the angle of arrival:

- **ESPRIT method**: Based on the principle of spatial smoothing, the first and last rows of the signal subspace matrix are removed to form two submatrices, $\mathbf{U}_1$ and $\mathbf{U}_2$. The rotational invariance property is exploited by finding the matrix $\mathbf{\Psi}$ such that $\mathbf{U}_2 = \mathbf{\Psi}\mathbf{U}_1$. This equation is solved using the least squares method

  $$\mathbf{\Psi} = \mathbf{U}_2 \mathbf{U}_1^{\triangle},$$

  where $(\cdot)^{\triangle}$ denotes the pseudo-inverse of a matrix. The eigenvalues λ_i of $\mathbf{\Psi}$ are then computed, and the angles of arrival are estimated as

  $$\theta_i = -\arcsin\left(\frac{\arg(\lambda_i)}{2\pi\ell_i}\right), \quad i = 0, \ldots, K-1$$

  where $\ell_i = \frac{df_s}{cN} q_{0i} \sin\alpha_{0i}$. The computational complexity of this step is approximately $\mathcal{O}(L^3 + K^2L)$.

- **MUSIC method**: Given the noise subspace, the spatial spectrum for the k-th target can be calculated as

$$P_{\text{MUSIC}}(\theta) = \frac{1}{\mathbf{a}^{\mathsf{H}}(q_{0k}, \alpha_{0k}, \theta)\mathbf{U}_n\mathbf{U}_n^{\mathsf{H}}\mathbf{a}(q_{0k}, \alpha_{0k}, \theta)},$$

where $\mathbf{a}(q_{0k}, \alpha_{0k}, \theta) \in \mathbb{C}^{L\times 1}$ is the steering vector in the DFrFT domain corresponding to the k-th target and angle θ. The peaks of $P_{\text{MUSIC}}(\theta)$ correspond to the estimated directions of arrival (DoAs). For N_a angle samples, each projection requires $\mathcal{O}(L^2)$ operations, resulting in a total complexity of $\mathcal{O}(L^3 + KN_aL^2)$. In this context, the efficiency of the method can be improved using techniques such as those proposed in (BARABELL, 1983; LAN et al., 2023a).

6.2.2 Multi-Line Fitting

The multi-line fitting problem involves partitioning a dataset into segments, each of which can be approximated by a straight line (see Figure 14). In this work, the problem is addressed in two ways: slope fitting, where the goal is to fit multiple linear models to the data while minimizing the overall error, and line detection, where lines in an image formed by peaks are detected using the Hough transform to determine their slopes.

Figure 14 – Representation of peaks as K lines in the fractional Fourier domain: (a) non-intersecting lines and (b) intersecting lines

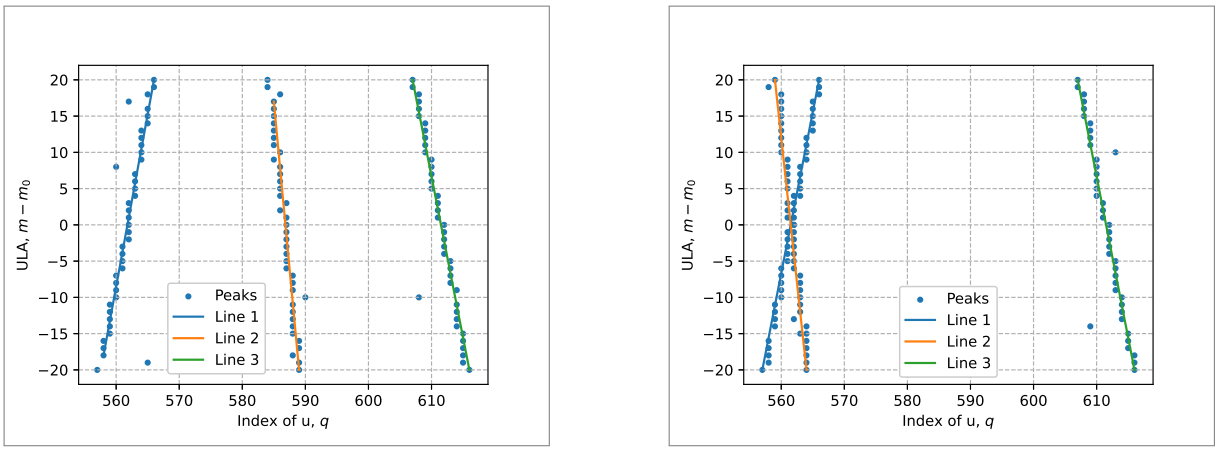

(a) Non-intersecting lines.

(b) Intersecting lines.

Source: The author (2025).

6.2.2.1 Piecewise Linear Regression

The least squares method can be extended to fit multiple lines when the peaks indices can be divided into segments, with each segment corresponding to one line (see Figure 14b). To be more specific, piecewise linear regression involves dividing the data set into K segments, each of which is fitted with a straight line. The procedure can be summarized as follows:

- Let the set of N_p points be $\{(x_n, y_n)\}$, where $n = 0, 1, \ldots, N_p - 1$. The goal is to fit K straight lines so that the piecewise model approximates the data points.
- Breakpoints define the boundaries between the K segments. Let the breakpoints be denoted as x_{M_i} for $i = 1, 2, \ldots, K-1$. Taking into account the start and end indices $M_0 = 0$ and $M_K = N_p$, the data is then partitioned into K segments as

$$S_k = \{(x_n, y_n) | M_k \leq n < M_{k+1}\}, \quad k = 0, 1, ..., K-1. \tag{6.8}$$

  These breakpoints may be predefined (for example, $M_i = i \lfloor N_p/K \rfloor$) or selected using optimization techniques.
- For each segment S_k, the slope of a linear model is fitted using CLSM.

The algorithmic complexity of this method is $\mathcal{O}(KM^3)$. However, that way of piecewise linear regression fails when the lines intersect, as depicted in Figure 14a.

6.2.2.2 Line detection in Hough space

In this context, an alternative approach is line detection using the Hough transform (DUDA; HART, 1972). In short, a straight line in the image space (x, y) can be represented in the Hough space by the parameters (ρ, θ), where ρ is the perpendicular distance from the origin to the line and θ is the angle between the normal line and the x-axis. This line can be represented as a single point (ρ, θ) in the Hough space, as illustrated in Figure 15. The geometric interpretation of the Hough transform (HT) is as follows: for any point $P = (x, y)$ on a straight line, the vector $P - P_0$, where $P_0 = (\rho \cos\theta, \rho \sin\theta)$ is the intersection of the line and the perpendicular to the origin, must be orthogonal to the vector $P_0 - 0 = P_0$. This orthogonality condition leads to equation $(P - P_0) \cdot P_0 = 0$. Therefore, the equation of the line in polar coordinates is given by

$$x \cos\theta + y \sin\theta = \rho. \tag{6.9}$$

This equation represents the fundamental relationship used in the Hough transform to map a straight line from Cartesian space to Hough space.

The algorithm for fitting K lines to a set of N_p points $\{x_i, y_i\}$ in the fractional Fourier domain is detailed in the following items:

1. **Convert the sequence to an image**: Define a 2D binary image $I(x, y)$ of size $L \times M$, where L is the number of points from the minimum index to the maximum index of the detected peaks. The white lines correspond to the sequence $S = \{(x_i, y_i)\}_{i=1}^{N_p}$ onto the image, setting $I(x_i, y_i) = 1$.
2. **Compute the Hough transform**: Discretize the Hough space in the polar representation of a line $\rho_j = x_i \cos\theta_j + y_i \sin\theta_j$, where ρ_j is the perpendicular distance from the origin,

Figure 15 – Representation of a straight line in Hough space.

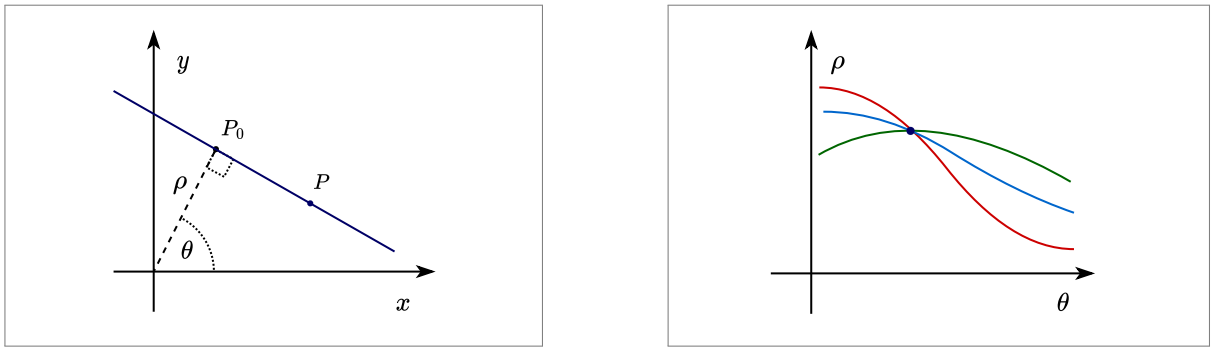

(a) Image domain. (b) Hough domain.

Source: Adapted from Duda e Hart (1972).

and θ_j is the angle in the discretized range. Let N_θ be the number of discrete angles θ_j, $j = 1, \ldots, N_\theta$. Initialize an accumulator array $H(\rho, \theta)$ with zeros. After that, for each white pixel (x_i, y_i) in $I(x, y)$, find the closest discretized ρ for each θ_j.

3. **Detect peaks in Hough space**: Identify the K highest peaks in the accumulator array $H(\rho, \theta)$. Each peak (ρ_k, θ_k) represents a detected line with a slope given as $-\frac{\cos\theta_k}{\sin\theta_k}$, when $\theta_k \neq 0$.

The time complexity of this multi-line fitting algorithm is given by $\mathcal{O}(N_p N_\theta)$, where $N_p{=}KM$ is the maximum number of peaks (M being the number of elements in the ULA). Note that HT can be more efficient than CLSM when $N_\theta < M^2$ (see Table 9). The HT-based algorithm can be improved using the probabilistic Hough transform (PHT), which is particularly useful since it processes only a random subset of edge points rather than all points (MATAS; GALAMBOS; KITTLER, 2000). The time complexity for PHT is given as $O(N_s N_\theta)$, where $N_s \ll N_p$ and N_s represents the number of sampled points. Since N_s is much smaller than N_p, the computational cost is significantly reduced. The computational complexity of DoA estimation, excluding the stages DFrFT and DSmFrFT, is summarized in Table 9. The operations required for peak alignment are not included as they are negligible compared to the overall complexity of the complete algorithm.

Table 9 – The Time complexity of DoA estimation for K targets.

Algorithm	Time Complexity
FBSS-MUSIC	$\mathcal{O}(PL^2N + L^3 + KN_aL^2)$
FBSS-ESPRIT	$\mathcal{O}(PL^2N + L^3 + K^2L)$
CLSM	$\mathcal{O}(KM^3)$
HT	$\mathcal{O}(KMN_\theta)$

Source: The author (2025).

7 RESULTS AND COMPUTER SIMULATIONS

In this chapter, we first present an analysis of the arithmetic complexity of the sampling-type DFrFT by decomposing it into a circular convolution over the ring of integers modulo $2^b + 1$. This analysis includes comparisons between the 1D and 2D convolution schemes. Following this, the circular convolution-based algorithms are compared to the decomposition into two chirp multiplications and one FFT algorithm; this analysis is based on the time complexity determined by the equivalent number of additions. Furthermore, error analysis and applications are also provided for a better understanding of the proposed algorithms. Including computer experiments related to obtaining the amplitude spectrum of a single-component LFM signal, radar echo modeling, estimation of the DoA in the so-called simplified fractional Fourier domain. All numerical simulations[1] are performed in the interactive Jupyter Notebook using Python programming language (version 3.9.7).

7.1 COMPLEXITY ANALYSIS

As a preliminary comparison, we consider chirp-convolution-based decompositions for DFrFT, Figure 16a presents a bar graph illustrating the number of multiplications, while Figure 16b exhibits the number of additions. In both figures, we also include the DFrFT decomposed into two chirp multiplications and one FFT algorithm (ZAYED, 1996; CARIOLARO et al., 1998; PEI; DING, 2000a; LAN et al., 2023b); this refers to the CM–FFT–CM decomposition. Note that the decomposition into a 2D convolution (mod $2^{32} + 1$ or $2^{64} + 1$) requires the fewest multiplications, although this comes at the expense of an increased number of additions. However, neither of the aforementioned bar graphs reflects realistic performance, as they do not consider the number of bits in data representation. To address this issue, we establish theoretical metrics to facilitate comparisons. These metrics are based on arithmetic operations using floating-point and diminished-1 representations. In the diminished-1 case, we neglect the minor effects of b-bit inversion and ICS, as they have a negligible impact on the overall resources of the entire system. In the bar representation shown in Figure 17, the overall time complexity represents the algorithm's runtime in unitless terms; it is quantified by a weighted sum of the number of additions and multiplications, with multiplications assigned a higher weight due to their greater computational complexity. In such a representation, we define the mean case as requiring $b/3$ b-bit additions for multiplications by other constants. At the same time, the upper values are based on the worst-case scenario of needing up to $b/2$ b-bit additions (VORONENKO; PÜSCHEL, 2007). After determining the equivalent number of additions, we adopt a logarithmic time complexity, which means that each b-bit addition is performed using a parallel-prefix IEAC adder (VERGOS; EFSTATHIOU; NIKOLOS, 2002), which has a delay given by

$$\tau_{\text{adder}}(b) = 2\left\lceil \log_2 b \right\rceil + 3, \tag{7.1}$$

[1] Code available at: https://github.com/egutierrezhu/doa-frft-chirps

where $\lceil \cdot \rceil$ denotes the ceil of the argument. The lower values in the bar representation for the CM–CC–CM modulo $2^b + 1$ correspond to the multipliers proposed in (VERGOS; EFSTATHIOU, 2007).

Figure 16 – Bar graph illustrating the arithmetic complexity of a 2^n-point DFrFT, showing the number of (a) multiplications and (b) additions.

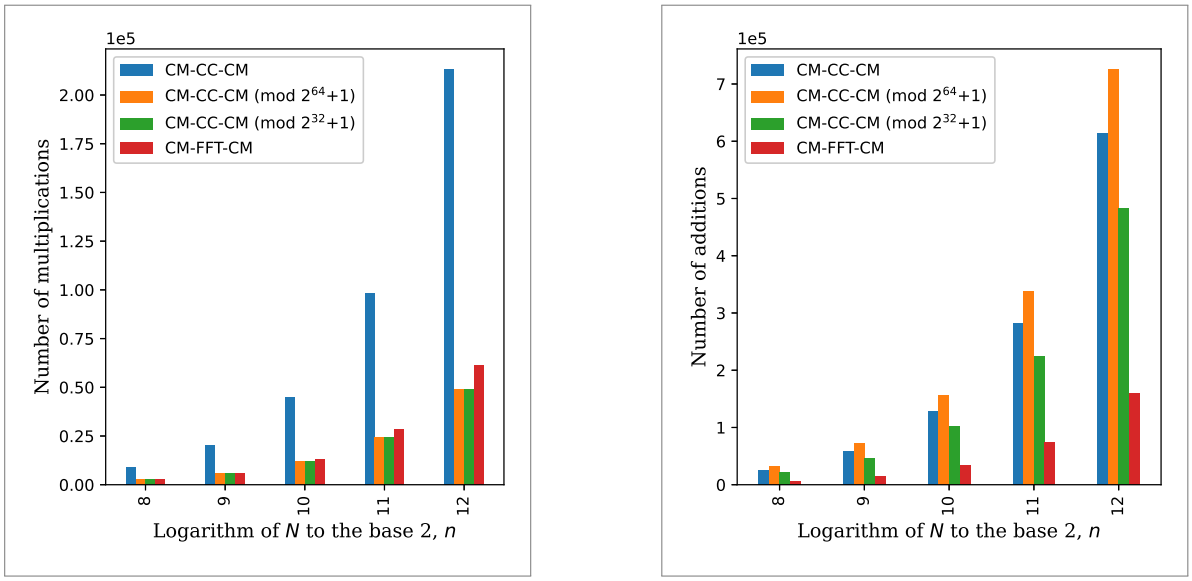

(a) (b)

Source: The author (2025).

For comparison, we consider that a precise method for implementing (3.3) can use floating-point operations based on the IEEE 754 standard. In double precision (64 bits): 1 bit for the sign, 11 bits for the exponent, and 52 bits for the significand. The complexity of floating-point arithmetic can be evaluated by the required fixed-point operations: adding two floating-point numbers involves aligning exponents, adding significands (one fixed-point addition), normalizing, and rounding, while multiplying them requires multiplying significands (one fixed-point multiplication), adding exponents (one fixed-point addition), normalizing, and rounding (WASSON, 2011). To ensure similar evaluation contexts, we assume that fixed-point additions are performed using parallel-prefix adders, allowing the delay for this operation to be specified by (7.1). When fixed-point multiplications of significands are performed in CSD representation, using the speed of bit-shifts over repeated fixed-point additions, it is essential to note that the number of bits in the adders is twice that of the mantissa (WASSON, 2011). Upon inspecting the results, it becomes evident that the method based on CM–CC–CM (mod $2^{32} + 1$) can be more efficient than DFrFT affine one FFT when represented in double precision format (64-bit CM–FFT–CM).

Although CM–CC–CM over $\mathbb{Z}_{2^b+1}$ achieves a substantial reduction in the number of multiplications, this advantage comes at the cost of an increased number of additions. Such trade-offs may affect hardware efficiency depending on the arithmetic architecture, as diminished-1

Figure 17 – Bar graph representing the arithmetic complexity of a 2^n-point DFrFT; expressed in addition-equivalent units under a logarithmic-time adder model.

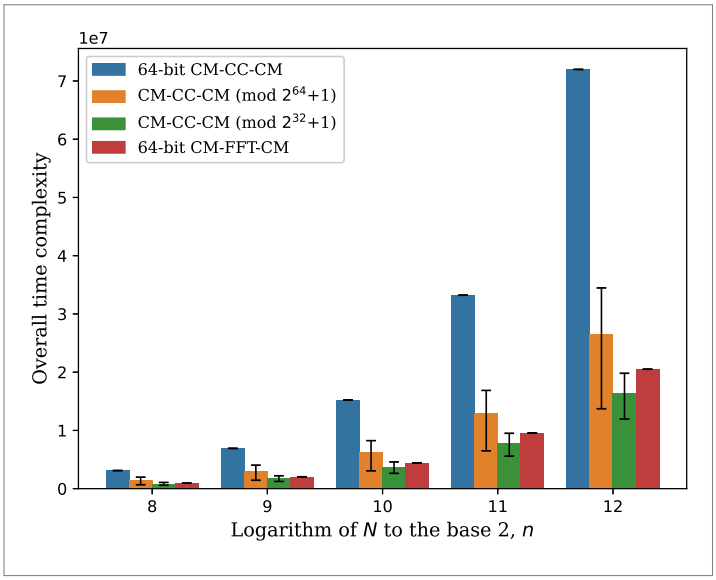

Source: The author (2025).

arithmetic, with minimal carry propagation, is well suited to field-programmable gate array (FPGA) designs using IEAC adders, ICS operations, and CSD multipliers, whereas its benefits may diminish on general-purpose processors with highly optimized floating-point units. Therefore, the results should be regarded as analytical upper limits, with practical performance determined by the underlying hardware and word-length constraints.

7.2 ERROR ANALYSIS

The validation of the proposed algorithms is essentially based on verifying the chirp signal parameters. The experiments focus on peak searching in the fractional Fourier domain. In the first analysis, numerical experiments were conducted to evaluate the performance of the GSS algorithm at various SNR levels for a single-component chirp signal centered at $20\,\text{kHz}$. The duration of the signal is $T = 5\,\mu\text{s}$, uniformly sampled with 1024 points. If we consider a bandwidth B from 5 to $100,\text{kHz}$, the corresponding chirp rate (B/T) ranges from 1 to $10,\text{MHz}/\mu\text{s}$. Figures 6(a–b) illustrate the mean absolute error (MAE) of fractional Fourier order, between the exact value (a_0) and its estimated value ($\widehat{a}_0$). Given the starting points of 1 and 1.2 for the GSS algorithm, a minimal error is observed in the chirp rate interval from 6 to $7,\text{MHz}/\mu\text{s}$; outside this range, the absolute error increases for lower SNR values. At certain intermediate SNR levels, DFrFT may be more accurate than DSmFrFT. Considering that the results show only minor inaccuracies when using DSmFrFT instead of DFrFT, we conclude that the GSS method can be an efficient approach to estimate the fractional order of DFrFT or DSmFrFT. Consequently, it offers a low-complexity solution for estimating the parameters of a linear chirp.

Figure 18 – Error in selecting the fractional order for (a) DFrFT and (b) DSmFrFT. The curves are fitted with fifth-order polynomial regression for visual inspection

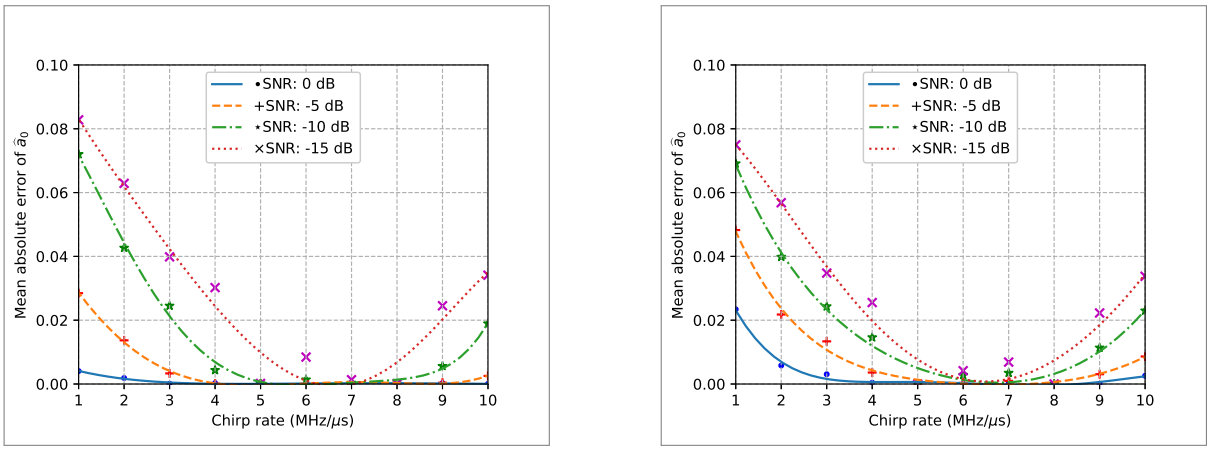

(a) DFrFT

(b) DSmFrFT

Source: The author (2025).

As a second analysis, we provide examples to illustrate the method for avoiding amplitude overlap when circular convolution is represented in the ring of integers modulo 2^b+1. In which we determine the number of bits to represent them without overflow and the error due to amplitude quantization. Our analysis consists of three numerical experiments described below. In the first experiment, we consider as the input signal a single-component chirp signal, which is modulated by the inner chirp, and the resulting in-phase and quadrature components are represented as integers in the range $\left[-2^{d-1}, 2^{d-1}\right]$, $d = 4, 8, 16$. The chirp that convolves is also encoded in the same range. After that, we proceed to bound the maximum absolute value in the output as indicated in (4.10), that is

$$\vartheta(N, d) = 2^{d-1} \sum_{i=0}^{N-1} \sqrt{c_i^2 + \hat{c}_i^2},$$

where c_i and $\hat{c}_i$ are integer representation of the real and imaginary part of $h(t) = e^{j\pi t^2 \csc \alpha}$, $\alpha = a\pi/2$, with fractional order a in the range $[0.5, 1.5]$. The exponent b in $2^b + 1$ is calculated as $b(N, d) = \lceil \log_2(2\vartheta(N, d) - 1) \rceil$. This parameter as a function of n and d is shown in Table 10. In amplitude quantization by $d = 4$, performing the described analysis, one can conclude that a 2^n-point DFrFT, $3 \leq n \leq 8$, can be calculated over $\mathrm{GF}(2^{16} + 1)$ without amplitude aliasing, since the calculated value $b(N, 4)$ is not greater than 16. If the input signal is encoded as in the cases when d is 8 and 16, one concludes that the modulus of the arithmetic operations must be $2^{32} + 1$ and $2^{64} + 1$, respectively.

In the third analysis, the difference between the two results is calculated in the second experiment as the root mean square error (RMSE). Specifically, a single-component chirp signal is used to evaluate the error as a function of the transform length. The Latin hypercube sampling (LHS) method is applied to generate random samples of parameters: $a \in [0.5, 1.5]$, $f_c \in [0, 1000]$

and $\mu \in [0, 50]$. The duration of the LFM signal is $T = 5$. Let $\epsilon(N, d)$ be the pointwise error in the amplitude spectrum between DFrFT decomposed into floating-point convolution, $X_a[q]$, and fixed-point convolution, $\widehat{X}_a^d[q]$. Specifically, fixed-point representation means that the in-phase and quadrature components are represented as integers by multiplying them by 2^{d-1} and applying the rounding function, and the result of multiplication (or convolution) is divided by 2^{d-1} twice. After that, we determine the RMSE as a function of the length transforms ($N = 2^n$, $n = 3, 4, \ldots, 13$) and the amplitude quantization levels ($d = 4, 8, 16$), that is

$$\epsilon(N, d) = \sqrt{\frac{1}{N} \sum_{q=-N/2}^{N/2-1} \left(|X_a[q]| - \left| \widehat{X}_a^d[q] \right| \right)^2}.$$

This measure is included in Table 10. In that way, considering floating-point representation in double precision format, $\epsilon(N, 16)$ is practically null, when d is 16.

Table 10 – Bit length and RMSE for DFrFT computed via integer convolution.

n	$d = 4$		$d = 8$		$d = 16$	
	$b(N, d)$	$\epsilon(N, d)$	$b(N, d)$	$\epsilon(N, d)$	$b(N, d)$	$\epsilon(N, d)$
3	11	0.0454	19	0.0030	35	0.0
4	12	0.0515	20	0.0032	36	0.0
5	13	0.0500	21	0.0032	37	0.0
6	14	0.0527	22	0.0033	38	0.0
7	15	0.0518	23	0.0033	39	0.0
8	16	0.0527	24	0.0033	40	0.0
9	17	0.0525	25	0.0033	41	0.0
10	18	0.0535	26	0.0033	42	0.0
11	19	0.0549	27	0.0033	43	0.0
12	20	0.0563	28	0.0033	44	0.0

Source: The author (2025).

In the fourth analysis, we perform numerical simulations to investigate amplitude aliasing when the CM–CC–CM decomposition is implemented using modulo-$2^b + 1$ arithmetic. The results are shown in Table 10, where it is observed that the criterion in (4.10) is not satisfied when n exceeds 8 for $b = 16$. In this context, there is no clearly noticeable amplitude overflow for $n = 9$. In the case of $n = 10$, Figure 19a presents the DFrFT spectrum (in logarithmic scale) of a single-component LFM signal in double-precision floating-point format. The magnitude spectrum, also expressed in decibels (dB), corresponding to the calculations over $\mathrm{GF}(2^{16} + 1)$, is depicted in Figure 19c. There is evident overflow in the peak values, with a magnitude difference reaching up to $-1\,\mathrm{dB}$ (see Figure 19e). The error outside the peak position reaches $-21\,\mathrm{dB}$, which can be attributed to quantization ($d = 4$). In contrast, the same representation over the ring of integers modulo $2^{32} + 1$ is shown in Figure 19b. In this case, the upper quantization error reaches $-30\,\mathrm{dB}$, which is lower than in the previous case, and there is no amplitude overflow

(see Figure 19d). In conclusion, these numerical simulations confirm that the bounding criterion provided in (4.10) can effectively help avoid amplitude aliasing. Finally, it can be observed that a minimum quantization error is achieved at the optimal fractional order of the DFrFT. In contrast, for other values, the error remains below $-18\,\mathrm{dB}$, as illustrated in Figure 19f. These upper-bound values indicate that the associated inaccuracies are within a tolerable range. The figure also includes the case where the chirp–convolution stage is implemented in the ring $\mathbb{Z}_{2^b+1}$, denoted as CM–CC$\,(\mathrm{mod}\ 2^b+1)$–CM. In this case, the error reaches a lower value of $-35\,\mathrm{dB}$ at the optimal order.

Figure 19 – The 2^{10}-point DFrFT spectrum of a single-component LFM signal (with $f_0 = 20$, $\mu = 8$, and $T = 5$) at the optimal fractional Fourier order, including the magnitude error due to quantization and overflow.

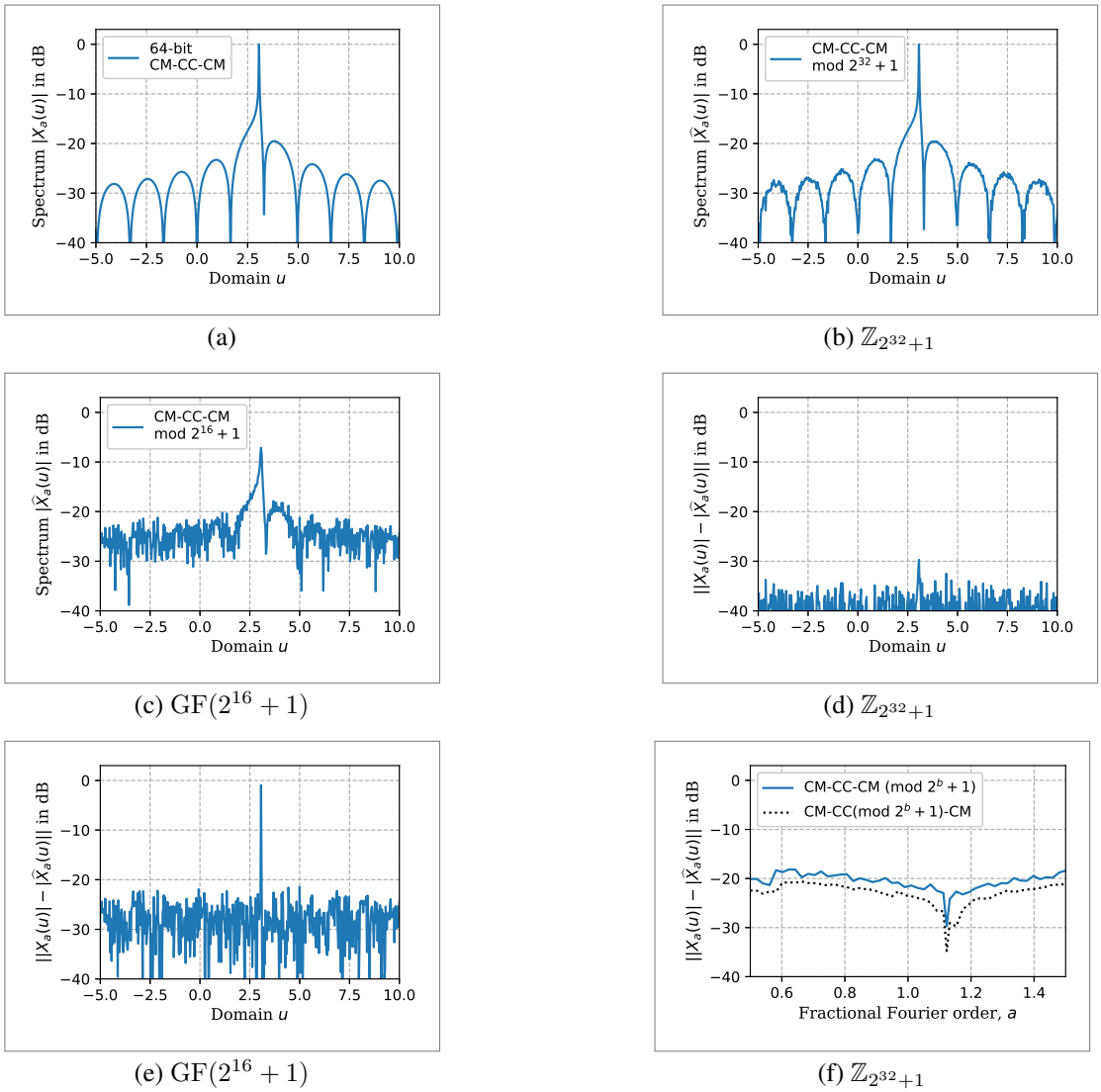

(a) (b) $\mathbb{Z}_{2^{32}+1}$

(c) $\mathrm{GF}(2^{16}+1)$ (d) $\mathbb{Z}_{2^{32}+1}$

(e) $\mathrm{GF}(2^{16}+1)$ (f) $\mathbb{Z}_{2^{32}+1}$

Source: The author (2025).

7.3 APPLICATIONS

In this section, we examine two cases to demonstrate the application of the proposed decompositions. First, we apply LDFrFT for radar echo modeling, using modulo-$2^b + 1$ convolutions. Second, we employ DSmFrFT to estimate the direction of arrival of incoming signals on a uniform linear array.

7.3.1 LDFrFT and Simulated Radar Signals

In this section, we examine the application of LDFrFT to radar echo modeling using FMCW signals (BARRICK, 1973; STOVE, 1992). Radar echo modeling using frequency-modulated continuous-wave (FMCW) signals (BARRICK, 1973; STOVE, 1992) involves a continuous wave signal with frequency modulation over time, typically in a sawtooth pattern (PATOLE et al., 2017; ERDOGAN et al., 2017). The transmitted FMCW signal can be expressed mathematically as

$$s_{\mathrm{T}}(t) = Ae^{j\left(2\pi f_c t + \pi \frac{B}{T} t^2\right)}, \quad t_1 \leq t \leq t_2,$$

where A is the amplitude, f_c is the carrier frequency, B is the bandwidth, T is the sweep time, and B/T is the frequency modulation rate. When the radar signal encounters a target, it reflects to the radar. The received echo is delayed based on the distance to the target. Specifically, the echo model for two stationary point targets located at different distances, R_i, $i = 1, 2$, can be expressed as

$$s_{\mathrm{R}}(t) = \sum_{i=1}^{2} A_i e^{j\left(2\pi f_c (t-\tau_i) + \pi \frac{B}{T} (t-\tau_i)^2\right)},$$

where $\tau_i = 2R_i/v_c$, and v_c is the speed of light. This model is approximated under the assumption that $\tau_i \ll T$, leading to the following result

$$s_{\mathrm{R}}(t) \approx \sum_{i=1}^{2} A_i e^{-j2\pi f_c \tau_i} e^{j\left(2\pi (f_c - \frac{B}{T}\tau_i) t + \pi \frac{B}{T} t^2\right)}.$$

In this way, the received signal becomes a two-component LFM signal. These signals can be processed using LDFrFT to extract range and velocity information from the beat frequency. From the geometric representation in Figure 5 and considering scaled coordinates, one obtains that

$$\underbrace{\left(f_c - \frac{B}{T}\tau_i\right)}_{f_{0i}} \underbrace{\frac{\sqrt{N}}{f_s}}_{s} = \underbrace{\frac{q_i}{\sqrt{N}}}_{u_{0i}} \csc \alpha_0, \quad i = 1, 2,$$

where α_0 is the optimal rotation angle of the time-frequency axis. Here, q_i denotes the index of the i-th peak in the DFrFT spectrum. Consequently, the formula for R_i is given by

$$R_i = \frac{v_c T}{2B} \left(f_c - \frac{q_i f_s}{N \sin \alpha_0}\right), \quad i = 1, 2. \tag{7.2}$$

Our LDFrFT method does not use axis scaling depending on α in numerical calculations. In contrast, the method proposed in (MIAO, 2023) adjusts the kernel through axis scaling, leading to a different corresponding formula

$$R_i' = \frac{v_c T}{2B}\left(f_c - \frac{q_i f_s}{N}\right), \quad i = 1, 2.$$

If we assume $R_1 > R_2$ and a given number of consecutive points (i.e., $q_2 - q_1$ is consistent for both cases), we obtain the relationship $R_1' - R_2' = (R_1 - R_2)\sin\alpha_0$. This suggests that the distance coverage for the two targets of our LDFrFT can be wider than that of the method proposed in (MIAO, 2023), which means $|R_1' - R_2'| \leq |R_1 - R_2|$. The relationship between α_0 and the parameters of the FMCW signal can be determined using the trigonometric relationship in scaled coordinates as

$$\cot\alpha_0 = \frac{s f_{0i}}{-\frac{f_{0i}}{\mu s}} = -\frac{NB}{f_s^2 T},$$

where μ represents the frequency slope B/T.

Table 11 – Parameters in simulated radar signals.

Parameter	Description	Value
A_1, A_2	amplitude	1
f_c	carrier frequency	24 GHz
B	bandwidth	10 GHz
T	sweep time	300 μs
N	number of sampling points	65536

Source: The author (2025).

Simulations are performed in a way similar to that presented in (MIAO, 2023). First, the sampling frequency is set to $f_s = 3(f_c + B)$, resulting in 102 GHz. Figure 20a illustrates the DFrFT spectrum (64-bit CM–CC–CM) corresponding to the parameters given in Table 11, considering $\tau_1 = 10\,\mu s$ and $\tau_2 = 10\,\mu s$. When applying the LDFrFT proposed in Section 5.3, a number of consecutive points higher than $2b$ (up to $4b^2$) results in each column convolution corresponding to a 2D scheme. Figure 20b shows the spectrum obtained for $Q = 2048$ consecutive points, starting at $q = 46843$, corresponding to the CM–LCC–CM (mod $2^{32} + 1$) decomposition, where the local circular convolution is mapped as 2D schemes, with peak indices at $q_1 = 47760$ and $q_2 = 47974$. The distances from the two point targets to the radar can be estimated using the formula given in (7.2), yielding $R_1 \approx 3000$ m and $R_2 \approx 1500$ m, thereby confirming the relation $\tau_i = 2R_i/v_c$.

In complexity comparisons, we observe that the LDFrFT proposed in (MIAO, 2023) is no longer efficient than the global version (CM–FFT–CM) in terms of the number of multiplications when $Q \geq 2^{10}$ (see Figure 21a). In contrast, our method requires lower multiplications than

Figure 20 – Fractional Fourier spectrum of the simulated radar-echo signal; corresponding to (a) the floating-point DFrFT using CM–CC–CM and (b) the LDFrFT using CM–LCC–CM modulo $2^b + 1$.

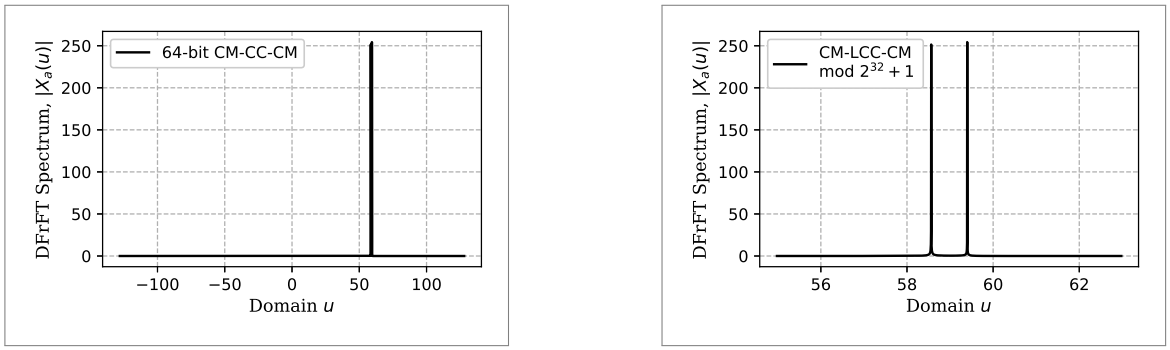

(a) (b)

Source: The author (2025).

Figure 21 – Bar graph illustrating the arithmetic complexity of DFrFT and LDFrFT, showing (a) the number of multiplications, (b) the number of additions, and (c) the time complexity based on the equivalent number of additions.

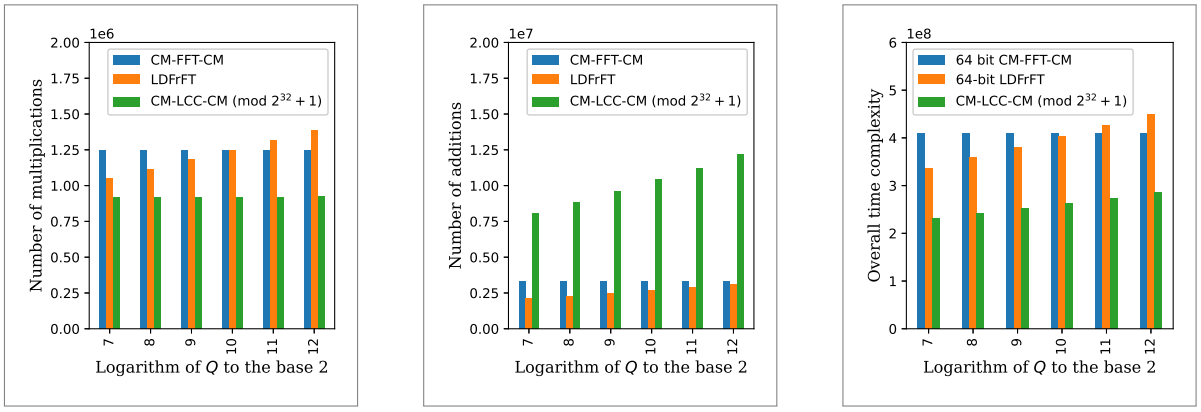

(a) (b) (c)

Source: The author (2025).

the aforementioned methods; however, this comes at the cost of a higher number of required additions (see Figure 21b). Considering the number of equivalent additions and the logarithmic time complexity outlined in (7.1), as illustrated by the bars in Figure 21c, it is clear that the LDFrFT proposed as two chirp multiplications and a local chirp convolution, CM–LCC–CM (mod $2^{32} + 1$), is faster than the LDFrFT presented in (MIAO, 2023), when it employs floating-point operations in double precision.

7.3.2 DoA Estimation in the Fractional Fourier Domain

For DoA estimation in the Fractional Fourier Domain, we consider both single-target and multi-target scenarios. In the first case, we account for factors such as the number of snapshots, noisy environments, and a wide range of incidence angles. In the second case, we conduct

experiments with both stationary and non-stationary sources. As in the first case, we also include experiments involving noise, as well as multi-carrier scenarios.

7.3.2.1 Single-Target Scenario

In the first experiment, we consider that there is a single target. The difference between the direction of arrival, θ, and its estimated value, $\widehat{\theta}$, is determined by Monte Carlo simulation. To be more specific, we calculate the root mean square error (RMSE) of the estimated DoA as

$$\text{RMSE} = \sqrt{\frac{1}{R}\sum_{r=1}^{R}\left(\widehat{\theta}_r - \theta_r\right)^2},$$

where R is the count of the simulation per point, $R = 500$. The fixed parameters are $T = 2\,\mu$s, $f_c = 20$ MHz, the antenna array is a ULA of 40 elements, and the distance between adjacent elements d is set as half wavelength corresponding to the highest frequency with a bandwidth of 20 MHz. As in (ZHONG et al., 2023), the DoA estimation algorithm consists of taking snapshots of $x_m(t)$, obtaining the peak position q_m, detecting and rejecting outliers of q_m, and determining $\hat{\theta}$ by CLSM. In Figure 22, the root mean square error (RMSE) versus the number of snapshots (N) is presented, comparing the CLSM method with subspace-based algorithms. The basic subspace-based methods are denoted as DFrFT-MUSIC and DFrFT-ESPRIT. Two array configurations are considered: a non-symmetric uniform linear array (ULA) with $m_0 = 0$ and a centered ULA with $m_0 = 20$. In both scenarios, it is observed that the application of peak snapping results in a lower RMSE. The improved versions of the algorithms are referred to DFrFT†-MUSIC and DFrFT†-ESPRIT, where $(\cdot)^\dagger$ denotes the **peak alignment** in the pre-processing step. For non-symmetric ULA, when $N > 512$, CLSM outperforms the aforementioned basic methods in terms of estimation efficiency.

Figure 22 – RMSE of DoA estimated as a function of the number of snapshots (N) when $\theta = \pi/8$ and SNR $= -15$ dB.

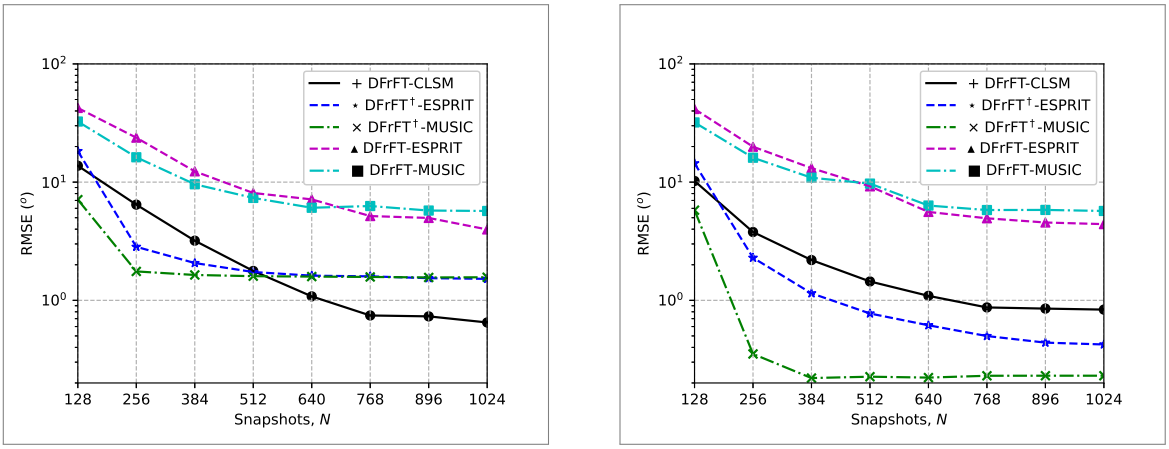

(a) $m_0 = 0$ (b) $m_0 = 20$

Source: The author (2025).

In the second experiment, the DSmFrFT is included and the RMSE is plotted against the signal-to-noise ratio (SNR). For the non-symmetric ULA, CLSM outperforms the subspace-based methods at SNR levels above -18 dB (see Figure 23). However, for the centered ULA configuration, the trend is reversed; subspace-based methods exhibit a lower RMSE, with the DFrFT†-ESPRIT algorithm achieving the highest accuracy for SNR values greater than -15 dB. The simplification of the transform, replacing DFrFT with DSmFrFT, improves the accuracy of the DoA estimation.

Figure 23 – RMSE of DoA estimated as a function of SNR when $\theta = \pi/8$ and $N = 1024$.

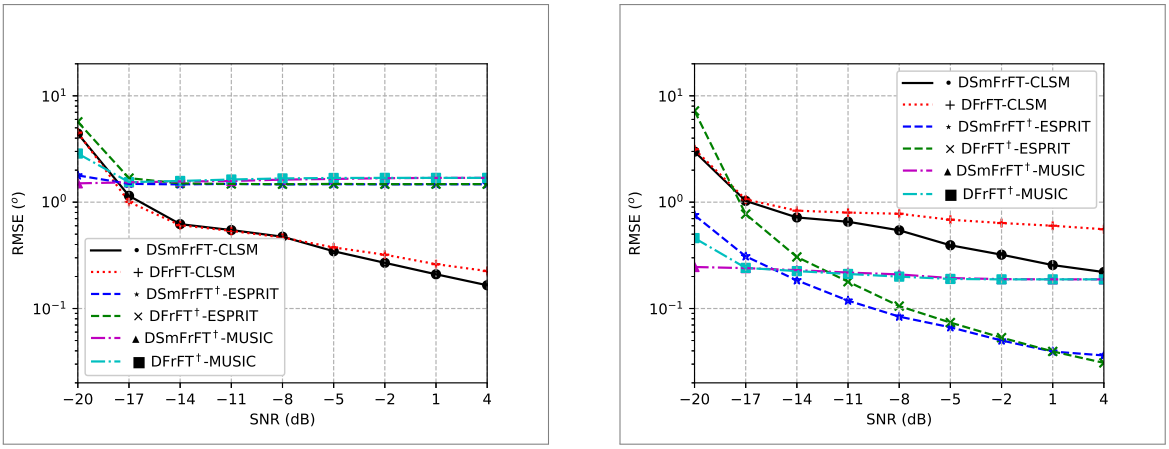

(a) $m_0 = 0$ (b) $m_0 = 20$

Source: The author (2025).

In the third experiment, for different angles of arrival, $\theta \in [20^{\text{o}}, 70^{\text{o}}]$, if $m_0 = 0$, the RMSE using subspace-based techniques and DSmFrFT increases considerably as θ increases within the given range (see Figure 24a). However, the RMSE remains smaller than 1^{o} when CLSM is used. On the other hand, if $m_0 = 20$, CLSM is no longer more accurate than subspace-based techniques and reaches RMSE above 1^{o} (see Figure 24b). In this example, only the DSmFrFT is considered, as substituting the DFrFT in its place does not significantly affect the accuracy of DoA estimation.

7.3.2.2 Multi-Target Scenario

As a first experiment, we consider two moving sources. When an underwater acoustic source moves with velocity v_s, the received frequency at a stationary observer is affected by the **Doppler effect**. The observed frequency f_r changes over time as the source moves. The Doppler-shifted frequency f_r is given by: $f_r = \frac{c}{c \pm v_s} f_0$, where the $+$ sign denotes a source moving away, while the $-$ sign indicates a source approaching. For $v_s \ll c$, the propagation speed of the wave in an aquatic medium is usually given by $c = 1500$ m/s, the frequency change is approximately linear when the source accelerates along the direction of incidence. In mathematical terms, it is an approximation of Taylor's series, given by $f_r \approx \left(1 \mp \frac{v_s}{c}\right) f_0$.

Figure 24 – RMSE of DoA estimated as a function of θ when SNR $= -10$ dB and $N = 1024$.

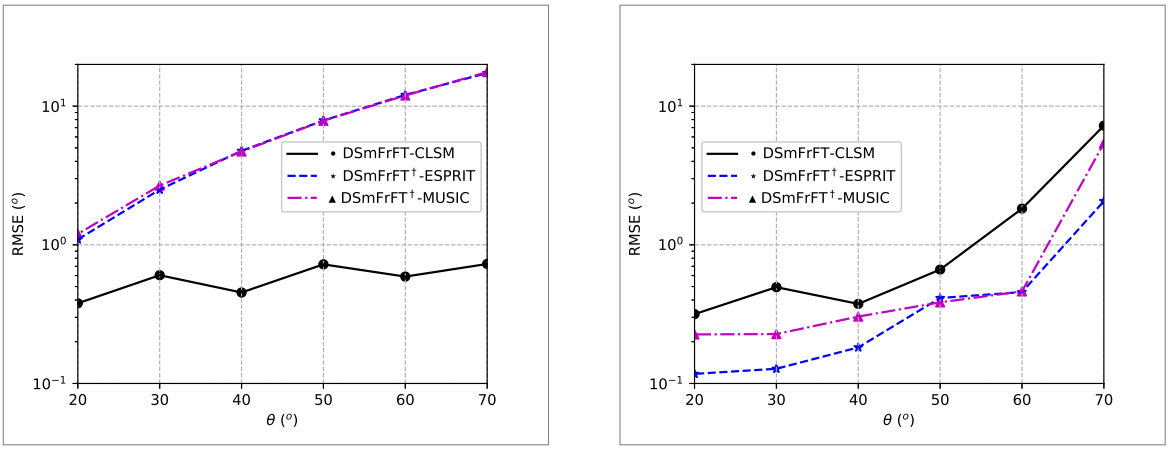

(a) $m_0 = 0$ (b) $m_0 = 20$

Source: The author (2025).

Figure 25 shows the spatial spectrum of the MUSIC algorithm with forward and backward smoothing (the size of the subarrays is half of the total). In this case, two moving sources with the same velocity are considered, approaching a 41-element center-symmetric ULA; the internal spacing between the elements is half the wavelength corresponding to the maximum frequency when $v_s = 200$ m/s. The initial frequency f_0 is 15 kHz and the observation time is 20 ms. The results show that replacing a DFrFT with a DSmFrFT provides a similar accuracy. In both cases, as speed increases, the sidelobe levels in the spatial spectrum increase, but the source directions remain determinable.

Figure 25 – The spatial spectrum of the MUSIC algorithm with forward–backward smoothing for DoA estimation of two non-stationary sources moving at the same velocities 0, 10, and 200 m/s.

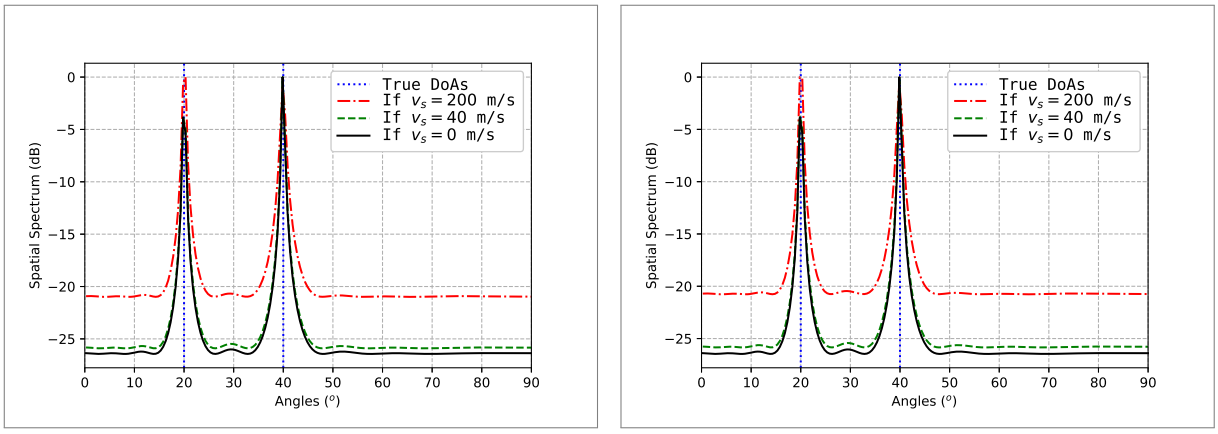

(a) DFrFT-FBSS-MUSIC (b) DSmFrFT-FBSS-MUSIC

Source: The author (2025).

In the second experiment, we consider two wide-band linear chirps, which causes the shift in the fractional Fourier domain to remain significant. Both signals have the same center

frequency of 20 kHz and the observation time is $2\,\mu$s. The distance d is half the wavelength corresponding to the maximum frequency when the bandwidth is 20 kHz. In Figure 26, it is observed that the MUSIC algorithm with forward and backward smoothing remains effective when using the peak-position fitted DFrFT, denoted as DFrFT†, as well as when using the simplified fitted version, which is denoted as DSmFrFT†. For a chirp rate of $10\,\text{MHz}/\mu$s, the use of the aforementioned algorithms results in an increase of sidelobes in the spatial spectrum, but they still accurately determine the direction of arrival. In other words, the incorporation of DFrFT and DSmFrFT into a subspace narrowband algorithm, along with their respective shift adjustments in the fractional Fourier domain, remains accurate. Significantly, the sidelobes are lower than those observed in the previously presented non-stationary case.

Figure 26 – The spatial spectrum of the MUSIC algorithm with forward–backward smoothing for DoA estimation of two wideband linear chirps with the same center frequency and chirp rates 1, 2, and 10 MHz/μs.

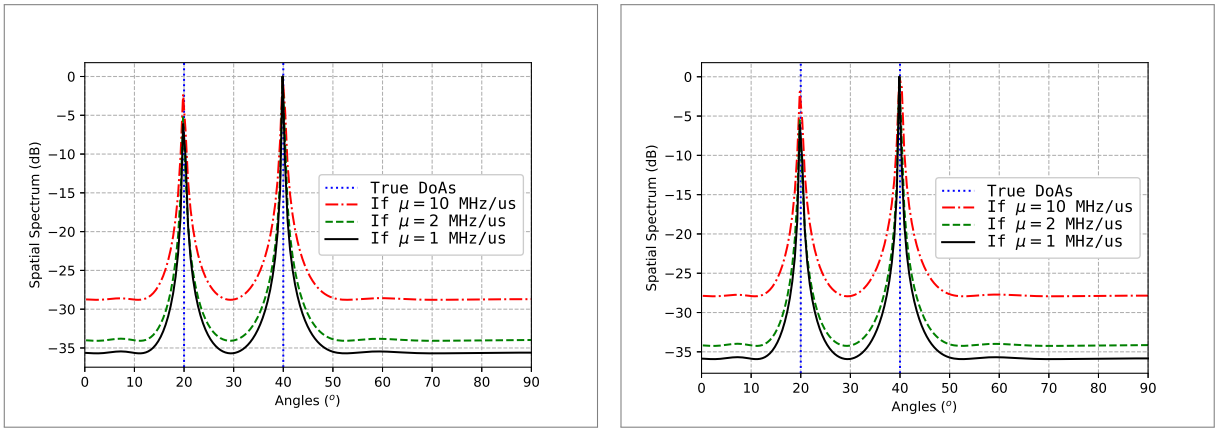

(a) DFrFT†-FBSS-MUSIC (b) DSmFrFT†-FBSS-MUSIC

Source: The author (2025).

In the third experiment, we focus on three incident chirp signals with directions of arrival (DoA) at $-40°$, $20°$, and $40°$, with center frequencies of $f_{c0}{=}10$, $f_{c1}{=}15$, and $f_{c2}{=}20$ MHz. The signal observation time is 5 μs, and the bandwidth of each signal is 20 MHz. The corresponding peaks in the fractional Fourier domain are shown in Figure 14b. The peaks when $f_{c1} = 10$ MHz are depicted in Figure 14a. In this context, the MUSIC algorithm is not included because it exhibits cross-null interference, which is well-knwon in a multi-carrier case (AMIN, 1993; LIU et al., 2019), leading to replicas of the interference angles of arrival in the spatial spectrum. For error analysis, we use the mean absolute error (MAE), defined as

$$\text{MAE} = \frac{1}{K}\sum_{k=0}^{K}|e_k|,$$

where e_k represents the RMSE for the k-th target. The representations of MAE versus SNR of these multi-carrier cases are shown in Figure 27(a-b). For comparison purposes, we consider the ESPRIT algorithm with spatial smoothing and forward-backward averaging (FBSS-ESPRIT).

Figure 27 – Representation of the mean absolute error (MAE) of the multi-target DoA estimation versus SNR, considering the ESPRIT algorithm with forward–backward averaging, as well as spatial smoothing, piecewise slope fitting, and the Hough transform-based multi-line fitting.

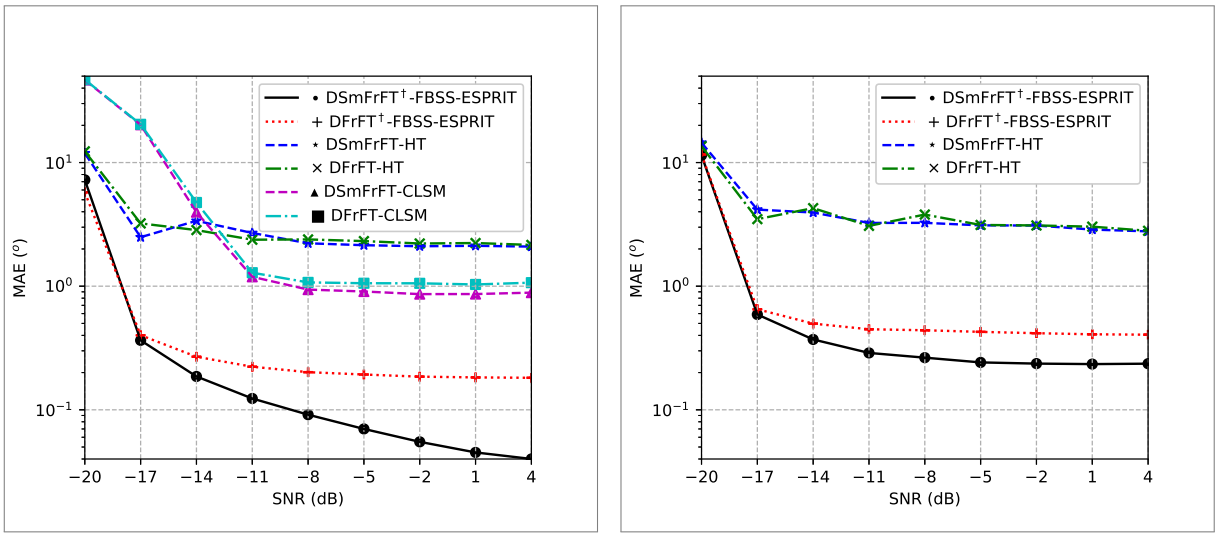

(a) Multi-target signals with $f_{c0} \neq f_{c1} \neq f_{c2}$

(b) Multi-target signals with $f_{c0} = f_{c1} \neq f_{c2}$

Source: The author (2025).

The size of the smoothing subarray is given as $L = \lfloor M/2 \rfloor$. Numerical simulations indicate that subspace-based techniques exhibit higher accuracy compared to slope-fitting methods. In both multi-target scenarios, the integration of DSmFrFT into the FBSS-ESPRIT algorithm, combined with peak-position fitting, yields a more precise DoA estimator for wideband linear chirps. Consequently, DSmFrFT serves as an effective preprocessing operator to enhance DoA estimation for chirp signals using ULA configurations.

In Figure 27b, the MAE measurement is presented for a correlated case, where $f_{c0} = f_{c1}$. In this scenario, given that the lines formed by peaks in the fractional Fourier domain intersect and cannot be segmented into K distinct lines, where K denotes the number of targets, the piecewise linear regression approach (CLSM method) is consequently inapplicable. An alternative approach is multiline fitting based on the Hough transform (HT), which yields lower absolute error than the CLSM method at SNR levels below approximately $-14\,\text{dB}$. The HT method, as well as CLSM, exhibits small differences in MAE calculations when applied with either DFrFT or DSmFrFT, indicating that the simplified FrFT operator is a valid low-complexity alternative for multiline fitting. In the case of using the HT method for DoA estimation of wideband linear chirps, increasing the number of elements in ULA can further reduce the estimation error.

8 CONCLUDING REMARKS

In this thesis, low-complexity numerical algorithms for digital computation of the FrFT are proposed, with a focus on the sampling-type DFrFT and its application to chirp signal analysis. This type of DFrFT serves as an alternative tool for time-frequency analysis or for systems with physical interpretability, such as radar and sonar systems. Considering the number of arithmetic operations, especially for long one-dimensional signals, the sampling-type DFrFT is more efficient than the eigenvector decomposition DFrFT, which is mathematically robust and possesses all essential properties. The choice of the type of DFrFT depends on the application's focus, practice utility, and theoretical rigor.

The most widely used numerical algorithm for the sampling-type DFrFT is the chirp-convolution-based method, specifically the CM–CC–CM decomposition. This type of decomposition is performed involving normalized domains. In this context, we have outlined that the chirp convolution in discrete form becomes a circular convolution, as it corresponds to partial points of an infinite linear convolution following the overlap-and-save procedure, which decomposes a linear convolution into smaller circular convolutions. In other words, an N-point DFrFT can be decomposed into two $(2N)$-length element-wise multiplications and one $(2N)$-length circular convolution. Subsequently, we demonstrated that the algorithm can be accelerated using Fermat number transforms by representing discrete-time signals over the ring of integers modulo $2^b + 1$.

Considering a 1D convolution modulo $2^b + 1$, which can be part of a DFrFT, where half of the input sequence is padded with zeros and only the latter half of the output sequence is required, we introduced local Fermat number transforms to eliminate operations involving null values and focus on relevant points. This optimization results in saving a total of $6N$ additions for an N-point DFrFT. Furthermore, we introduced a radix-$(4b)$ algorithm for computing a 2^n-point FNT in GF$(2^b + 1)$, with $b = 8$ or 16, where $\log_2(4b) < n \leq b$. In particular, when the kernel is chosen as the m-th root of 2, its $(m/2)$-th power is the square root of 2, which can occasionally be given by $2^{\frac{b}{4}}(1 - 2^{\frac{b}{2}})$ (modulo $2^b + 1$). This operand reduces to left-bit shifts and one subtraction when used in a multiplication. The radix-$(4b)$ is more efficient in terms of multiplications than the radix-$(2b)$ method. However, a reduction in the number of multiplications may lead to an increase in additions. Despite this, the proposed algorithm offers an alternative to achieve larger transform lengths with a given Cooley-Tukey mapping.

In applications such as radar signals, Fermat primes F_t, with $t = 0, 1, \ldots, 4$, may be too small to represent the CM–CC–CM decomposition. Therefore, it is necessary to use Fermat numbers F_t, with $t = 5, 6$. In this way, the maximum length of an FNT is 2^{t+2}. For long one-dimensional signals, a low-complexity alternative involves using a 2D convolution scheme alongside 2D-FNTs. In this scheme, only one-fourth of the input matrix contains the sequence to be processed, and one-fourth of the output matrix contains the required sequence. In an N-point DFrFT, local input/output adaptations can reduce arithmetic operations by at least $18N$ additions.

In low-complexity algorithms based on computing partial points, the LDFrFT based on local circular convolution can provide a wider coverage in terms of target distance compared to the previous LDFrFT algorithm when calculating a specified number of consecutive points in the DFrFT. For comparisons, we use the CSD representation to estimate the equivalent number of additions and a logarithmic time complexity for modulo $2^b + 1$ adders. Simulations of radar signals show that our LDFrFT, decomposed into a local circular convolutions modulo $2^{32} + 1$, achieves a lower time complexity with minimal inaccuracies compared to the double precision floating point LDFrFT decomposed into fast Fourier transforms.

An alternative numerical algorithm for the sampling-type DFrFT involves using axis scaling, which enables its decomposition into a single DFT and two chirp multiplications. This is referred to as the CM–FFT–CM decomposition when the DFT is implemented within the framework of fast Fourier transforms. The method has been generalized as a discrete transform with a free sampling parameter, and in essence it is a scaled DFrFT, as it involves axis scaling based on the angle of rotation in the time-frequency plane. As a result, greater efficiency can be achieved in comparison to the chirp-convolution-based decomposition when a floating-point representation is used. Additionally, the differences between the methods in terms of time-shift properties and the relationship between the optimal order and the parameters of a linear chirp were detailed.

Considering the ways in which a linear canonical transform becomes an FrFT, we explored versions with amplitude simplification and those that can be decomposed into a single Fourier transform. Here, we demonstrate that the frequency-scaled simplified FrFT (referred to as SmFrFT) admits high chirp rates. The discrete form of this transform, defined in normalized domains, is denoted as DSmFrFT and possesses the convertibility property. This property enables the elimination of high oscillations when the fractional order approaches 0 or ± 2.

In the context of chirp signal processing using the FrFT, the DSmFrFT offers substantial advantages for linear chirps, particularly by reducing the peak search dimension when the center frequency is known. This has been validated through numerical simulations, which involved analyzing the amplitude spectrum of a single-component LFM signal and estimating the DoA of a single target in the fractional Fourier domain. In this scenario, we have demonstrated how the local DSmFrFT algorithm can reduce the number of multiplications and additions. Furthermore, it can be concluded that the DSmFrFT enhances the range of chirp rates and provides a robust capability for estimating the parameters of chirp signals.

For both single- and multi-objective DoA estimation, it has been shown that applying peak alignment during the preprocessing stage of subspace-based algorithms significantly reduces the estimation error when using a center-symmetric ULA. In the multi-carrier scenario, where chirp signals have different center frequencies and their peaks in the fractional Fourier domain can be clustered such that non-intersecting lines can be fitted, piecewise linear regression has been shown to be effective. However, when the lines formed by these peaks intersect, the CLSM

method becomes inapplicable. In such cases, multi-line fitting using the HT presents an efficient alternative, when the number of angles in the Hough space is smaller than the square of the number of sensors in the ULA. Finally, it is important to note that both the CLSM and the HT methods may offer lower computational complexity compared to subspace-based algorithms. However, the forward-backward spatial smoothing technique generally provides high accuracy. In this context, the ESPRIT algorithm integrated with the simplified fractional Fourier transform is particularly effective, whereas the MUSIC algorithm may exhibit cross-null interference under the same conditions.

Future work may be directed toward the development of low-complexity algorithms for the digital computation of the fractional Fourier transform and its applications, as outlined in the following items:

1. *Hardware implementation:* Future work will focus on FPGA-based implementation of the CM–CC–CM structure in the ring $\mathbb{Z}_{2^b+1}$, using IEAC adders, ICS operations, and CSD multipliers to improve modular arithmetic efficiency and latency performance.

2. *Two-dimensional FrFT:* Future work will extend the proposed chirp-based decompositions for two-dimensional FrFT (2D-FrFT), exploiting separable forms for image rotation, filtering, and encryption, and nonseparable forms for coupled chirp synthesis, joint time–frequency analysis, and radar imaging.

3. *Centered DFrFT:* Future research may explore low-complexity algorithms for the centered DFrFT (CDFrFT), leveraging the structure of the Grünbaum tridiagonal operator as well as Krylov subspace methods. Such approaches could enhance the practical applicability of the CDFrFT in resource-constrained systems, including real-time radar and quantum signal processing.

4. *Receiver for FMCW radar:* The fractional correlation-based receiver for FMCW signals plays a critical role in applications such as automotive radar. The problem can be addressed through decomposition based on chirp convolutions in the ring $\mathbb{Z}_{2^b+1}$, or by using simplied FrFT with frequency-variable scaling for a more efficient correlation process.

5. *Localization of mobile agents:* In IoV or IoUT applications, future studies may focus on multi-target DoA estimation of mobile agents based on wideband chirp signals in the fractional Fourier domain, encompassing Cramér–Rao bound analysis and scalable array geometries such as uniform rectangular arrays.

BIBLIOGRAPHY

ABDUH, Z. et al. Classification of heart sounds using fractional Fourier transform based mel-frequency spectral coefficients and traditional classifiers. **Biomedical Signal Processing and Control**, Elsevier, v. 57, p. 101788, 2020. Cited on page 17.

AGARWAL, R.; BURRUS, C. Fast convolution using Fermat number transforms with applications to digital filtering. **IEEE Transactions on Acoustics, Speech, and Signal Processing**, IEEE, v. 22, n. 2, p. 87–97, 1974. Cited 4 times on pages 19, 47, 48, and 51.

AGARWAL, R.; BURRUS, C. Fast one-dimensional digital convolution by multidimensional techniques. **IEEE Transactions on Acoustics, Speech, and Signal Processing**, IEEE, v. 22, n. 1, p. 1–10, 1974. Cited 5 times on pages 25, 37, 51, 54, and 55.

AHMAD, M. I.; LIU, Z.; XU, Y. Order selection in fractional Fourier transform based beamforming. **Journal of Systems Engineering and Electronics**, BIAI, v. 21, n. 3, p. 361–369, 2010. Cited on page 20.

AHMED, N. et al. Performance analysis of efficient computing techniques for direction of arrival estimation of underwater multi targets. **IEEE Access**, IEEE, v. 9, p. 33284–33298, 2021. Cited on page 21.

ALDIMASHKI, O.; SERBES, A. Performance of chirp parameter estimation in the fractional Fourier domains and an algorithm for fast chirp-rate estimation. **IEEE Transactions on Aerospace and Electronic Systems**, IEEE, v. 56, n. 5, p. 3685–3700, 2020. Cited 4 times on pages 20, 21, 28, and 38.

ALMEIDA, L. B. The fractional Fourier transform and time-frequency representations. **IEEE Transactions on Signal Processing**, IEEE, v. 42, n. 11, p. 3084–3091, 1994. Cited on page 30.

AMIN, M. Sufficient conditions for alias-free direction of arrival estimation in periodic spatial spectra. **IEEE Transactions on Antennas and Propagation**, IEEE, v. 41, n. 4, p. 508–511, 1993. Cited on page 86.

BAOZHOU, Z. et al. Diminished-1 Fermat number transform for integer convolutional neural networks. In: IEEE. **2019 IEEE 4th International Conference on Big Data Analytics (ICBDA)**. [S.l.], 2019. p. 47–52. Cited 2 times on pages 19 and 51.

BARABELL, A. Improving the resolution performance of eigenstructure-based direction-finding algorithms. In: IEEE. **ICASSP'83. IEEE International Conference on Acoustics, Speech, and Signal Processing**. [S.l.], 1983. v. 8, p. 336–339. Cited on page 71.

BARRICK, D. E. **FM/CW radar signals and digital processing**. [S.l.]: Environmental Research Laboratories, 1973. v. 55. Cited on page 80.

BERNSTEIN, D. J. Multidigit multiplication for mathematicians. **Advances in Applied Mathematics**, p. 1–19, 2001. Cited on page 101.

BISPO, B. C.; NETO, J. R. de O.; LIMA, J. B. Hardware architectures for computing eigendecomposition-based discrete fractional Fourier transforms with reduced arithmetic complexity. **Circuits, Systems, and Signal Processing**, Springer, v. 43, n. 1, p. 593–614, 2024. Cited on page 19.

BLAHUT, R. E. **Fast algorithms for signal processing**. New York: Cambridge University Press, 2010. Cited 3 times on pages 19, 49, and 101.

BLOCH, S. Introduction to chirp concepts with a cheap chirp radar. **American Journal of Physics**, v. 41, n. 7, p. 857–864, 1973. Cited 2 times on pages 20 and 28.

BULTHEEL, A.; SULBARAN, H. E. M. Computation of the fractional Fourier transform. **Applied and Computational Harmonic Analysis**, Elsevier, v. 16, n. 3, p. 182–202, 2004. Cited on page 30.

CANDAN, C.; KUTAY, M. A.; OZAKTAS, H. M. The discrete fractional Fourier transform. **IEEE Transactions on Signal Processing**, IEEE, v. 48, n. 5, p. 1329–1337, 2000. Cited 2 times on pages 19 and 21.

CARIOLARO, G. et al. A unified framework for the fractional Fourier transform. **IEEE Transactions on Signal Processing**, IEEE, v. 46, n. 12, p. 3206–3219, 1998. Cited 3 times on pages 18, 30, and 74.

CARIOW, A.; PAPLIŃSKI, J.; MAJORKOWSKA-MECH, D. Some structures of parallel VLSI-oriented processing units for implementation of small size discrete fractional Fourier transforms. **Electronics**, MDPI, v. 8, n. 5, p. 509, 2019. Cited on page 19.

CHEN, X. et al. Maneuvering target detection via radon-fractional Fourier transform-based long-time coherent integration. **IEEE Transactions on Signal Processing**, IEEE, v. 62, n. 4, p. 939–953, 2014. Cited on page 21.

CHEN, Z.; GOKEDA, G.; YU, Y. **Introduction to Direction-of-arrival Estimation**. [S.l.]: Artech House, 2010. Cited 2 times on pages 28 and 29.

CHONG, H.; XIAOMIN, Z. DoA estimation of multi-component LFM in complex environment using ESPRIT based on FRFT. In: IEEE. **2011 IEEE International Conference on Signal Processing, Communications and Computing (ICSPCC)**. [S.l.], 2011. p. 1–4. Cited 4 times on pages 20, 21, 32, and 69.

CONDON, E. Immersion of the Fourier transform in a continuous group of functional transformations. **Proceedings of the National academy of Sciences of the United States of America**, National Academy of Sciences, v. 23, n. 3, p. 158, 1937. Cited on page 17.

COOLEY, J. W.; TUKEY, J. W. An algorithm for the machine calculation of complex Fourier series. **Mathematics of Computation**, JSTOR, v. 19, n. 90, p. 297–301, 1965. Cited 5 times on pages 17, 19, 39, 42, and 47.

CUI, Y. et al. Gridless underdetermined DOA estimation of wideband LFM signals with unknown amplitude distortion based on fractional Fourier transform. **IEEE Internet of Things Journal**, IEEE, v. 7, n. 12, p. 11612–11625, 2020. Cited on page 20.

DAHER, A. et al. Fast algorithm for optimal design of Fermat number transform based block digital filters. **Digital Signal Processing**, Elsevier, v. 113, p. 103029, 2021. Cited on page 47.

DAI, Z.-P. et al. Propagation and transformation of four-petal Gaussian vortex beams in fractional Fourier transform optical system. **Optik**, Elsevier, v. 245, p. 167644, 2021. Cited on page 17.

DASGUPTA, S.; PAPADIMITRIOU, C. H.; VAZIRANI, U. **Algorithms**. [S.l.]: McGraw-Hill, Inc., 2006. Cited on page 101.

DE OLIVEIRA NETO, J. R. et al. Computation of an eigendecomposition-based discrete fractional Fourier transform with reduced arithmetic complexity. **Signal Processing**, Elsevier, v. 165, p. 72–82, 2019. Cited on page 19.

DING, M.; WEI, Y.; YU, L. Parameter estimation of a single chirp in the presence of wiener phase noise with unknown variance. **IEEE Transactions on Signal Processing**, v. 72, p. 3171–3186, 2024. Cited 2 times on pages 20 and 28.

DUDA, R. O.; HART, P. E. Use of the Hough transformation to detect lines and curves in pictures. **Communications of the ACM**, ACM New York, NY, USA, v. 15, n. 1, p. 11–15, 1972. Cited 3 times on pages 25, 72, and 73.

DUHAMEL, P.; HOLLMANN, H. 'Split radix' FFT algorithm. **Electronics Letters**, IET Digital Library, v. 20, n. 1, p. 14–16, 1984. Cited 2 times on pages 102 and 105.

DUHAMEL, P.; PIRON, B.; ETCHETO, J. M. On computing the inverse DFT. **IEEE Transactions on Acoustics, Speech, and Signal Processing**, IEEE, v. 36, n. 2, p. 285–286, 1988. Cited on page 105.

DUHAMEL, P.; VETTERLI, M. Fast Fourier transforms: a tutorial review and a state of the art. **Signal Processing**, Elsevier, v. 19, n. 4, p. 259–299, 1990. Cited 2 times on pages 17 and 48.

ERDOGAN, A. Y. et al. FMCW signal detection and parameter extraction by cross Wigner–Hough transform. **IEEE Transactions on Aerospace and Electronic Systems**, IEEE, v. 53, n. 1, p. 334–344, 2017. Cited on page 80.

FANG, X. et al. Radar maneuvering target detection based on two steps scaling and fractional Fourier transform. **Signal Processing**, Elsevier, v. 155, p. 1–13, 2019. Cited on page 17.

FARAH, M. B. et al. A novel chaos based optical image encryption using fractional Fourier transform and DNA sequence operation. **Optics & Laser Technology**, Elsevier, v. 121, p. 105777, 2020. Cited on page 17.

GOERTZEL, G. An algorithm for the evaluation of finite trigonometric series. **American Math. Monthly**, v. 65, p. 34–35, 1958. Cited on page 18.

GÓMEZ-ECHAVARRÍA, A.; UGARTE, J. P.; TOBÓN, C. The fractional Fourier transform as a biomedical signal and image processing tool: A review. **Biocybernetics and Biomedical Engineering**, Elsevier, v. 40, n. 3, p. 1081–1093, 2020. Cited on page 22.

GORBUNOV, M.; DOLOVOVA, O. Fractional Fourier transform and distributions in the ray space: Application for the analysis of radio occultation data. **Remote Sensing**, MDPI, v. 14, n. 22, p. 5802, 2022. Cited on page 17.

HEALY, J. J. et al. **Linear canonical transforms: Theory and applications**. [S.l.]: Springer, 2015. v. 198. Cited on page 33.

HEIDEMAN, M.; JOHNSON, D.; BURRUS, C. Gauss and the history of the fast Fourier transform. **IEEE ASSP Magazine**, IEEE, v. 1, n. 4, p. 14–21, 1984. Cited on page 17.

HRICHA, Z.; YAALOU, M.; BELAFHAL, A. Introduction of a new vortex cosine-hyperbolic-Gaussian beam and the study of its propagation properties in fractional Fourier transform optical system. **Optical and Quantum Electronics**, Springer, v. 52, p. 1–18, 2020. Cited on page 17.

HUANG, G.; ZHANG, F.; TAO, R. Sliding short-time fractional fourier transform. **IEEE Signal Processing Letters**, IEEE, v. 29, p. 1823–1827, 2022. Cited on page 18.

IRFAN, M.; ZHENG, L.; SHAHZAD, H. Research article review of computing algorithms for discrete fractional Fourier transform. **Research Journal of Applied Sciences, Engineering and Technology**, v. 6, n. 11, p. 1911–1919, 2013. Cited 2 times on pages 19 and 30.

JACOBSEN, E.; LYONS, R. The sliding dft. **IEEE Signal Processing Magazine**, IEEE, v. 20, n. 2, p. 74–80, 2003. Cited on page 18.

JIA, S. et al. Multi-block sparse bayesian learning channel estimation for OFDM underwater acoustic communication based on fractional Fourier transform. **Applied Acoustics**, Elsevier, v. 192, p. 108721, 2022. Cited on page 17.

KARATSUBA, A. A.; OFMAN, Y. P. Multiplication of many-digital numbers by automatic computers. In: RUSSIAN ACADEMY OF SCIENCES. **Doklady Akademii Nauk**. [S.l.], 1962. v. 145, n. 2, p. 293–294. Cited on page 101.

KIM, M. et al. Direction finding for multiple wideband chirp signal sources using blind signal separation and matched filtering. **Signal Processing**, Elsevier, v. 200, p. 108642, 2022. Cited 3 times on pages 20, 28, and 29.

KLAUDER, J. R. et al. The theory and design of chirp radars. **Bell System Technical Journal**, Wiley Online Library, v. 39, n. 4, p. 745–808, 1960. Cited 2 times on pages 20 and 28.

KNUTH, D. E. **The Art of Computer Programming Vol. 2: Seminumerical Methods**. [S.l.]: Addison-Wesley, Reading, Mass, 1981. Cited 2 times on pages 101 and 102.

KOC, A. et al. Digital computation of linear canonical transforms. **IEEE Transactions on Signal Processing**, IEEE, v. 56, n. 6, p. 2383–2394, 2008. Cited on page 18.

KRISHNAN, R.; JULLIEN, G.; MILLER, W. Complex digital signal processing using quadratic residue number systems. **IEEE Transactions on Acoustics, Speech, and Signal Processing**, IEEE, v. 34, n. 1, p. 166–177, 1986. Cited 2 times on pages 19 and 54.

LAN, C. et al. Underwater acoustic DOA estimation of incoherent signal based on improved GA-MUSIC. **IEEE Access**, IEEE, v. 11, p. 69474–69485, 2023. Cited on page 71.

LAN, T. et al. Intrinsic spectrum analysis of laser dynamics based on fractional Fourier transform. **Journal of Lightwave Technology**, IEEE, v. 41, n. 14, p. 4777–4785, 2023. Cited 2 times on pages 18 and 74.

LEE, D.-H. et al. Robust LFM target detection in wideband sonar systems. **IEEE Transactions on Aerospace and Electronic Systems**, IEEE, v. 53, n. 5, p. 2399–2412, 2017. Cited on page 20.

LEIBOWITZ, L. A simplified binary arithmetic for the Fermat number transform. **IEEE Transactions on Acoustics, Speech, and Signal Processing**, IEEE, v. 24, n. 5, p. 356–359, 1976. Cited 2 times on pages 51 and 52.

LI, N. et al. Graph linear canonical transform based on CM-CC-CM decomposition. **Digital Signal Processing**, Elsevier, v. 159, p. 105015, 2025. ISSN 1051-2004. Cited on page 18.

LIU, A. et al. Combined root-MUSIC algorithms for multi-carrier MIMO radar with sparse uniform linear arrays. **IET Radar, Sonar & Navigation**, Wiley Online Library, v. 13, n. 1, p. 89–97, 2019. Cited on page 86.

LIU, X.; XIAO, B.; WANG, C. Frequency estimation of chirp signals based on fractional Fourier transform combined with Otsu's method. **Optik**, Elsevier, v. 240, p. 166945, 2021. Cited 5 times on pages 20, 28, 35, 36, and 46.

LIU, X.; XIAO, B.; WANG, C. Optimal target function for the fractional Fourier transform of LFM signals. **Circuits, Systems, and Signal Processing**, Springer, v. 41, n. 7, p. 4160–4173, 2022. Cited on page 20.

LIU, Y. et al. The hopping discrete fractional fourier transform. **Signal Processing**, Elsevier, v. 178, p. 107763, 2021. Cited on page 18.

LOAN, C. V. **Computational frameworks for the fast Fourier transform**. [S.l.]: SIAM, 1992. Cited on page 105.

LUO, Y. et al. An unassisted super-resolution satellite navigation receiver using GPS L5 signals. **IEEE Transactions on Aerospace Electronic Systems**, v. 59, n. 6, p. 7666–7680, 2023. Cited on page 18.

MADANAYAKE, A. et al. Fast radix-32 approximate DFTs for 1024-beam digital RF beamforming. **IEEE Access**, IEEE, v. 8, p. 96613–96627, 2020. Cited on page 101.

MAHADI, M. et al. Low-complexity robust beamforming for a moving source. In: IEEE. **2020 28th European Signal Processing Conference (EUSIPCO)**. [S.l.], 2021. p. 1846–1850. Cited on page 20.

MAJORKOWSKA-MECH, D.; CARIOW, A. A low-complexity approach to computation of the discrete fractional Fourier transform. **Circuits, Systems, and Signal Processing**, Springer, v. 36, n. 10, p. 4118–4144, 2017. Cited on page 19.

MARINHO, F. J.; BERNARDO, L. M. Numerical calculation of fractional Fourier transforms with a single fast-Fourier-transform algorithm. **JOSA A**, Optica Publishing Group, v. 15, n. 8, p. 2111–2116, 1998. Cited 2 times on pages 18 and 34.

MATAS, J.; GALAMBOS, C.; KITTLER, J. Robust detection of lines using the progressive probabilistic Hough transform. **Computer Vision and Image Understanding**, Elsevier, v. 78, n. 1, p. 119–137, 2000. Cited on page 73.

MIAO, H. Local discrete fractional Fourier transform: An algorithm for calculating partial points of DFrFT. **Signal Processing**, Elsevier, v. 210, p. 109080, 2023. Cited 7 times on pages 19, 25, 35, 44, 45, 81, and 82.

MOORE, C.; MERTENS, S. **The nature of computation**. [S.l.]: Oxford University Press, 2011. Cited on page 101.

MOUSAVI, M.; SHAHZADI, A. Hyperbolic FrFT-OFDM system BER analysis over high Doppler Rician fading channels. **Electronics Letters**, Wiley Online Library, v. 51, n. 24, p. 2003–2005, 2015. Cited on page 21.

MULINDE, R.; ATTYGALLE, M.; AZIZ, S. M. Experimental validation of direction of arrival estimation for high chirp-rate linear frequency modulated radar signals. **IET Radar, Sonar & Navigation**, Wiley Online Library, v. 15, n. 6, p. 627–640, 2021. Cited 2 times on pages 20 and 34.

MUNRO, I. Some results concerning efficient and optimal algorithms. In: **Proceedings of the Third Annual ACM Symposium on Theory of Computing**. [S.l.: s.n.], 1971. p. 40–44. Cited on page 102.

NAMIAS, V. The fractional order Fourier transform and its application to quantum mechanics. **IMA Journal of Applied Mathematics**, Oxford University Press, v. 25, n. 3, p. 241–265, 1980. Cited on page 17.

NIEWELT, B. et al. Experimental implementation of the optical fractional Fourier transform in the time-frequency domain. **Physical Review Letters**, APS, v. 130, n. 24, p. 240801, 2023. Cited on page 17.

NUSSBAUMER, H. Complex convolutions via Fermat number transforms. **IBM Journal of Research and Development**, IBM, v. 20, n. 3, p. 282–284, 1976. Cited 3 times on pages 19, 51, and 54.

OKTEM, F. S.; OZAKTAS, H. M. Exact relation between continuous and discrete linear canonical transforms. **IEEE Signal Processing Letters**, IEEE, v. 16, n. 8, p. 727–730, 2009. Cited on page 21.

OTTERSTEN, B.; KAILATH, T. Direction-of-arrival estimation for wide-band signals using the ESPRIT algorithm. **IEEE Transactions on Acoustics, Speech, and Signal Processing**, IEEE, v. 38, n. 2, p. 317–327, 1990. Cited on page 20.

OZAKTAS, H. M. et al. Digital computation of the fractional Fourier transform. **IEEE Transactions on Signal Processing**, IEEE, v. 44, n. 9, p. 2141–2150, 1996. Cited 6 times on pages 17, 30, 35, 36, 38, and 42.

OZAKTAS, H. M.; KUTAY, M. A.; MENDLOVIC, D. Introduction to the fractional Fourier transform and its applications. In: **Advances in Imaging and Electron Physics**. US: Elsevier, 1999. v. 106, p. 239–291. Cited 3 times on pages 30, 31, and 36.

PANAHI, F.; RASHIDI, S.; SHEIKHANI, A. Application of fractional Fourier transform in feature extraction from electrocardiogram and galvanic skin response for emotion recognition. **Biomedical Signal Processing and Control**, Elsevier, v. 69, p. 102863, 2021. Cited on page 17.

PARK, C.-S.; KO, S.-J. The hopping discrete fourier transform [sp tips&tricks]. **IEEE Signal Processing Magazine**, IEEE, v. 31, n. 2, p. 135–139, 2014. Cited on page 18.

PATOLE, S. M. et al. Automotive radars: A review of signal processing techniques. **IEEE Signal Processing Magazine**, IEEE, v. 34, n. 2, p. 22–35, 2017. Cited on page 80.

PEACOCK, D. J.; SANTHANAM, B. **Multicomponent Subspace Chirp Parameter Estimation Using Discrete Fractional Fourier Analysis.** [S.l.], 2011. Cited on page 20.

PEI, S.-C.; DING, J.-J. Closed-form discrete fractional and affine Fourier transforms. **IEEE Transactions on Signal Processing**, IEEE, v. 48, n. 5, p. 1338–1353, 2000. Cited 6 times on pages 18, 19, 31, 35, 39, and 74.

PEI, S.-C.; DING, J.-J. Simplified fractional Fourier transforms. **JOSA A**, Optica Publishing Group, v. 17, n. 12, p. 2355–2367, 2000. Cited 4 times on pages 18, 31, 34, and 41.

PEI, S.-C.; DING, J.-J. Fractional cosine, sine, and Hartley transforms. **IEEE Transactions on Signal Processing**, IEEE, v. 50, n. 7, p. 1661–1680, 2002. Cited 2 times on pages 18 and 33.

PETROV, N.; YAROVOY, A. G. Fractional Fourier transform receiver for modulated chirp waveforms. **IEEE Transactions on Microwave Theory and Techniques**, IEEE, v. 71, n. 2, p. 818–826, 2022. Cited 2 times on pages 17 and 18.

QU, H. et al. DOA estimation of coherent wideband LFM signals based on fractional Fourier transform. In: IEEE. **First International Conference on Innovative Computing, Information and Control-Volume I (ICICIC'06)**. [S.l.], 2006. v. 3, p. 18–21. Cited on page 69.

ROY, R.; KAILATH, T. ESPRIT-estimation of signal parameters via rotational invariance techniques. **IEEE Transactions on Acoustics, Speech, and Signal Processing**, IEEE, v. 37, n. 7, p. 984–995, 1989. Cited 2 times on pages 20 and 21.

SANJAY, K. Convolution, product and correlation theorems for simplified fractional Fourier transform: A mathematical investigation. **Research Journal of Quantum Computations and Physical Systems**, v. 1, p. 1, 2018. Cited on page 18.

SCHMIDT, R. Multiple emitter location and signal parameter estimation. **IEEE Transactions on Antennas and Propagation**, IEEE, v. 34, n. 3, p. 276–280, 1986. Cited 2 times on pages 20 and 21.

SEJDIĆ, E.; DJUROVIĆ, I.; STANKOVIĆ, L. Fractional Fourier transform as a signal processing tool: An overview of recent developments. **Signal Processing**, Elsevier, v. 91, n. 6, p. 1351–1369, 2011. Cited on page 22.

SERBES, A. Compact fractional Fourier domains. **IEEE Signal Processing Letters**, IEEE, v. 24, n. 4, p. 427–431, 2017. Cited on page 21.

SHEN, A. K. Gauss multiplication trick? **Mathematical Enlightenment**, Independent Moscow University – MCCME, v. 24, n. 0, p. 19–33, 2019. Cited on page 101.

SHI, J. et al. Synchrosqueezed fractional wavelet transform: A new high-resolution time-frequency representation. **IEEE Transactions on Signal Processing**, IEEE, v. 71, p. 264–278, 2023. Cited on page 21.

SHI, J. et al. Generalized convolution theorem associated with fractional Fourier transform. **Wireless Communications and Mobile Computing**, Wiley Online Library, v. 14, n. 13, p. 1340–1351, 2014. Cited on page 18.

SINGLETON, R. C. An algorithm for computing the mixed radix fast Fourier transform. **IEEE Transactions on Audio and Electroacoustics**, IEEE, v. 17, n. 2, p. 93–103, 1969. Cited on page 102.

SONG, P.-F. et al. An efficient FPGA-based accelerator design for convolution. In: IEEE. **2017 IEEE 8th International Conference on Awareness Science and Technology (iCAST)**. [S.l.], 2017. p. 494–500. Cited on page 19.

STOVE, A. G. Linear FMCW radar techniques. In: IET. **IEE Proceedings F (Radar and Signal Processing)**. [S.l.], 1992. v. 139, n. 5, p. 343–350. Cited on page 80.

STRANG, G. Wavelets. **American Scientist**, JSTOR, v. 82, n. 3, p. 250–255, 1994. Cited on page 17.

SU, X.; TAO, R.; KANG, X. Analysis and comparison of discrete fractional Fourier transforms. **Signal Processing**, Elsevier, v. 160, p. 284–298, 2019. Cited 2 times on pages 17 and 33.

TALLA, N.; BATTULA, T. K. A novel intelligent ground moving target indication using meta-heuristic-based simplified fractional Fourier transform. **Cybernetics and Systems**, Taylor & Francis, v. 55, n. 2, p. 351–379, 2024. Cited 2 times on pages 18 and 30.

TAN, Y. et al. Heart sound classification based on fractional Fourier transformation entropy. In: IEEE. **2022 IEEE 4th Global Conference on Life Sciences and Technologies (LifeTech)**. [S.l.], 2022. p. 588–589. Cited on page 17.

TAO, R.; ZHOU, Y. S. Novel method for the direction of arrival estimation of wideband linear frequency modulated sources based on fractional Fourier transform. **Transaction of Beijing Institute of Technology**, Beijing Institute of Technology, v. 25, n. 10, p. 895–899, 2005. Cited 3 times on pages 20, 21, and 32.

TREES, H. L. V. **Optimum array processing: Part IV of detection, estimation, and modulation theory**. [S.l.]: John Wiley & Sons, 2002. Cited on page 28.

TU, T. et al. Chirp-modulated visual evoked potential as a generalization of steady state visual evoked potential. **Journal of Neural Engineering**, IOP Publishing, v. 9, n. 1, p. 016008, 2011. Cited on page 32.

VARGAS-RUBIO, J. G.; SANTHANAM, B. On the multiangle centered discrete fractional fourier transform. **IEEE Signal Processing Letters**, IEEE, v. 12, n. 4, p. 273–276, 2005. Cited on page 20.

VERGOS, H.; DIMITRAKOPOULOS, G.; NIKOLOS, D. Efficient diminished-1 modulo $2^n + 1$ multipliers. **IEEE Transactions on Computers**, v. 54, n. 4, p. 491–496, 2005. Cited on page 53.

VERGOS, H. T.; EFSTATHIOU, C. Design of efficient modulo $2^n + 1$ multipliers. **IET Computers & Digital Techniques**, IET, v. 1, n. 1, p. 49–57, 2007. Cited on page 75.

VERGOS, H. T.; EFSTATHIOU, C.; NIKOLOS, D. Diminished-one modulo $2^n + 1$ adder design. **IEEE Transactions on Computers**, IEEE, v. 51, n. 12, p. 1389–1399, 2002. Cited on page 74.

VISWANATHAN, M. **Digital Modulations Using Python**. [S.l.]: Mathuranathan Viswanathan, 2019. Cited on page 43.

VORONENKO, Y.; PÜSCHEL, M. Multiplierless multiple constant multiplication. **ACM Transactions on Algorithms (TALG)**, ACM New York, NY, USA, v. 3, n. 2, p. 11–es, 2007. Cited 3 times on pages 53, 61, and 74.

WANG, W.-Q. Moving target indication via three-antenna SAR with simplified fractional Fourier transform. **EURASIP Journal on Advances in Signal Processing**, Springer, v. 2011, p. 1–10, 2011. Cited 2 times on pages 18 and 30.

WASSON, G. IEEE-754 Compliant algorithms for fast multiplication of double precision floating point numbers. **International Journal of Research in Computer Science**, Citeseer, v. 1, n. 1, p. 1–7, 2011. Cited on page 75.

WEI, D.; SHEN, J. Multi-spectra synchrosqueezing transform. **Signal Processing**, Elsevier, v. 207, p. 108940, 2023. Cited on page 18.

WIENER, N. Hermitian polynomials and Fourier analysis. **Journal of Mathematics and Physics**, Wiley Online Library, v. 8, n. 1-4, p. 70–73, 1929. Cited on page 17.

WINOGRAD, S. On multiplication of 2×2 matrices. **Linear Algebra and its Applications**, Elsevier, v. 4, n. 4, p. 381–388, 1971. ISSN 0024-3795. Cited on page 101.

XING, Y. et al. Low-complexity chromatic dispersion compensation using high-radix Fermat number transform. **Journal of Lightwave Technology**, IEEE, v. 42, n. 15, p. 5190–5203, 2024. Cited 6 times on pages 19, 49, 50, 52, 54, and 55.

XU, W.; YOU, X.; ZHANG, C. Using Fermat number transform to accelerate convolutional neural network. In: IEEE. **2017 IEEE 12th International Conference on ASIC (ASICON)**. [S.l.], 2017. p. 1033–1036. Cited on page 19.

YETIK, I. S.; NEHORAI, A. Beamforming using the fractional Fourier transform. **IEEE Transactions on Signal Processing**, IEEE, v. 51, n. 6, p. 1663–1668, 2003. Cited 2 times on pages 20 and 28.

YIN, J.-w. et al. Fractional Fourier transform based underwater multi-targets direction-of-arrival estimation using wideband linear chirps. **Applied Acoustics**, Elsevier, v. 169, p. 107477, 2020. Cited 3 times on pages 20, 21, and 32.

YU, J. et al. Separation and localization of multiple distributed wideband chirps using the fractional Fourier transform. **EURASIP Journal on Wireless Communications and Networking**, Springer, v. 2015, p. 1–8, 2015. Cited 2 times on pages 20 and 35.

ZAYED, A. I. On the relationship between the fourier and fractional fourier transforms. **IEEE Signal Processing Letters**, IEEE, v. 3, n. 12, p. 310–311, 1996. Cited 4 times on pages 18, 30, 33, and 74.

ZHANG, C. et al. A novel MuLoRa modulation based on fractional Fourier transform. **IEEE Communications Letters**, IEEE, v. 25, n. 9, p. 2993–2997, 2021. Cited on page 17.

ZHANG, D. et al. Multitarget AOA estimation using wideband LFMCW signal and two receiver antennas. **IEEE Transactions on Vehicular Technology**, IEEE, v. 67, n. 8, p. 7101–7112, 2018. Cited on page 20.

ZHANG, K. et al. A fast time delay estimator of cubic phase signal based on simplified fractional Fourier transform. In: IET. **IET International Radar Conference 2015**. [S.l.], 2015. p. 1–4. Cited on page 18.

ZHANG, X. et al. A pre-estimation algorithm for LFM signal based on simplified fractional Fourier transform. **Journal of Information and Computational Science**, v. 8, n. 4, p. 645–652, 2011. Cited on page 18.

ZHANG, Y. et al. A comprehensive survey on fractional Fourier transform. **Fundamenta Informaticae**, IOS press, v. 151, n. 1-4, p. 1–48, 2017. Cited on page 22.

ZHANG, Y. et al. Hyperchaotic image encryption using phase-truncated fractional Fourier transform and DNA-level operation. **Optics and Lasers in Engineering**, Elsevier, v. 143, p. 106626, 2021. Cited on page 17.

ZHAO, W. et al. Fast gridless direction-of-arrival estimation for wideband linear frequency modulated signals based on fractional Fourier transform. **Signal, Image and Video Processing**, Springer, v. 19, n. 1, p. 1–14, 2025. Cited on page 21.

ZHAO, Z.; LI, G. Synchrosqueezing-based short-time fractional Fourier transform. **IEEE Transactions on Signal Processing**, IEEE, v. 71, p. 279–294, 2023. Cited 2 times on pages 18 and 31.

ZHONG, J. et al. Direction of arrival estimation based on slope fitting of wideband array signal in fractional Fourier transform domain. **IET Radar, Sonar & Navigation**, Wiley Online Library, v. 17, n. 3, p. 422–434, 2023. Cited 8 times on pages 21, 29, 35, 36, 66, 67, 68, and 83.

ZHONG, J. et al. Two-dimensional DOA estimation using slope fitting of wideband LFM signal based on fractional Fourier transform. **Signal, Image and Video Processing**, Springer, v. 19, n. 15, p. 1272, 2025. Cited on page 35.

APPENDIX A – COMPLEX MULTIPLICATION TRICKS

In this appendix, we present a brief explanation of how a chirp multiplication can be performed efficiently, which is commonly encountered in numerical algorithms for the sampling-type DFrFT. First, in its natural form, the product of two complex numbers is given as

$$(a + jb)(c + jd) = ac - bd + j(ad + bc), \tag{A.1}$$

which involves four multiplications and two additions over the real field. This result can be found as a special case of the multiplication of two polynomials modulo a third; specifically, it means that $(a_0 + a_1u)(b_0 + b_1u)$ modulo $u^2 + 1$ (KNUTH, 1981, p. 647). In (MADANAYAKE et al., 2020), for example, the authors mention that twiddle-factor multiplications in fast Fourier transforms can be implemented using 3 real-valued multipliers and 5 real-valued adders by employing Gauss's algorithm for complex multiplication. However, there is some debate about whether the mathematician Carl Friedrich Gauss (1777–1855) developed this algorithm or whether he was the first to propose it (SHEN, 2019). Blahut (2010) comments that:

> Algorithms for complex multiplication using three real multiplications became generally known in the late 1950s, but the origin of these algorithms is a little hazy (BLAHUT, 2010, p. 20).

In this context, we can identify three methods for reducing the number of real multiplications in (A.1), one of which is particularly significant in computing fast Fourier transforms. These methods, involving only three multiplications, are:

1. The term $ad + bc$ can be replaced by its equivalent as follows

   $$ad + bc = (a + b)(c + d) - ac - bd,$$

   therefore, the three multiplications in (A.1) are ac, bd, and $(a + b)(c + d)$. This trick has been attributed to Gauss (DASGUPTA; PAPADIMITRIOU; VAZIRANI, 2006, p.55). However, in earlier years, this algorithm was presented in (WINOGRAD, 1971) without any mention of Gauss. According to Knuth (KNUTH, 1981, p.647), this formula was suggested by Peter Ungar in 1963. In (BERNSTEIN, 2001), original sources for each algorithm are presented, and this particular one is referred to as Karatsuba's trick rather than Gauss's trick. In (MOORE; MERTENS, 2011, p.37), the authors state that Karatsuba and Ofman (1962) discovered the algorithm for multiplying n-digit integers in 1962, but the concept of reducing four multiplications to three originated with Gauss.

2. Another approach involves using the equations:

   $$ac - bd = a(c + d) - d(a + b),$$
   $$ad + bc = a(c + d) + c(b - a).$$

In this case, the three multiplications in (A.1) are $a(c+d)$, $d(a+b)$, and $c(b-a)$. This optimization method appears in (MUNRO, 1971), once again without reference to Gauss. In Exercise 41 of (KNUTH, 1981, p. 501), it is described as:

> Show that the real and imaginary parts of $(a+jb)(c+jd)$ can be obtained by performing 3 multiplications and 5 additions of real numbers, where two of the additions involve a and b only (KNUTH, 1981, p. 501).

3. In a similar way of item 1), when $ac-bd$ is substituted by its equivalent

$$ac - bd = (a+b)(c-d) + ad - bc,$$

in consequence, the three multiplications in (A.1) are ad, bc, and $(a+b)(c-d)$. According to Singleton (1969), this alternative was pointed out by Golub.

In conclusion, the method described in item 2) can be more efficient, as two additions can be saved by pre-computing the operations $a+b$ and $b-a$, which is feasible in fast Fourier transform algorithms (DUHAMEL; HOLLMANN, 1984).

Returning to DFrFT and DSmFrFT, chirp multiplications in (3.3) and (3.20) can be expressed as $\tilde{x}[r] = e^{j\phi_\alpha[r]}x[r]$, where $\phi_\alpha[r] = \frac{\pi}{N}r^2\mu_\alpha$ is a generic phase and μ_α denotes a chirp rate depending on α, specifically $-\tan\left(\frac{\alpha}{2}\right)$ and $\cot(\alpha)$, respectively. For a specific rotation angle $\alpha = a\pi/2$, with a being the fractional order, pre-computing techniques can be applied as:

$$y[r] = \cos\phi_\alpha[r] + \sin\phi_\alpha[r],$$
$$z[r] = \sin\phi_\alpha[r] - \cos\phi_\alpha[r].$$

Subsequently, with $w[r] = \cos\phi_\alpha[r]\,(\mathfrak{Re}\{x[r]\} + \mathfrak{Im}\{x[r]\})$, the real and imaginary parts of $\tilde{x}[r]$ are given by:

$$\mathfrak{Re}\{\tilde{x}[r]\} = w[r] - y[r]\mathfrak{Im}\{x[r]\},$$
$$\mathfrak{Im}\{\tilde{x}[r]\} = w[r] + z[r]\mathfrak{Re}\{x[r]\}.$$

Therefore, an N-point element-wise chirp modulation requires $3N$ real-valued multiplications and $3N$ real-valued additions.

APPENDIX B – PARTIAL LINEAR CONVOLUTION

In this appendix, we begin by observing that an N-point DFrFT corresponds to a subset of samples from an infinite-length linear convolution. These points can be efficiently computed using a $(2N-1)$-point circular convolution, following the overlap-and-save (OaS) algorithm, which decomposes the linear convolution into smaller circular convolutions. Furthermore, we describe how this circular convolution can be optimized when the input is zero-padded and only the last N output samples are of interest.

OVERLAP-AND-SAVE APPROACH

The sampling-type DFrFT, through its decomposition presented in (3.3), can be formally expressed as a linear convolution problem, given by

$$y[r] = (g * h)[r], \tag{B.1}$$

where:

- $g[r]$ is a finite-length sequence of length N, supported on $r \in [-N/2, N/2)$.
- $h[r]$ is an infinite-length sequence.
- The output $y[r]$ is an infinite-length sequence, whose values within $r \in [-N/2, N/2)$ are the points of interest.

The above referred partial output of $y[r]$ can be computed via a circular convolution by applying the overlap-and-save (OaS) algorithm, which avoids directly computing the full linear convolution, as described in the following items:

- Block division of the infinite sequence: Split $h[r]$ into overlapping blocks of length $L = 2N - 1$. Each block is indexed by an integer m as

  $$h_m[r] = h[r + mN] \text{ for } r \in (-N, N).$$

- Circular convolution within each block: Perform the $(2N-1)$-point circular convolution between the finite-length signal $g[r]$ and each block $h_m[r]$: $y_m[r] = (g \circledast h_m)[r]$, where $\circledast$ denotes circular convolution. This operation efficiently computes the valid part of the linear convolution within the portion of $h[r]$ covered by the block m.
- Selection of valid output: Due to circular convolution, some points correspond to linear convolution aliases (wrap-around effects). Therefore, only the last N points in the output are retained, as they correspond to the desired partial linear convolution.

CALCULATING THE POINTS OF INTEREST

Note that the N-point DFrFT given by (3.3) can be computed exactly for $m = 0$ by applying the OaS algorithm to the linear convolution in (B.1). In this specific case, the above decomposition can be efficiently implemented using N-point DFTs, as follows:

1. Pre-computing DFT of $\mathbf{h}$: $\mathbf{h}=[h_0, \ldots, h_{2N-1}]$ is a $2N$-length vector whose elements are given by the chirp function $e^{j\frac{\pi}{N}r^2 \csc\alpha}$, $-N \leq r < N$, so that its DFT, $\mathbf{H}=[H_0, \ldots, H_{2N-1}]$, can be computed in advance.

2. Computing DFT of $\mathbf{g}$: $\mathbf{g} = [g_0, \ldots, g_{2N-1}]$ is a $2N$-length vector whose first non-null elements are computed as $x[r]e^{-j\frac{\pi}{N}r^2 \tan\left(\frac{\alpha}{2}\right)}$, $-N/2 \leq r < N/2$. By definition, the DFT of $\mathbf{g}$, $\mathbf{G}=[G_0, \ldots, G_{2N-1}]$, is a matrix-vector product given by

$$G_k = \frac{1}{\sqrt{2N}} \sum_{n=0}^{2N-1} g_n \omega_{2N}^{kn}, \quad k = 0, 1, \ldots, 2N-1, \tag{B.2}$$

where $\omega_p = e^{-j\frac{2\pi}{p}}$, $p = 2N$. Particularly, the DFT of $\mathbf{g}$ can be separated into two smaller summations by the decimation-in-frequency procedure, as follows

$$G_k = \frac{1}{\sqrt{2N}} \left(\sum_{n=0}^{N-1} g_n \omega_{2N}^{kn} + \sum_{n=N}^{2N-1} g_n \omega_{2N}^{kn} \right).$$

Observe that the second summation is null ($g_n=0$), so that the even elements, G_{2k}, and the odd elements, G_{2k+1}, $k = 0, 1, \ldots, N-1$, can be computed as

$$G_{2k} = \frac{1}{\sqrt{2N}} \sum_{n=0}^{N-1} g_n \omega_N^{kn},$$
$$G_{2k+1} = \frac{1}{\sqrt{2N}} \sum_{n=0}^{N-1} g_n \omega_{2N}^{n} \omega_N^{kn}.$$

As demonstrated, the DFT of $\mathbf{g}$ involves N complex multiplications and two N-point DFTs.

3. Pointwise product: the convolution theorem states that the DFT of a circular convolution, $\mathbf{y} = \mathbf{g} \circledast \mathbf{h}$, is the same as the product of their respective DFTs, that is, $Y_k = G_k H_k$, $k = 0, \ldots, 2N-1$.

4. Inverse DFT of $[Y_0, \ldots, Y_{2N-1}]$: let $\mathbf{y} = [y_0, \ldots, y_{2N-1}]$ be the vector resulting from the aforementioned circular convolution whose last N elements corresponds to summation term of (3.3). Then, $\mathbf{y}$ can be obtained by the inverse DFT (IDFT) as

$$y_n = \frac{1}{\sqrt{2N}} \sum_{k=0}^{2N-1} Y_k \omega_{2N}^{-kn}, \quad n = 0, 1, \ldots, 2N-1.$$

Analogous to the decimation-in-time procedure in DFT, the elements of interest y_{n+N}, $n{=}0, \ldots, N-1$, can be calculated as the addition of the N-point IDFTs of the even and odd indices, that is

$$y_{n+N} = \frac{1}{\sqrt{2N}} \sum_{k=0}^{N-1} Y_{2k} \omega_N^{-kn} - \frac{\omega_{2N}^{-n}}{\sqrt{2N}} \sum_{k=0}^{N-1} Y_{2k+1} \omega_N^{-kn}.$$

In that way, calculating the last N points of $\mathbf{y}$ requires N complex multiplications, N complex additions, and two N-point IDFTs.

Notice that a total of $3N$ complex additions is reduced by the procedure explained in items 2) and 4). An alternative approach to implement (3.4) is illustrated in Figure 28. In which a decimation-in-frequency (DIF) approach is first applied to avoid operations with zero-padding values when calculating the DFT (DUHAMEL; HOLLMANN, 1984), resulting in a reduction of $2N$ complex additions. Subsequently, after pointwise multiplication ($\otimes$), only the last N points of the inverse DFT (IDFT) are calculated, saving an additional of N complex additions. The IDFT is implemented by swapping the real and imaginary parts of the input ($\bowtie$), applying the decimation-in-time (DIT) procedure and then swapping the parts again, following the method described in (DUHAMEL; PIRON; ETCHETO, 1988).

Figure 28 – The signal flow graph of an n-point circular convolution, implemented using DFT in recursive form of split-radix FFT algorithm (LOAN, 1992, p. 111); the dotted lines represent either null input signals or neglected output signals. In which, given $m = n/2$ and $p = m/2$, the twiddle-factors are represented by diagonal matrix $\Delta_p = \text{diag}\,(1, \omega_n, \ldots, \omega_n^{p-1})$, where $\omega_n = e^{-j\frac{2\pi}{n}}$.

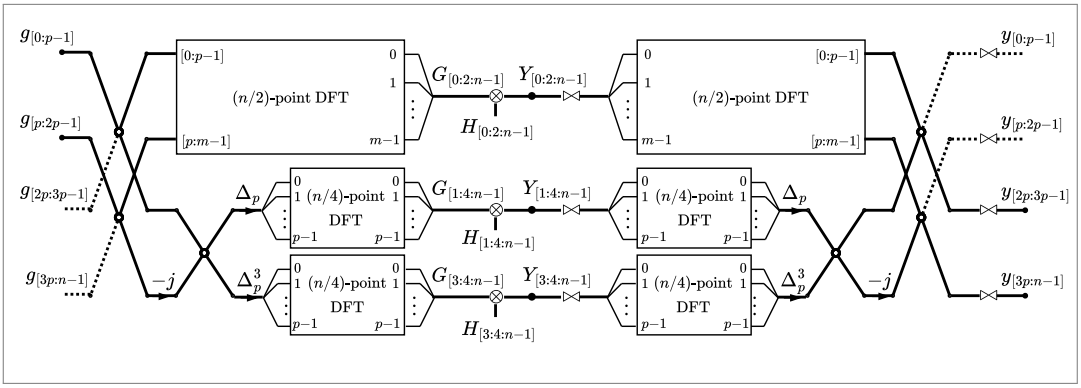

Source: The author (2025).